University of Glasgow

Asgari-Targhi, Ameneh (2017) *Action potential duration alternans in mathematical models of excitable cells.* PhD thesis.

http://theses.gla.ac.uk/8460/

Copyright and moral rights for this work are retained by the author

A copy can be downloaded for personal non-commercial research or study, without prior permission or charge

This work cannot be reproduced or quoted extensively from without first obtaining permission in writing from the author

The content must not be changed in any way or sold commercially in any format or medium without the formal permission of the author

When referring to this work, full bibliographic details including the author, title, awarding institution and date of the thesis must be given

Enlighten:Theses
http://theses.gla.ac.uk/
theses@gla.ac.uk

Action potential duration alternans in mathematical models of excitable cells

by

Ameneh Asgari Targhi

A thesis submitted to the

College of Science and Engineering

at the University of Glasgow

for the degree of

Doctor of Philosophy

July 2017

Dedication

This thesis is dedicated to the memory of my beloved father whose gentleness, altruism and generosity have been the true inspiration in my life. And to the memories of two fine and loving young ladies that I had the privilege to know and love; my cousin and my childhood friend Elahe Tarah who very suddenly perished because of a heart failure at the beginning of my PhD research and my sister Vajiheh Asgari Targhi whose kindness and warmth in her beautiful short life has taught me how to live life to the full.

Abstract

Action potential duration alternans has been associated with the onset of one of the most common forms of abnormal heart rhythm, atrial fibrillation (Cherry et al., 2012; Nattel, 2002). This thesis concerns identifying variables and parameters responsible for inducing action potential duration alternans. In order to achieve this, we apply asymptotic reduction methods to models of cardiac electrophysiology described by a system of ordinary differential equations and derive explicit discrete restitution maps which specify the action potential duration as a function of the preceding diastolic interval. The bifurcations of equilibria of these maps are studied to determine regions in the parameter space of the models where normal response and alternans occur. Furthermore, explicit parametric representations of both the normal and the alternans equilibrium branches of the restitution map are found.

We also develop a framework formulated in terms of a boundary value problems for studying cardiac restitution. This framework can be used to derive analytically or compute numerically different branches of the action potential duration restitution map from the full excitable models. Our method is validated by comparing the asymptotic restitution map with the boundary value problem formulated restitution curves.

The proposed method is applied to investigate the restitution properties of three excitable models: one generic excitable model and two ionic cardiac models. The first model is the McKean (1970) model which is a simplified version of the classical FitzHugh (1961) model. The other two models are the Caricature version of the Noble (1962) model derived by Biktashev et al. (2008) and an asymptotically reduced version of the Courtemanche et al. (1998) model of the atrial cell, reduced by Suckley (2004). After deriving the action potential duration restitution map for each of the mentioned model, the region of the models parameters in which alternans occurs is determined.

We conclude that alternans appears if the dynamics in the diastolic stage of an action potential are faster than the dynamics in the systolic stage. Furthermore, we show that the time scale for the slow gating variable is responsible for inducing alternans. We outline that the oscillation in the slow activation of the K^+ current and the slow inactivation of the L-type Ca^{+2} current can induce or suppress alternans.

Contents

List of Figures

Acknowledgements

I wish to express my sincere appreciation to the Lord Kelvin and Adam Smith scholarship for providing me with the opportunity to undertake this research.

I would like to thank my primary supervisor Dr Radostin Simitev for supervising this thesis and for all of his guidance and mathematical support throughout this research. I would also like to thank my other two supervisors, Dr Antony Workman for being such a thoughtful teacher and mentor and for his encouragement throughout my PhD research, and Professor Andrew Rankin for being a great support. I would like to express my heartfelt thanks to Professor Rankin and wish him a wonderful retirement to come.

I would like to express my appreciation to my thesis committee members Professor Xiaoyu Luo and Dr Ruediger Thul. It was a great pleasure to present my work for them and benefit from their expertise.

I would like to thank my mother for her unconditional love and support during my PhD studies. She has always been a shining and inspiring example of hope and strength in my life.

I would also like to thank my siblings, in particular my brother Mr Masoud Asgari Targhi for being the most caring and loving brother in the world, and for being so encouraging and an absolutely amazing companion during the long Scottish winter nights, while I was writing up.

I wish to express my deep gratitude to Dr Hiroshi Ashikaga for his insights, encouragement and support during many discussions we had over the past year of my PhD research.

I would like to thank my friends and fellow graduate students in the school of Mathematics and Statistics. In particular I would like to express my sincere thanks and appreciation to Dr Spiros Adams-Florou for reading the manuscript and providing me with helpful comments and suggestions.

I would like to show my gratitude to Mrs Sandy Wotton for all her support during the first year of my PhD at the time I was dealing with my family tragedy and settling in a new environment. She was a great mentor, support and a true blessing in my life.

I wish to express my sincere thanks to Mrs Alison Gray for being such a loving neighbour and friend, for her prayers, positive attitude and for being my adopted Scottish Godmother.

Last but not least, I would like to thank my adorable niece Sophie Setareh Voss who was born during my PhD studies and has brought tremendous joy and happiness to my life.

Glasgow, Winter. 2017

Declaration of Authorship

I, Ameneh Asgari Targhi, declare that, except where explicit reference is made to the contribution of others, this thesis is the result of my own work and has not been submitted for any other degree at the University of Glasgow or any other institution.

Chapter 1

Introduction

1.1 Atrial fibrillation and alternans

Atrial fibrillation is a disturbance of the normally rhythmical electrical beating of the cardiac atria (Li et al., 1999; Nattel, 2002). The electrical impulses (action potentials) that usually travel down the normal pathways instead spread through the atria in a chaotic fashion, as illustrated in Figure 1.1. This causes the atria to beat in a rapid, disorganised manner and the ventricles to contract in a rapid, irregular way. This irregularity may be a precondition for heart failure and stroke. Hence, atrial fibrillation may predispose to heart failure and stroke by completely different mechanisms: stroke by increased tendency for blood clotting in the atria due to loss of atrial contraction and heart failure from influences such as reduced ventricular filling because of reduced atrial contraction (Li et al., 1999; Nattel, 2002) Indeed, heart failure and stroke are among the most common causes of death in patients with atrial fibrillation (Leong et al., 2013; Tsadok et al., 2012). Current treatments for atrial fibrillation have limited efficacy and also safety concerns (organ toxicity and/or ventricular pro-arrhythmia risk). Therefore, there is an urgent need to develop new treatments for atrial fibrillation and this requires an improved understanding of the various and complex electrophysiological mechanisms of atrial fibrillation initiation and maintenance (Comtois and Nattel, 2012; Workman et al., 2008). Studies suggest that action potential duration (APD) alternans which is a beat-to-beat alternation of the action potential duration, may contribute to the development of atrial fibrillation (Franz et al., 2012). Therefore, in order to understand possible triggers of atrial fibrillation, an improved understanding of the mechanisms of APD alternans is required (Evans et al., 2000; Nattel, 2002).

Thus, the motivation for this work is to gain insight into the onset of atrial fibrillation and other

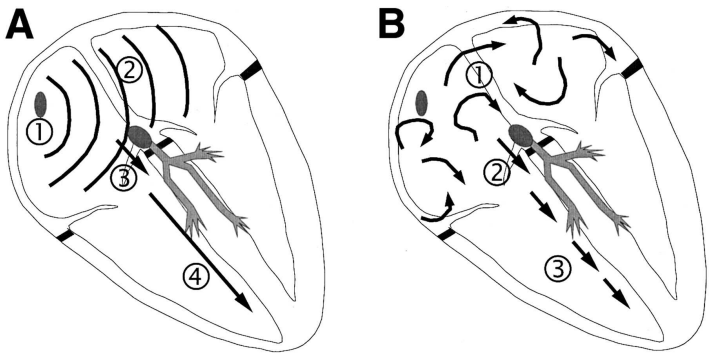

Figure 1.1: A schematic depiction of regular and irregular electrical activity in the atria. A denotes a healthy heart heartbeat. The electrical signals start from the sinoatrial node -the normal pacemaker- in the heart as shown in (1). After spreading across the atria as denoted in (2) and passing through the atrioventricular (AV) node in (3), the signals travel to the ventricles in (4). Figure B illustrates atrial fibrillation. Multiple electrical signals fire in (1) and the atria are activated in a chaotic manner. The extra signals reach the AV node as can be seen in (2) and some of them travel down to the ventricle as shown in (3) (Waktare, 2002).

irregular cardiac rhythms. To this end, understanding alternans and other cardiac arrhythmias, requires studying the restitution properties of cardiac cells. The term *restitution* describes the shortening of the action potential durations as the heart rate increases and is one of the most important characteristics of cardiac cells (Kalb et al., 2004; Schaeffer et al., 2007). In the following section we will introduce some concepts needed to formulate and describe alternans. Then we present mathematical models that have been developed to study restitution and alternans so far.

1.2 Preliminary concepts

In this subsection we will describe some basic phenomenology and introduce several concepts that are needed in order to formulate the aims and objectives of this work.

Action potential When a cardiac cell is depolarised by an electrical stimulus, such as one arising from the natural pacemaker the sinoatrial node, the transmembrane voltage rises rapidly and the cell depolarises. This is followed by a plateau phase in which the cell cannot be reactivated and finally the voltage returns to its resting potential which corresponds to the repolarisation of the cell. This is called

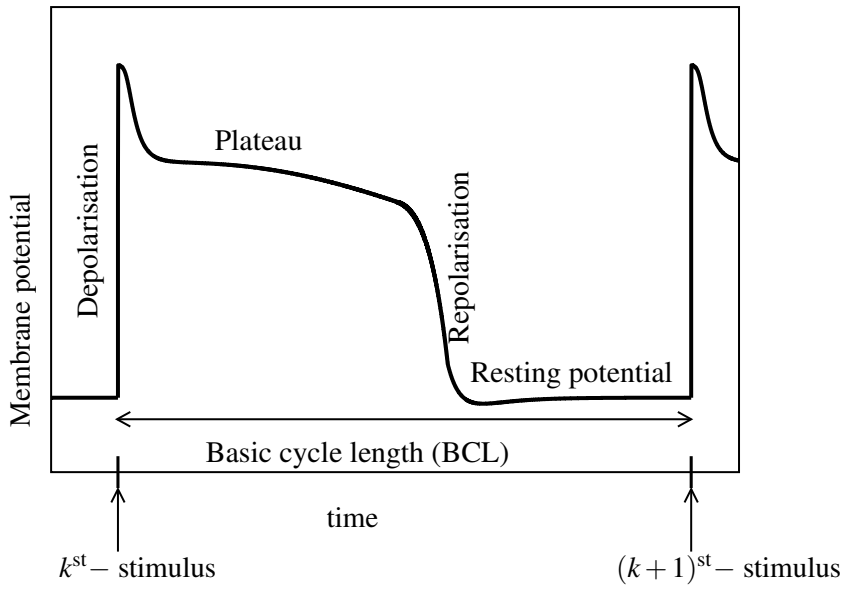

Figure 1.2: A schematic representation of the cardiac action potential with the major cardiac ionic currents. Depolarisation or "fast upstroke": during the fast upstroke phase the membrane potential rises from negative to positive. Plateau: calcium Ca^{+2} ions enter the cell and potassium K^{+} ions leave the cell. The balance between these two causes the membrane to shape the plateau phase of an AP. Repolarisation: K^{+} ions leave the cell and the membrane potential reduces to a negative value. Resting potential: there is almost no ion exchange across the cellular membrane and membrane potential is at its resting value.

an action potential and is depicted in Figure 1.2. The movement of ions through the transmembrane ion channels generates action potentials in the cardiac cells. The time required for the cell to achieve repolarisation after a depolarising stimulus, is called the action potential duration (A). The period between the end of one action potential and the start of the next is called the diastolic interval (D) and the time between stimuli is called the basic cycle length which is $B = \mathrm{A} + \mathrm{D}$ (Cain et al., 2004). Throughout this thesis, the action potential duration is referred to as A, the diastolic interval is denoted as D, B stands for basic cycle length and k refers to the number of action potentials.

Excitable cells All cells in the body can be divided into two groups of excitable cells and non-excitable cells. When a sufficiently strong current is applied to the membrane of an excitable cell for a short time, the cell's membrane potential (voltage difference between inside and outside of the cell) ascends rapidly before returning gradually to its resting state. Thus, resulting in the generation

of an action potential. Excitable cells such as cardiac cells, most neurons and muscle cells, use the membrane potential as a signal, hence their functions are dependent on the generation and propagation of electrical signals (Alberts et al., 1994; Keener and Sneyd, 1998)

The rest of the cells in the body are non-excitable, meaning that if a current is applied to their membrane, their potential changes but as soon as the current is removed their potential returns to its equilibrium value. Non-excitable cells do not carry electrical information and do not generate action potentials (Keener and Sneyd, 1998).

Cardiac cells under repeated simulation For a cardiac cell which has been subjected to a periodic train of electrical stimuli a variety of periodic responses have been observed in experiments. Examples include bullfrog cardiac muscles (Hall et al., 1999) and Langendorff-perfused rabbit hearts (Visweswaran et al., 2013).

At a slow rate for example 75 beats per minute corresponding to a basic cycle length of 800 (ms), every stimulus produces an identical action potential which is called a 1:1 response. At a faster pacing rate, a 1:1 response is replaced with a response pattern in which every stimulus may excite an action potential, but even and odd action potentials may be different. This is known as an alternans 2:2-response. At an even faster pacing rate, the above mentioned responses become unstable and only every second stimulus may excite an action potential, and all action potentials may be identical, this is called a 2:1 response. It is commonly believed that the 1:1 response represents the healthy function of the cardiac cell while the other responses are viewed as instabilities of the normal response that may progressively lead to the onset of cardiac arrhythmias in tissue including atrial fibrillation (Cherry et al., 2012). Figure 1.3 illustrates a sequence of action potentials. The membrane potential E is plotted as a function of time for a 1:1 response and a 2:2 response in Figures 1.3(a) and 1.3(b), respectively.

Restitution As explained previously, electrical restitution is one of the most crucial aspects of cardiac cells in which action potential duration is shortened as the heart rate increases (Kalb et al., 2004). The mechanism of restitution is not fully understood, but studies suggest that a decrease in the restitution of ionic currents determines the action potential duration restitution (Qu et al., 1999). It has been shown that restitution is associated with the role of repolarisation currents such that when D is shortened, repolarisation currents do not reactivate fully i.e.decrease in Ca^{+2} current, or fail to deactivate outward currents i.e. increase in K^{+} current, therefore generating a shorter action potential

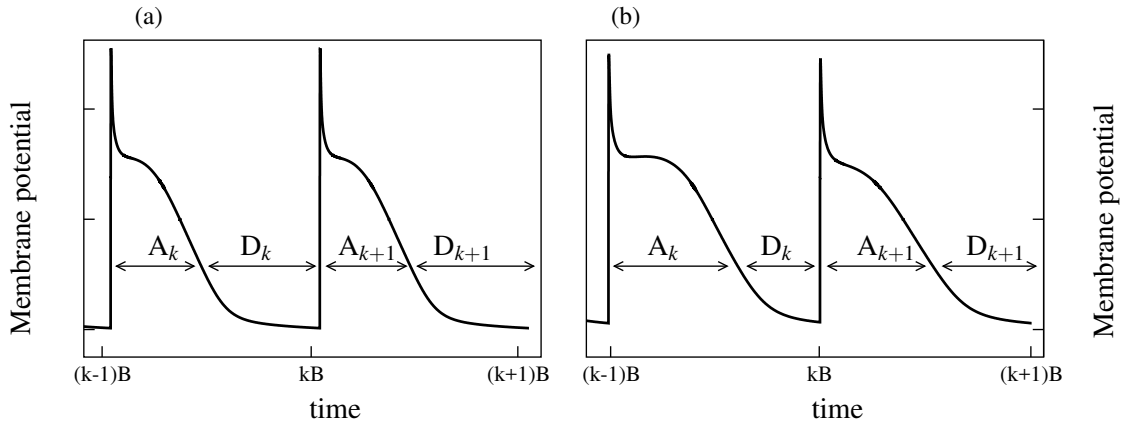

Figure 1.3: Typical examples of a normal 1:1 response in a healthy cardiac cell in Figure (a), where $A_{k+1} = A_k \ \forall k \in \mathbb{N}$. Figure (b) is a 2:2 response called alternans where $A_{k+1} = A_{k-1}$ but $A_k \neq A_{k+1} \ \forall \ k \in \mathbb{N}$.

duration (Tolkacheva et al., 2006; Walker and Rosenbaum, 2003).
This indicates that at faster heart rates, the consequently shorter APD allows a long enough diastolic interval for the cardiac cells, thus alternans occur. This property plays an essential role in the heart function (Kalb et al., 2004). The electrical restitution is studied using the restitution curve which is a graph of the action potential duration plotted against the preceding diastolic interval. Restitution curves can be modelled in various ways, including: (i) exponential functions fitted to experimental data (Guevara et al., 1984; Nolasco and Dahlen, 1968), (ii) difference equations derived from a simplified ionic model of the cardiac membrane (Mitchell and Schaeffer, 2003; Tolkacheva et al., 2002).

Studying the restitution curve and analysing the stability of the restitution properties of cardiac cells has been the focus of many studies (Aliev and Panfilov, 1996; Evans et al., 2000; Tolkacheva et al., 2002, 2003). For example Aliev and Panfilov (1996) fitted a restitution curve to the experimental data of the canine myocardium of Elharrar and Surawicz (1983) and found the parameter values for a simplified model. They then studied the dynamics of propagation of action potential waves in 3-dimensions.

Previous studies indicate that the restitution curve depends on the pacing protocol that is used to obtain it, hence it is known as a phenomenon called ”rate-dependent” restitution (Cain et al., 2004; Elharrar and Surawicz, 1983; Kalb et al., 2005). Therefore, prior to introducing different restitution maps, we will explain different pacing protocols by which the restitution curve is obtained.

Pacing protocols Two of the most commonly used pacing protocols are *the dynamic protocol* and *the $S_1 - S_2$ protocol*. Tolkacheva et al. (2003) illustrated that restitution curves derived from each of these protocols, capture different aspects of restitution dynamics.

The *dynamic protocol* is also called the steady state protocol, since it is a measure of the steady state response. In this protocol the cardiac cell periodically receives an external stimulus at a fixed interval known as the basic cycle length. When it settles into a stable periodic response, the steady state is recorded for a given basic cycle length and the pair $(\mathrm{D}_{ss}, \mathrm{A}_{ss})$ is recorded for each basic cycle length. Then the basic cycle length is changed and the process is repeated. By plotting the $(\mathrm{D}_{ss}, \mathrm{A}_{ss})$ pairs, the dynamic restitution curve is obtained over a range of different values of the basic cycle length.

The $S_1 - S_2$ *protocol* is a measure of the immediate response to a change in basic cycle length. This protocol begins with applying a stimulus S_1 and pacing the cardiac cell at $B = B_1$ until it settles down into a steady state response after k APs. Then at $K = k+1$ a stimulus S_2 is applied to the cell at an interval of $B = B_2$. The diastolic interval of the S_1 stimulus (D_k) and the action potential duration of the S_2 stimulus (A_K) are recorded. The pairs $(\mathrm{D}_k, \mathrm{A}_K)$ are plotted. Note that, the dynamic restitution protocol results in only one restitution curve, whereas the $S_1 - S_2$ restitution protocol produces a different restitution curve for each $B = B_1$ (Cain et al., 2004; Kalb et al., 2004; Schaeffer et al., 2007).

Modelling restitution by discrete iterative maps In order to model the electrical restitution behaviour of the cardiac cells, different restitution maps have been proposed.

One-dimensional restitution map without memory: The first mathematical formulation for the one-dimensional restitution map without memory was proposed in 1984 by Guevara et al. (1984), in which action potential duration is a function ϕ of the preceding diastolic interval as given in (1.1). Degree of memory in the mapping models corresponds to the number of variables previous to diastolic interval (DI). This means that only the previous beat plays a role in determining the action potential duration of the next one.

$$\mathrm{A}_{k+1} = \phi(\mathrm{D}_k), \tag{1.1}$$

where A_{k+1} denotes the durations of the $(k+1)^{\mathrm{st}}$ action potential and D_k the k^{th} diastolic interval. Here the basic cycle length is kept fixed and $\phi(\mathrm{D})$ is an increasing function of the diastolic interval. For each basic cycle length (B), $\mathrm{A}_k + \mathrm{D}_k = B$. Inserting $\mathrm{D}_k = B - \mathrm{A}_k$, we see that A_{k+1} is determined by an iteration of a one-dimensional map.

One-dimensional restitution map with memory: The second type of restitution map was first presented based on experimental data by Gilmour and Otani (1997) when the A_{k+1} was modelled as a function of not only the preceding diastolic interval D_k but also the action potential duration A_k.

$$A_{k+1} = F(D_k, A_k). \tag{1.2}$$

Since $B = A_k + D_k$, this map is also one-dimensional but it contains one beat memory, i.e. memory is considered as the dependence of the the action potential duration on more previous APDs and DIs. These types of maps are called "one-dimensional restitution maps with memory" and can be generalised to contain more variables previous to the D_k, i.e.

$$A_{k+1} = F\left(D_k, A_k, D_{k-1}, A_{k-1}, ...\right).$$

Two-dimensional restitution map with memory: in addition to these two types of maps, the third map was introduced theoretically and experimentally by Gulrajani (1987), Chialvo et al. (1990) and Gilmour et al. (2002) in which the role of the longer term memory was studied in more detail. A memory variable M_k was added to the model which accumulates during the action potential duration and dissipates during the diastolic interval. Thus, the model called the "Two-dimensional restitution map with memory" and according to Chialvo et al. (1990) is described by:

$$A_{k+1} = (1 - M_{k+1})G(D_k), \tag{1.3a}$$

$$M_{k+1} = \psi(M_k), \tag{1.3b}$$

where

$$\psi(M_k) = \left(1 - (1 - M_k)\exp\frac{-A_k}{\tau_2}\right)\exp\frac{-D_k}{\tau_2},$$

and

$$G(D_k) = a_1 - a_2\exp\frac{-D_k}{\tau_1}.$$

The parameters $a_1, a_2, \tau_1,$ and τ_2 describe properties of the tissue. Scientists such as Kalb et al. (2004); Schaeffer et al. (2007); Tolkacheva et al. (2002) suggested that memoryless one-dimensional maps are not comparable with experimental data since they do not contain a sufficient amount of memory. Therefore, one-dimensional maps with memory or two-dimensional maps have been widely researched and role of memory in the stability of these maps, has been investigated. These studies argue that the more variables restitution maps have, the more history of the membrane potential is taken into account and consequently the more qualitatively comparable to the experimental data they

are (Cain et al., 2004; Schaeffer et al., 2007; Tolkacheva et al., 2002, 2003). In contrast, little attention has been paid to the fact that much of the the valuable predictions of the onset of instability in cardiac cells, is based on analysis of the most simple restitution maps (Kalb et al., 2005). Hence, studies on the maps of type (1.1), are still lacking. We believe that studying the most simple maps, are essential as they provide knowledge about the role of the parameters and variables of a model in inducing alternans and ind establishing the normal responses of a cardiac cell.

Furthermore, once the right criteria is developed to study the stability of the one dimensional memoryless map (1.1), one can always expand it and study the role of memory too. Restitution maps that are derived from the ionic models and are based on the physiology of the cells can provide vital information about different parameters or variables in the model. Focusing on this is one of the main aims of this thesis.

We remark that, the restitution curve obtained from the one-dimensional memoryless map (1.1) is independent of the pacing protocol. Since all the points (D_k, A_{k+1}) lie on a single curve $A_{k+1} = \phi(D_k)$, whereas the other two types of maps (1.2) and (1.3) provide different curves under different pacing protocols. Thus, the pacing protocol does not play any role in memoryless restitution maps and the use of either protocol will result in a same solution.

Prediction of Alternans The existence of alternans in the memoryless one-dimensional map (1.1) was first found by Nolasco and Dahlen (1968) in which they explained the relationship between action potential duration alternans and action potential duration restitution based on the slope of the restitution curve. They suggested that when the slope of the curve is less than one, the system is stable. At the faster rates (smaller basic cycle length) the slope of the action potential duration restitution curve is greater than one and the system becomes unstable and alternans occurs as can be seen in Figure 2.3. This condition which is called the "restitution condition" in Kalb et al. (2004) has been used by many researchers such as Chialvo et al. (1990) to study the stability of arrhythmia. Karma (1994) also studied the breakup of spiral waves in two dimensions and the occurrence of cardiac arrhythmias, using restitution condition. It was suggested by Evans et al. (2000) that studying the restitution curve provides more insight into an understanding of the occurrence of the arrhythmia and how the arrhythmia can be controlled. Furthermore, based on the slope of an action potential duration restitution curve, the onset of arrhythmia can be determined (Evans et al., 2000). However, in more recent experimental and theoretical studies it has been suggested that the traditional restitution condition fails and does not

predict alternans (Kalb et al., 2004). Hence, when the slope of the standard map is one, the prediction of the origin of alternans is not accurate. This indicates that the study of temporal alternans needs to be modelled by more complex maps Echebarria and Karma (2002). There are different criteria based on the slope of restitution curves for the maps of (1.2) and (1.3), but since the focus of this thesis is on the memoryless maps (1.1), we don't concentrate on those criteria.

There are other types of cellular alternans that believed to cause arrhythmias such as Ca^{+2} alternans, spatially-dis/concordant alternans (Fenton and Karma, 1998; Fox et al., 2002; Merchant and Armoundas, 2012; Weiss et al., 2006). Ca^{+2} plays a vital role in excitation-contraction coupling, therefore, it is an important ion in inducing cardiac arrhythmia and alternans. At the cellular level, the relationship between membrane voltage and Ca^{+2} dynamics is complex. Membrane voltage and calcium dynamics are bidirectionally coupled and it is not clear which leads to the other. There are data in support of two main hypotheses (Merchant and Armoundas, 2012; Valdivia, 2015; Weiss et al., 2006): (i) Alternation in ionic currents and membrane voltage leads to alternation in intracellular Ca^{+2} concentration.(ii) Alternation of intracellular Ca^{+2} concentration causes alternation of membrane voltage. With respect to the first hypothesis, which is the influence of voltage on $[Ca^{+2}]_i$ cycling, Weiss et al. (2006) argue that the L-type Ca^{+2} current plays an important role such that if action potential duration alternates, L-type Ca^{+2} current alternates and in response to this $[Ca^{+2}]_i$ fluctuates. Fox et al. (2002); Merchant and Armoundas (2012) also stated that alternation of sarcolemmal Ca^{+2} and K^+ currents due to change in action potential morphology have an affect on alternation in $[Ca^{+2}]_i$ cycling. With regard to the second hypothesis, the role of Ca^{+2}-alternans on producing voltage alternans is considered and many experimental studies have demonstrated that $[Ca^{+2}]_i$ alternans causes voltage alternans (Merchant and Armoundas, 2012; Valdivia, 2015; Weiss et al., 2006).

1.3 Aims and objectives

In this section we outline the aims and objectives of this thesis. We will provide justifications for each of the objectives by referring to and explaining the gaps in the current literature. We will then briefly describe our approach. This is followed by introducing the outlines of each chapter in this thesis.

- We aim to develop an approach for the solution of the restitution boundary value problem which will make it possible to derive discrete restitution maps directly from the set of ordinary differential equations (ODEs) via asymptotic reduction. Such low-dimensional maps have the advan-

tage of being more directly related to the differential equations governing cell's electrophysiology. This approach has been employed previously by Tolkacheva et al. (2002) and Mitchell and Schaeffer (2003), but they used a simplified version of the Fenton and Karma (1998) model. Hence, their model does not closely match the real physiology of the cardiac cell. In our approach, however, we derive a map from more realistic models such as those of Noble (1962) and Courtemanche et al. (1998), thereby providing more insights into these physiologically based models, which are closer to the cardiac cell's functions.

- We aim to apply the tools developed in this process to analyse typical models of atrial excitability. We aim to identify mechanisms in which alternans, fibrillation and other irregular rhythms appear and how they behave in these models.

- In complicated ionic models, one-dimensional maps act as a guide to determining the important factors in producing alternans. Therefore it is vital to be able to compare the mapping results directly to the ionic model and this provides testable predictions as a result of repetitive stimulation of a cardiac cell (Michaels et al., 1990). We wish to propose a generally applicable framework for studying cardiac restitution, formulated in terms of a boundary value problem for forced periodic oscillations in the ordinary differential equations governing cellular electrophysiology. This formulation should be applicable to any detailed cardiac excitation model. Present day models for the electrical excitation of cardiac cells incorporate a huge wealth of knowledge about the microscopic structure of the cells based on detailed experimental measurements. If successful, our formulation will allow to better relate these cellular properties to restitution properties and predict the onset of fibrillation and other irregular cardiac rhythms.

- In general, it will only be possible to solve such a boundary value problem for restitution numerically. We aim to devise a suitable formulation of the problem that can be implemented using standard numerical solvers for boundary value problems and software for numerical bifurcation and branching. Cardiac excitation models are characterised by a certain set of asymptotic properties and which we aim to exploit.

- We aim to draw conclusions on how this methodology can be applied to other related problems, for instance, Calcium alternans, alternans in spatially extended domains and realistic cardiac geometries.

1.4 Structure of the thesis

In Chapter 2 we provide more background in the mathematical as well as physiological context of the thesis. This is followed by Chapter 3 where we present the detailed methodology of this research. We explain two different approaches to study alternans and we emphasise that the restitution maps and the complete ionic models complement each other. The combined results of the studied models will provide a good understanding of the cellular dynamics (Michaels et al., 1990).

In Chapter 4 we apply the proposed methods on a caricature version of the FitzHugh-Nagumo system (FitzHugh, 1961; Nagumo et al., 1962) called the McKean (1970) model and we derive a restitution map. We then study the stability of the map based on its parameters. Although the system is very simple we show that at fast frequencies the diastolic interval can determine the behaviour of the system. This is an important step to justify the use of our chosen methodology. Also we will confirm this approach by applying our methodology on the more complicated models in Chapters 5 and 6.

In Chapter 5 we study a simplified version of Noble (1962) on the Purkinje fibres of the heart. The model is originally introduced by Biktashev et al. (2008), is called the "Caricature Noble Model". It is based on the physiology of a cardiac cell and at the same time is simple enough to be solved analytically. We apply the proposed method on this model and study the stability of the map derived from the full system of ODEs.

In Chapter 6 a reduced version of a healthy human atrial model by Courtemanche et al. (1998) is studied. The model was reduced via asymptotic reduction by Suckley (2004). The steps she followed in order to reduce the full system, are repeated and explained briefly in this chapter. We then derive a one-dimensional map of the form (1.1) and investigate different factors and mechanisms of alternans using the methodology described in Chapter 3. This is followed by Chapter 7 which consists of the conclusions and future research directions.

Chapter 2

Physiological and Mathematical Background

Restitution dynamics of cardiac cells are studied using functions that relate the action potential duration to its preceding diastolic interval (Kalb et al., 2005; Shaeffer et al., 2008). These functions are either empirical, therefore fitted to experimental data as it was done by Nolasco and Dahlen (1968), or they are derived from a system of ordinary differential equations that describes the electrical activity of the cells (Shaeffer et al., 2008; Tolkacheva et al., 2002).

In this chapter we begin by describing the physiology of excitable cells and explaining the basic principles of modelling the electrical activity of these cells. We then expand on the details of the ionic models, which are system of ordinary differential equations and we present the mapping approach in modelling the electrical restitution of cardiac cell. This is followed by explaining the mathematical tools that we use in order to study the asymptotic properties of these systems of equations and the behaviour of their solutions. We conclude this chapter by elucidating the relevance of these models to this research.

2.1 Physiology of excitable cells

As stated in Chapter 1 excitable cells have the ability to be electrically excited which results in the generation of action potentials. In this section, we explain the physiology of the cell membrane and the cellular mechanisms in each heartbeat.

The cell membrane The cell membrane is the boundary around the cell separating the internal environment of the cell from its external environment. It is a double layer of thick phospholipid (about 7.5 nm) molecules that is selectively permeable, permitting passage of some materials and restricting the passage of others. The cell membrane contains different types of pores. Protein-lined pores called channels allow the passages of certain type of molecules, but small uncharged molecules can pass between the phospholipid molecules by simple diffusion (Alberts et al., 1994; Keener and Sneyd, 1998).

Electrically charged particles (ions) pass through ion-specific channels called ion channels. The cell membrane has two kinds of ion channels: "non-gated" channels that are always open and "gated" channels which can open and close. Opening and closing the gated ion channels is mostly dependent on the membrane voltage. Hence, they are called voltage-gated ion channels. The cell membrane is constantly regulating the exchange with the external environment by permitting the passage to some materials and restricting the passage of others. The permeability of the membrane to a particular ion is dependent on the number of open channels for that specific ion (Alberts et al., 1994; Ermentrout and Terman, 2010). A cardiac cell beats when a complex series of gates open and close in an organised manner. When a cell is electrically stimulated, the cell membrane becomes selectively permeable/restrictive to certain ions and a transmembrane potential is formed which is called an action potential (Keener and Sneyd, 1998).

According to Ermentrout and Terman (2010), non-gated channels are believed to be responsible for the resting potential whereas most of the gated channels are considered to be closed during the resting state. Action potential is formed when gated channels open and permit the passage of certain ions across the cell membrane. The membrane potential at which a particular ion is in equilibrium across the membrane, is called the *Nernst potential* for that ion.

Cellular mechanisms in each heartbeat In each heartbeat the electrical stimulus activates and opens the voltage dependent Na^+ channels. Since the concentration of Na^+ outside the cell is substantially higher than inside the cell, Na^+ enters the cytoplasm. The increase in membrane permeability (conductance) to Na^+, allows the membrane potential to depolarise. Voltage then approaches Na^+ Nernst equilibrium potential ($E_{Na} = +50$ (mV)) at which Na^+ ions are in equilibrium across the membrane and the electrical and chemical driving forces balance. Na^+ channels at positive membrane potential close and voltage-dependent K^+ channels open due to depolarisation of the membrane.

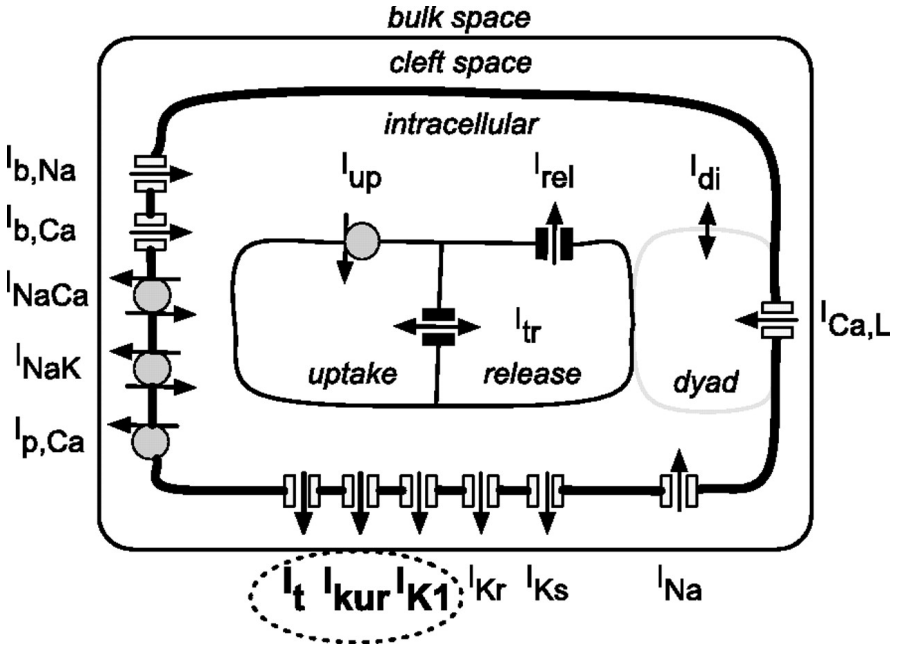

Figure 2.1: A schematic representation of the cell membrane in a human atrial action potential model. The extracellular, intracellular, cleft spaces, the uptake and release compartments within the sarcoplasmic reticulum are illustrated as well as the ionic currents and the ion exchanger currents. (Nygren et al., 1998).

Hence, K^+ ions leave the cell via I_{to}, causing the membrane potential a slight drop. A this stage, the voltage-dependent Ca^{+2} channel called the L-type calcium channel -where L stands for long lasting- (Bers., 2002) activates. Since the concentration of Ca^{+2} outside the cell is relatively high, Ca^{+2} enters the cytoplasm via the L-type calcium channels (Bers., 2002). The outward flow of K^+ and the inward flow of Ca^{+2} balance and form a plateau phase.

As Ca^{+2} enters the cytoplasm and concentration of Ca^{+2} increases, it binds to protein structures called ryanodine receptors (RyRs) and activates them. Then the Ca^{+2} stored in the sarcoplasmic reticulum (SR) is released via ryanodine receptors, by calcium-induced-calcium-release (CICR) mechanisms (Bers., 2002; Keener and Sneyd, 2008; Richards et al., 2011). This mechanism is such that if one local L-type calcium channel opens, calcium ions bind to RyRs and this activates the process of releasing Ca^{+2}. The large efflux from the sarcoplasmic reticulum activates the neighbouring ryanodine receptors and Ca^{+2} enters the cytoplasm. The Ca^{+2} inside the cell diffuses through the cytoplasm and binds to the contractor compartments called myofilaments. Myofilaments are chains of proteins inside

the muscle cells and cause contraction of the myocyte (Bers., 2002; Keener and Sneyd, 2008).

As stated before, the plateau phase of an action potential has a relatively large duration and K^+ and Ca^{+2} ions are believed to play vital role in maintaining this duration. After the plateau phase, there is a repolarisation phase of an action potential at which the L-type Ca^{+2} channels close. Ca^{+2} channels are voltage dependent and Ca^{+2} dependent, they inactivate and close while K^+ channels remain open and K^+ enters the cell. The voltage dependent K^+ channels are called delayed rectifier channels and are classified based on the speed at which they activate. There are slow delayed rectifier current I_{Ks}, rapid delayed rectifier current I_{Kr} and ultra rapid delayed rectifier current I_{Kur}. The currents responsible for the repolarisation are I_{Kr}, I_{Ks} and I_{K1} and they cause the membrane potential to reach its resting value. The delayed rectifier channels close after the repolarisation but the inward rectifier channels remain open during the resting phase of the action potential.

The myocyte then has to relax and for relaxation to happen, the amount of Ca^{+2} which entered the cytoplasm needs to be removed from the cytoplasm. If this didn't happen, the cell would gain or lose Ca^{+2} and the cell would lose its equilibrium state (Bers., 2002). Therefore in the relaxation phase, Ca^{+2} either returns to the sarcoplasmic reticulum or is pumped out of the cell across the plasma membrane. Figure 2.1 illustrates the intracellular compartments and the ionic currents in a human atrial cell model (Nygren et al., 1998).

Excitable systems A system is excitable if the equations that describe the temporal behaviour of the system, have one equilibrium point that is globally attracting the trajectories in the phase space. An excitable system has a resting state and an excited state. Hence, in excitable cells, a sufficiently large perturbation in voltage which is above a certain threshold, results in generating an action potential. If the perturbation is not large enough, the voltage decays back to its resting value (Ermentrout and Terman, 2010). In the next section mathematical models of action potentials and excitable systems are described.

2.2 Mathematical models of action potential

Electric circuit model of the cell membrane In mathematical models of action potentials the cell membrane is modelled as an electrical circuit. The cell membrane acts as an insulator for separating charges, and as a conductor for its ability of selective conductance (Keener and Sneyd, 1998). As illustrated in Figure 2.2, it is also assumed that the membrane acts like a capacitor in parallel with

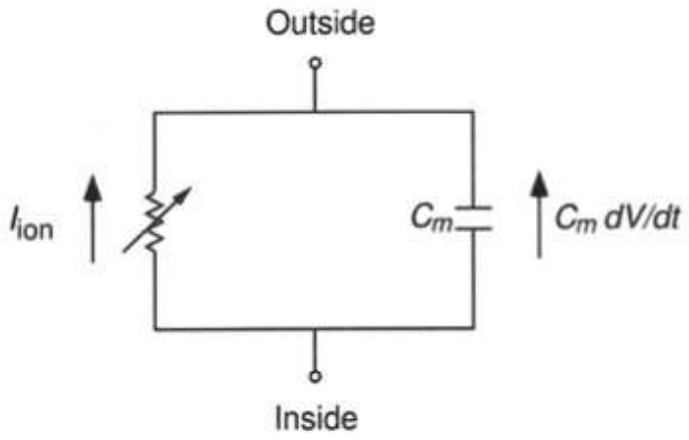

Figure 2.2: The electrical circuit model of the cell membrane where the capacitor and the resistor are in parallel. Keener and Sneyd (1998).

a resistor. The capacitance of the membrane C_M is a constant defined as the ratio of charge across a capacitor Q to the voltage potential needed E to hold that charge and their relationship is given by

$$C_M = \frac{\mathrm{Q}}{E}.$$

Since the current is $I = \dfrac{\mathrm{dQ}}{\mathrm{d}t}$, the capacitive current in the circuit is $C_M \dfrac{\mathrm{d}E}{\mathrm{d}t}$. The transmembrane potential E is defined as

$$E = E_{\mathrm{i}} - E_{\mathrm{e}},$$

where E_{i} is the voltage inside the cell and E_{e} is the extracellular potential. In an electrically stimulated cell by a stimulus current I_{stim}, according to Kirchhoff's voltage law there will be a change of charge inside and outside of the membrane and to balance this change, the stimulus current will be

$$-I_{\mathrm{stim}} = C_M \frac{\mathrm{d}E}{\mathrm{d}t} + I_{\mathrm{ion}}.$$

In order to obtain the capacitive current and therefore the transmembrane voltage as a function of time, it is vital to explain the ionic currents across the cell membrane.

The flow of any ion across the cell membrane is driven by the electrochemical gradient for that ion. The voltage gradient and the concentration gradient of the ion across the cell membrane control the electrochemical gradient for that ion. As stated previously, when these two forces balance each other the electrochemical gradient is zero and there is no net flow of the ion through the ion channel.

Hence, the membrane potential reaches its Nernst potential for that ion. At this equilibrium potential, the chemical and electrical gradients are equal and opposite in direction. For each ion of type S the Nernst potential is determined by the ratio of the concentrations of S on the two sides of the membrane and is given by

$$E_{\mathrm{S}} = \frac{RT}{zF} \ln \frac{[\mathrm{S}]_{\mathrm{o}}}{[\mathrm{S}]_{\mathrm{i}}}, \tag{2.1}$$

where E_{S} is the equilibrium potential for any ion of type S, $[\mathrm{S}]_{\mathrm{o}} and\ [\mathrm{S}]_{\mathrm{i}}$ are the concentration of the ion S outside and inside of the cell respectively, R is the universal gas constant $8.314\ \ JK^{-1}mol^{-1}$, T is the absolute temperature in Kelvin, F is Faraday's constant $96,485\ \ Cmol^{-1}$, z is the charge of the ion, where z is +1 for Na^{+}, +1 for K^{+}, +2 for Ca^{+2} and so on. According to (Keener and Sneyd, 1998) the membrane potential is assumed to drop due to the concentration difference given by (2.1) as well as an electrical current $r_{\mathrm{S}} I_{\mathrm{S}}$ provided the channel is ohmic. Hence, the membrane potential is given by

$$E = r_{\mathrm{S}} I_{\mathrm{S}} + E_{\mathrm{S}},$$

where r_{S} is the resistance of the channel S and I_{S} is the current of S. The current-voltage relationship is derived as:

$$I_{\mathrm{S}} = \frac{E - E_{\mathrm{S}}}{r_{\mathrm{S}}}.$$

It is important to notice that this ionic current is zero when the membrane potential reaches its Nernst potential i.e. when $E = E_{\mathrm{S}}$ and hence $I_{\mathrm{S}} = 0$. The current I_{S} in the above equation, is the product of the single channel conductance times the number of channels per unit area of membrane (Keener and Sneyd, 1998). In general the ionic current is described as below:

$$C_M \frac{\mathrm{d}E}{\mathrm{d}t} = -\sum_{\mathrm{S}} \left(g_{\mathrm{S}} \prod_{\mathrm{i}} (\mathbf{y}_{\mathrm{S,i}})^{k_{\mathrm{S,i}}} (E - E_{\mathrm{S}}) \right) - I_{\mathrm{stim}} \tag{2.2a}$$

where S is different types of ionic channels (i.e. sodium, calcium, ...), i is the type of gates for each channel, k is the multiplicity of the gates, $g_{\mathrm{S}} = 1/r_{\mathrm{S}}$ is the maximum conductivity for any ion channel of type S when all gates are open and E_{S} is at equilibrium voltage and $\mathbf{y}_{\mathrm{S,i}}$ is the gating variable for channel S. According to physiologically based models like Luo and Rudy (1991) the evolution of gating variable $\mathbf{y}(t)$ is described as below:

$$\frac{\mathrm{d}\mathbf{y}_{\mathrm{S,i}}}{\mathrm{d}t} = \frac{\overline{\mathbf{y}_{\mathrm{S,i}}}(E) - \mathbf{y}_{\mathrm{S,i}}}{\tau_{\mathbf{y}_{\mathrm{S,i}}}(E)} \tag{2.2b}$$

where $\overline{\mathbf{y}_{\mathrm{S,i}}}$ and $\tau_{\mathbf{y}_{\mathrm{S,i}}}(E)$ as continuous functions of E, define the quasi stationary value and the time in which the gate closes and opens respectively. As is clear from (2.2), mathematical models vary significantly in terms of modelling the I_{ion}. Some models like Courtemanche et al. (1998) and Nygren et al. (1998) are based on the physiology of the cells, hence they considered as Reaslistic models. In contrast, some models like Mitchell and Schaeffer (2003) model, mimic selected properties of excitable cells (nerve, ventricle, atrium, SA, etc ...) but the equations do not directly represent the physiological structures in the cell. Moreover, I_{stim} is the stimulus current which is a function of time. Stimulus current is applied experimentally to the cell membrane. A mathematical model for the experimental I_{stim} may be written as

$$I_{\mathrm{stim}}(t) = \sum_{k=0}^{\infty} J\delta(t - kB),$$

where δ is the Dirac delta function and this raises the voltage to J instantaneously. An alternative way to achieve the same is to pace our models using initial condition for one of the dynamical variables. In this thesis, I_{stim} is omitted from the equations and instead the initial condition for voltage is set at a stimulus value which may be called "Stimulation by voltage".

2.2.1 Realistic ionic models

Realistic models of excitable cells are sets of differential equations formulated in such a way that they faithfully represent the latest knowledge of the physiological structures in the cell. Besides, their solutions reproduce as many of the properties of the cells as possible. Realistic models of I_{ion} currents, incorporate the latest known details of the cardiac cells' physiology, such as the different type of ion channels, population of ion channels, changes in ionic concentration inside and outside of the membrane, mechanisms that regulate movement of the ions across the cell membrane, the structure of the cells, the geometry of the cells, temperature and volume. Hence, they are considered too detailed and complicated to analyse.

The first quantitative model of electrical activity of the excitable cell was introduced by two Nobel prize winner scientists Hodgkin and Huxley (1952). Their model was used to explain the action potential in the long giant axon of a squid nerve cell. Their idea has been applied to a variety of excitable cells ever since. One of the most important versions of their model is the Noble (1962) model for mammalian Purkinje fibres. We study and analyse a version of this model in Chapter 4 of this thesis.

Different mathematical models have been developed over the past 50 years to study the role of cellular and sub-cellular mechanisms in producing action potentials for different cells in the heart (Noble et al., 2012). Some of these models are amongst the first cardiac models that established this field, such as the Noble (1962) model of mammalian Purkinje fibres and the Beeler and Reuter (1977) model of mammalian ventricular myocytes Beeler and Reuter (1977). Furthermore, many of the realistic models are extensions of existing models. For example the Luo and Rudy (1991) model is a model of the ventricle of a Guinea pig, the Winslow et al. (1999) model is for canine ventricular myocytes. The Courtemanche et al. (1998) model and of the Nygren et al. (1998) model are the human atrial models . In recent years, as the experimental data has improved and provided more information about the cells, the mathematical models have been extended to fit these data (Noble et al., 2012).

One of the recent models of human atrial action potential is the Grandi et al. (2011) model, which is a continuation of the Grandi et al. (2010) model of human ventricle. Although such detailed models are ground-breaking tools for computational modelling, the level of their complexity makes their mathematical analysis rather challenging. Therefore, the simplified models that incorporate the primary elements of the complex ionic-based models provide a solid understanding of the behaviour of the solutions.

2.2.2 Conceptual models

The conceptual models of excitable cells are considerably simpler than the realistic models. They retain the essential features of the ionic-based models and present it in a simplified form. For example, these models generate action potentials and exhibit a threshold of excitation. To mimic the properties of excitable cells the mathematical models of excitable systems take the form

$$\frac{\mathrm{d}u}{\mathrm{d}t} = g(u) - v \equiv G(u,v), \tag{2.3}$$

$$\frac{\mathrm{d}v}{\mathrm{d}t} = bu - cv \equiv F(u,v), \tag{2.4}$$

where $b, c > 0$. The variable u behaves qualitatively like the transmembrane potential E, and v is a measure of the permeability. The function g is modeled such that captures the dynamical behavior of excitable cells. Reasonable requirements on g are: (1) $g(0) = 0$ and $g'(0) < 0$ (for local stability of the equilibrium $u = 0$), (2) there should exist an set $S > 0$ such that $g(S) = 0$ and $g'(S) > 0$ (allows S to be a repelling threshold) and (3) $g'(u) < 0$ for large values of u (allows (u,v) to return to $(0,0)$). Cubic polynomials and other cubic-like functions satisfies these requirements for $g(u)$.

An example of conceptual models, is a simple version of the Hodgkin and Huxley (1952) model which was first introduced by FitzHugh (1961); Nagumo et al. (1962). The FitzHugh-Nagumo system of equations is given by

$$\begin{aligned} \varepsilon \frac{\mathrm{d}E}{\mathrm{d}t} &= f(E) - w, \\ \frac{\mathrm{d}w}{\mathrm{d}t} &= E - \beta w, \end{aligned} \tag{2.5}$$

where $f(E) = E(E-\alpha)(1-E)$, and $\alpha,\ \beta,\ \varepsilon$ are constants such that $0 < \alpha < 1$, $0 < \varepsilon \ll 1$ and $\beta \geq 0$. Since ε is small, the recovery variable w is much slower than the voltage E.

This system is a typical example of fast-slow systems with different time scales involving both fast and slow motions. The fast processes correspond to the upstroke of the action potential and the slow processes correspond to the plateau stage and the repolarisation of the action potential. The conceptual models in general are either ad-hoc and thus suitable only for a particular application, or are modifications of the FitzHugh-Nagumo system (FitzHugh, 1961; Nagumo et al., 1962) that are relevant to nerve tissue but not to cardiac tissue. Therefore they contain parameters and variables that cannot be translated into the physiology. However, analysing these systems enables us to understand the behaviour of the solutions qualitatively. One of the examples of this type of model is the McKean (1970) model which is a caricature version of the the FitzHugh-Nagumo system (FitzHugh, 1961; Nagumo et al., 1962) model. In McKean's model $f(E)$ is a piecewise-linear function which allows explicit solutions and analysis. We will study this model in Chapter 4.

2.2.3 Asymptotically simplified realistic models

Another approach for modelling the electrical activity of a cardiac cell is to derive simplified mathematical models from the realistic models. The asymptotically simplified models include the essential components of the more complex physiologically based models. Hence by applying asymptotic analysis on the realistic models and separating time scale of their variables, complicated models for membrane dynamics can be simplified. For instance the Fenton and Karma (1998) or the Caricature Noble model derived byBiktashev et al. (2008), are amongst these models. The asymptotically simplified models are directly related to relevant physiological structures of the cells. One of the useful advantages of these models is their ability to reproduce essential features of cells and at the same time, provide mathematical simplicity similar to conceptual models.

Asymptotically simplified models may offer a good introduction to membrane dynamics and quan-

titatively reproduce the restitution behaviour of cardiac cells. In addition, due to the simplicity of their functions, they are computationally faster than the realistic models.

Biktashev et al. (2008) used an asymptotic embedding approach to develop a caricature model of the classical model of Purkinje fibres Noble (1962) model. The Caricature Noble model is amenable to analytical study but at the same time preserves the essential features of contemporary ionic models of cardiac excitation. This model is studied and analysed in Chapter 5 of this thesis.

Another, asymptotically simplified model studied in this thesis, is derived from the detailed human atrial model of the Courtemanche et al. (1998). The reduced model is derived by Suckley (2004) where she performed asymptotic analysis on the model to reduce it to a three variable model. Not only are the generic properties of Courtemanche et al. (1998) model preserved but also the detailed model of human atrial action potential is reduced to the extent that it can be studied and analysed with mathematical tools. We study the reduced model in Chapter 6 of this thesis.

Two important mathematical tools that have been mentioned in this section are asymptotic analysis and phase plane analysis. Later on in this chapter, these fundamental tools will be discussed.

2.3 Models of restitution

The functions that relate the action potential duration to its previous diastolic interval are of two types namely either (a) proposed based on heuristic arguments and then fitted to experimental data (Nolasco and Dahlen, 1968) or (b) derived from mathematical models of action potentials (Shaeffer et al., 2008; Tolkacheva et al., 2002) where the models of the action potential may be ad hoc. In this section we will describe these two types of mapping models. In addition, we will also provide justifications as to why the maps derived from the ionic models provide more insight into the physiology of the cell than the fitted maps.

2.3.1 Heuristic discrete restitution maps

The first theoretical explanation of action potential duration alternans was presented by Nolasco and Dahlen (1968) where they used a feedback relationship between the action potential duration and the diastolic interval. Nolasco and Dahlen (1968) considered the cardiac alternation's features to be similar to the oscillation in electrical circuits. They used negative feedback in the electrical circuit where X as a signal is part of the input I. When the input I is amplified to the output O=G(I) that is a

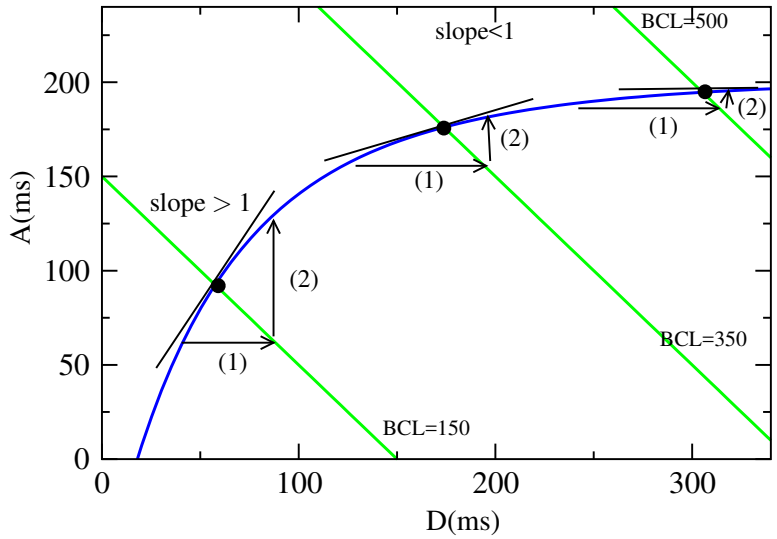

Figure 2.3: Projection method used by Nolasco and Dahlen (1968) to illustrate action potential duration alternans. D-lines are plotted for three different basic cycle lengths and the steady state for each BCL which is the intersection of D-line and A-curve is shown.

function G of I. A fraction F of the output O feeds back to the input i.e. I=X- F(O), where F(O) is a fraction of output O.

In the cardiac cells, the signal X is the stimulus interval (basic cycle length) and contributes to the input that is the diastolic interval, and the diastolic interval influences the next action potential duration by $A_1 = f(D_0)$. The whole action potential duration feeds back into the next diastolic interval and therefore $D_1 = B - A_1$. For a fixed basic cycle length the diastolic interval as a function of action potential duration is a straight line with slope -1 which was called by Nolasco and Dahlen (1968) the D-line. The D-lines are denoted in green in Figure 2.3. Consequently, they measured action potential duration and diastolic interval at different basic cycle length in the steady state and drew a graph $A = f(D_0)$ which is called the A-curve is plotted in blue in Figure 2.3. The intersection of the A-curve and the D-line is the steady state (D_{ss}, A_{ss}) at that basic cycle length. In order to get successive values of the action potential duration and the diastolic intervals Nolasco and Dahlen (1968) used a projection method such that from the A-curve, a horizontal line is drawn to the D-line (number (1) in the figure) and the intersection of these two is the value of D at the new basic cycle length and a vertical line from this point to the A-curve (number (2) in the figure) is the value of action potential duration at the new basic cycle length. By applying the cobweb methods and the conditions

for stability (Strogatz, 2001), the slope of the A-curve (i.e. $S = \left[\frac{dA}{dD}\right]_{(D_{ss},A_{ss})}$) at the steady state was studied by Nolasco and Dahlen (1968) and the following cases were established:

(i) If $S < 0$ the action potential duration reaches the steady state without oscillation.

(ii) If $S = 0$ the iteration converges immediately to the steady state.

(iii) If $0 < S < 1$ the action potential duration and the diastolic interval oscillate around the steady state. The steeper the A-curve, the slower the convergence to the steady state.

(iv) If $S = 1$ and the A-curve is symmetric around the D-line, therefore alternans with different amplitude could be observed.

(v) If $S > 1$ the projection line quickly moves away from the intersection point. Either persistent alternans occur or not every stimulus gets a response.

Using experimental data and drawing the A-curve for each of the above cases, Nolasco and Dahlen (1968) showed that for slow rates the change in action potential duration is minimal and at rapid rates the slope of the A-curve becomes very steep. Furthermore, they changed the rate, recorded the first two cycles immediately after the change and observed non-steady state responses. At rapid rates and at the slow rates the non-steady state curves were above and below the steady state curve, respectively. Hence, a family of non-steady state curves was considered to be approaching the steady state curve. They also performed further experiments to analyse how alternating the basic cycle length affects the occurrence of persistent alternans. They concluded that at the persistent alternans, the slope of the curve is greater than one, which is in agreement with their graphical model in Figure 2.3. Nolasco and Dahlen (1968) reported that looking at the A-curve provides a greater understanding of the system than the D-line, since the slope of the *D*-line is always -1 and the only important value of the D-line is its intersection with the A-curve. Moreover, they concluded that when the slope of the A-curve is negative or zero the system is stable and alternans does not occur, whereas at the faster rates the system becomes unstable and alternans occurs. Since the A-curve can be drawn for different cardiac tissues, studying the effect of different parameters of a tissue on the A-curve will certainly help to understand the occurrence of alternans in cardiac cells. Figure 2.4 illustrates a typical action potential duration restitution curve similar to that of Figure 2.3. The intersection of the A-curve and the D-line is a steady state point (D_{ss}, A_{ss}). In Figure 2.4 two different basic cycle lengths are chosen and the D-line for each of them is plotted in green. In order to see if action potential duration alternates at

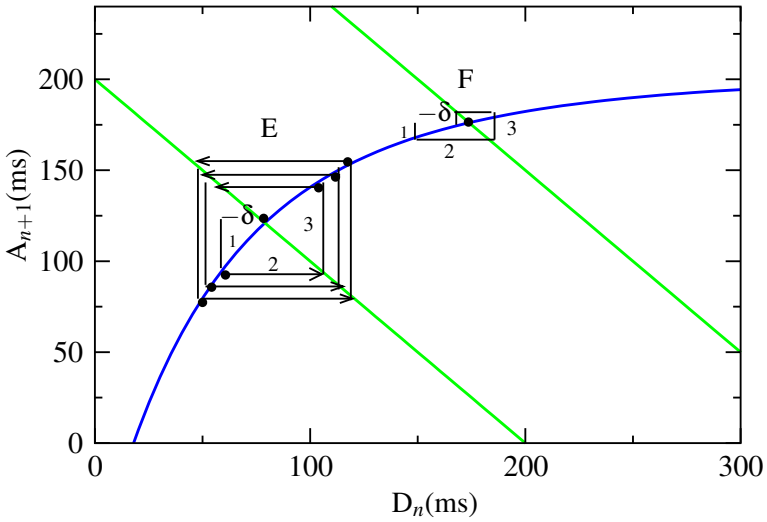

Figure 2.4: Analysing the stability of the steady states. The intersections of the blue A-curve with the green D-line is the steady state. The point E corresponds to $B = 200$ (ms) and F corresponds to $B = 500$ (ms). The stability of the points is examined under a small perturbation of $-\delta$ from the steady state. E is unstable and F is a stable equilibrium.

these basic cycle lengths, the stability of the steady state point $(D_n, A_{n+1}) = (D_{ss}, A_{ss})$ is checked at points E and F corresponding to $B = 200$ (ms) and $B = 500$ (ms) respectively. The local stability can be determined by a small perturbation of the D. If we perturb the D by shortening it by a small amount δ to D_{n+1}, this generates a shorter A_{n+2} which can be determined by dropping a vertical line (labelled (1) in the Figure 2.4) to the intersection with the action potential duration restitution curve. The shorter A_{n+2} creates a long D_{n+2} and this can be determined by drawing a horizontal line (labelled (2)) to its intersection with the D-line. This D_{n+2} produces a long A_{n+3} which is determined by the intersection of the vertical line (3) with the action potential duration restitution curve and so on and so forth. As can be seen in Figure 2.4, around the point E the amplitude of action potential duration alternans progressively increases and finally settles at a steady-state alternans. This indicates that the equilibrium point E is unstable.

Physiologically the process at the point E means that if the diastolic interval D_{n+1} is short, the cell needs enough time to fully recover its resting electrical properties before the next stimulus which then produces a shorter A_{n+2} Echebarria and Karma (2002). The period doubling nature of this instability was demonstrated mathematically in Guevara et al. (1984) which we discuss here. The same methodology applies to the point F. However, at the point F the action potential duration amplitude

decreases and settles at the steady state indicating that F is a stable steady state.

Guevara et al. (1984) also performed an experimental study to derive the electrical restitution curve. They used a mathematical approach and predicted the occurrence of alternans at the fast rate where at a critical frequency the 1:1 response loses its stability and a 2:2 response occurs. They periodically stimulated a heart cell and recorded the action potential duration and diastolic interval. They did that with two sets of data: one for short stimulation frequencies and one for a wide range of stimulation frequencies. The data sets were fitted respectively to single and double exponential functions. The action potential duration was derived as

$$\mathrm{A}_{k+1} = g(Nt_s - \mathrm{A}_k),$$

where t_s is the BCL, N is the smallest integer such that $Nt_s - \mathrm{A}_k > \theta$, for θ the refractory period. It was assumed by Guevara et al. (1984) that the electrical restitution curve is

$$g(\mathrm{D}) = \mathrm{A}_{\max} - \alpha \exp(-\mathrm{D}/\tau),$$

where $\mathrm{A}_{\max}$ is the maximum action potential duration at long recovery times, α and τ are positive constants, and $\mathrm{D} > \theta$.

The fixed point of the restitution function occurs at A_* when $\mathrm{A}_{k+1} = \mathrm{A}_k$ and is stable if

$$\left| \frac{\mathrm{dA}_{k+1}}{\mathrm{dA}_k} \right| < 1.$$

If the derivative at the steady state is -1 a period doubling bifurcation occurs and their experimental data is in agreement with their theoretical approach. Therefore, Guevara et al. (1984) formulated the response of the model to periodic stimulation as a bifurcation problem. The exponential maps do not provide explicit information about the details of cardiac dynamics. Therefore, over the last few years the maps that are derived from the system of ordinary differential equations have been studied more than the above mentioned maps.

2.3.2 Maps derived from system of ordinary differential equations

As stated above, the electrical activity of cardiac cells is described by a system of ordinary differential equations that keeps track of the transmembrane voltage and ionic currents. The second type of map is derived from this system of equations using a multi-scale analysis technique and asymptotic methods. One of the examples of this type of maps is presented in Tolkacheva et al. (2002)'s

paper, where a one-dimensional map is derived from the Fenton and Karma (1998) to approximate the response of the model. In the Fenton and Karma (1998) model voltage changes in the membrane in response to three ionic currents: a fast inward current, a slow inward and a slow outward current. By implementing asymptotic analysis they reduced the system and derived a map which describes action potential duration as a function of the preceding diastolic interval as well as the previous action potential duration

$$\mathrm{A}_{k+1} = G(\mathrm{A}_k, \mathrm{D}_k).$$

This was then followed by studying the stability of the map and illustrating different types of solutions corresponding to various dynamical behaviour of the cardiac cell.

Another example of maps derived from the system of ordinary differential equations, is the Mitchell and Schaeffer (2003) model. They used a simple version of the Fenton and Karma (1998) which has only two currents. Mitchell and Schaeffer (2003) applied asymptotic techniques to reduce the model and to derive an explicit action potential duration restitution map. They showed that the map derived in the Mitchell and Schaeffer (2003) is qualitatively similar to the exponential restitution curves. However, they demonstrated that the exponential maps do not provide a good understanding for smaller diastolic intervals. The one-dimensional action potential duration restitution map of this model has one variable unlike Tolkacheva et al. (2002) map.

We derive action potential duration restitution maps from the models that have physiological meaning. In Chapter 5 we use a version of the Caricature Noble model and in chapter 6 a reduced version of the Courtemanche et al. (1998) is used.

2.4 Mathematical tools

In this section we describe the essential mathematical tools that are needed to study and analyse solutions for models of action potentials. The *asymptotic reduction method* and *phase plane analysis* are the two fundamental tools in this field. Asymptotic methods enables us to reduce the order of the system to a readily solvable system and phase plane analysis helps us to study the behaviour of the system in more detail (Ermentrout and Terman, 2010). In the following we explain these two tools for a general dynamical system which is a family of differential equations of the form

$$\varepsilon \frac{\mathrm{d}\mathbf{x}}{\mathrm{d}t} = f(\mathbf{x}, \mathbf{y}), \tag{2.6a}$$

$$\frac{\mathrm{d}\mathbf{y}}{\mathrm{d}t} = g(\mathbf{x}, \mathbf{y}), \tag{2.6b}$$

where $\mathbf{x} \in \mathbb{R}^m$ are fast variables, $\mathbf{y} \in \mathbb{R}^n$ are slow variables and $0 < \varepsilon \ll 1$. The system has different time scales as the dynamic variable $\mathbf{x}$ have fast motions and the variables $\mathbf{y}$ are slow. If we assume that the variables are well separated into two groups of fast and slow variables at all times we can apply the "Tikhonov" approach and reduce the system (Tikhonov, 1952). However, it was confirmed by Biktashev et al. (2008) that in cardiac excitable systems some variables evolve differently during the time course of one solution, i.e. one variable is fast in some part of the solution and is slow in other regions of the solution. Tikhonov (1952)'s theorem cannot describe this feature, hence we observe "non-Tikhonov" characteristics of the variables. Biktashev et al. (2008) employed an asymptotic embedding approach and proposed that a complicated system which contains Tikhonov and non-Tikhonov features can be reduced in a systematic way until no further reduction is possible (Biktashev and Suckley, 2004). The parameter embedding that was proposed in Biktashev et al. (2008) is the following

Definition 2.1 *A parameter embedding with parameter* ε *of a function* $f(x)$ *is* $\underline{f}(x;\varepsilon)$ *such that*

$$\underline{f}(x;1) = f(x) \;\; \textit{for all } x \in \textit{dom}(f)$$

When $\varepsilon \to 0$ the parameter embedding is called an *asymptotic embedding*.

2.4.1 Singular perturbation analysis

Realistic models of action potentials usually contain small parameters since they cover multiple scales at the cellular and sub-cellular level. Therefore, there are two time scales in operation everywhere in the domain (Keener and Sneyd, 1998). One possible way to take advantage of these small parameters is to employ asymptotic methods and derive a simplified model from these detailed models.

Slow-fast systems A *slow-fast system* is a system whose variables evolve on two different timescales. Consider the system of equations (2.6) in which the dynamics of the system is dependent on ε. In the limit $\varepsilon \to 0$, equations (2.6) become a slow-time subsystem with one algebraic equation *i.e.* $f(x,y) = 0 \implies x = \mathcal{X}(y)$ and one differential equation (2.7b) which is the essential dynamical variable.

$$0 = f(x,\mathbf{y}), \tag{2.7a}$$

$$\frac{\mathrm{d}\mathbf{y}}{\mathrm{d}t} = g(x,\mathbf{y}). \tag{2.7b}$$

The equations (2.7) describe the motion along the slow manifold $f(x,\mathbf{y})=0$. We now consider this system in the fast-time and replace the independent variable t with $T=t/\varepsilon$:

$$\frac{\mathrm{d}}{\mathrm{d}t}=\frac{\mathrm{d}}{\mathrm{d}T}\frac{\mathrm{d}T}{\mathrm{d}t}=\frac{1}{\varepsilon}\frac{\mathrm{d}}{\mathrm{d}T},$$

to obtain

$$\begin{aligned}\frac{\mathrm{d}x}{\mathrm{d}T}&=f(x,\mathbf{y}),\\ \frac{\mathrm{d}\mathbf{y}}{\mathrm{d}T}&=\varepsilon g(x,\mathbf{y}).\end{aligned}$$

Taking the limit $\varepsilon\to 0$, the fast subsystem is obtained

$$\frac{\mathrm{d}x}{\mathrm{d}T}=f(x,\mathbf{y}), \tag{2.9a}$$

$$\frac{\mathrm{d}\mathbf{y}}{\mathrm{d}T}=0. \tag{2.9b}$$

In the limit $\varepsilon\to 0$, the essential dynamical variable is x and its evolution is obtained from equations (2.9a) and $\mathbf{y}$ is a constant according to the equation (2.9b).

2.4.2 Phase plane analysis

Phase plane analysis is a very useful tool in analysing excitable systems. The phase space for the system (2.6) is the (x,y) plane. The solution $(x(t),y(t))$ corresponds to a trajectory in the phase plane and the velocity vector of the solution curve at the point (x_i,y_i) is given by

$$\left(\frac{\mathrm{d}x}{\mathrm{d}t},\frac{\mathrm{d}y}{\mathrm{d}t}\right)=\left(\frac{1}{\varepsilon}f\left(x_i,y_i\right),g\left(x_i,y_i\right)\right).$$

In order to understand how trajectories behave in a phase plane, the *nullclines* of the system are studied. The $x-$nullcline is the curve $\frac{\mathrm{d}x}{\mathrm{d}t}=f(x,y)=0$ and the $y-$nullcline is the curve $\frac{\mathrm{d}y}{\mathrm{d}t}=g(x,y)=0$. As mentioned above, x is a fast variable and y is a slow variable. It is essential that the x-nullcline has three branches of solutions $f(x,y)=0\quad x=\mathcal{X}_j(y)$ for $j=1,2,3$. The middle branch is the unstable (repelling) branch and acts as a threshold of excitation $x=\mathcal{X}_2(y)$, while the other two branches, on the right and the left, are stable (attracting), i.e. $x=\mathcal{X}_j(y)$ where $j=1,3$. In order to explain the phase plane analysis, lets consider the FitzHugh-Nagumo system of equations given by (2.5) (FitzHugh, 1961; Nagumo et al., 1962). Then a typical example of the nullclines is shown in Figure 2.5

Since the dynamics of the system are defined by the slow variable y through $\frac{\mathrm{d}y}{\mathrm{d}t}=g\left(\mathcal{X}_j(y),y\right)$, the curve $f(x,y)=0$ is called the "slow manifold". Along the slow manifold the motion is governed

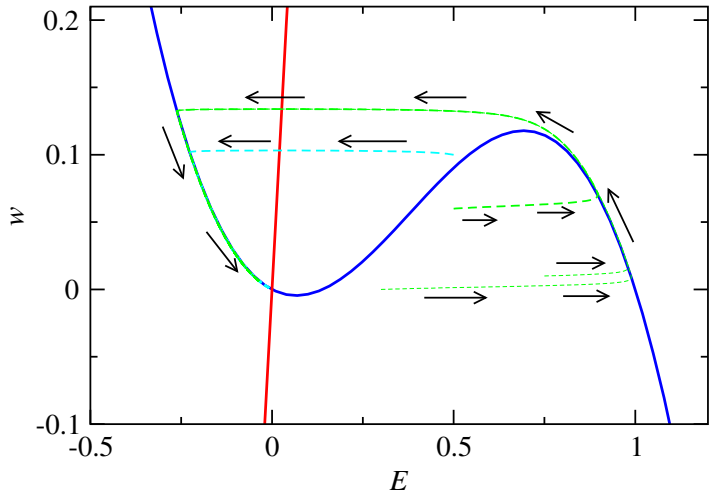

Figure 2.5: Phase portrait and trajectories for the FitzHugh-Nagumo system FitzHugh (1961); Nagumo et al. (1962) given by (2.5). The blue cubic curve is the E-nullcline, the red straight line is the w-nullcline and the trajectories for different initial conditions are illustrated as green and blue dashed curves. The parameter values are $\varepsilon = 0.001,\ \alpha = 0.139$ and $\beta = 0.2$.

by the slow subsystem (2.7), therefore, the solution moves slowly in the direction determined by the sign of $\frac{dy}{dt}$. If $\frac{dy}{dt} > 0$ the solution moves upward and if $\frac{dy}{dt} < 0$ the solution moves downward. Away from the slow manifold (along the y-nullcline), the motion is governed by the fast subsystem (2.9). Hence, the solution moves quickly in a horizontal direction, determined by the sign of $\frac{dx}{dt}$. If positive, the solution moves to the right and if negative the solution moves towards the left (Ermentrout and Terman, 2010; Keener and Sneyd, 1998).

The point (x_*, y_*) at which the two nullclines intersect is called a "fixed point" and after determining the stability of this point, via linearisation of the vector field around the point, we analyse the behaviour of the solution of this dynamical system (2.6).

Consider the fixed point to be a stable equilibrium (x_*, y_*) that is situated on the left stable branch $x = \mathcal{X}_1(y)$ of $f(x,y) = 0$. A small perturbation can excite the system if and only if it lies on the right of the middle branch. A perturbation that lies to the left of the middle branch of x-nullcline will return to rest quickly. Therefore the middle branch of the x-nullcline separates the firing of an action potential from the subthreshold return to rest (Ermentrout and Terman, 2010).

Now that we know the mathematical and physiological background and the necessary mathematical tools to study excitable system we introduce a methodology chapter. In the Methodology chapter

we provide a general formulation to study alternans (2:2 response) and other instabilities in excitable systems.

Chapter 3

Methods

3.1 Introduction

In this chapter we will summarise how action potential duration restitution maps can be used in order to distinguish between various responses to periodic stimulation. We will then, formulate a set of boundary value problems that can be applied to typical excitable models in order to derive analytically or compute numerically various branches of their action potential duration restitution maps. This methodology will be applied to investigate the restitution properties of several excitable models in subsequent chapters.

3.2 Action potential duration restitution maps

As stated previously, action potential duration restitution maps are either postulated heuristically which was explained in Section 2.3.1 or are derived from models of the action potentials as mentioned in Section 2.3.2. In this section deriving restitution maps from a system of ordinary differential equations is presented. Furthermore, by analysing the bifurcation and stability properties of discrete iterative maps, various responses to periodic stimulation are classified.

Consider the following system which is reduced systematically until it cannot be reducible any further:

$$f(x,y) = 0$$
$$\frac{\mathrm{d}y}{\mathrm{d}t} = g(x,y).$$

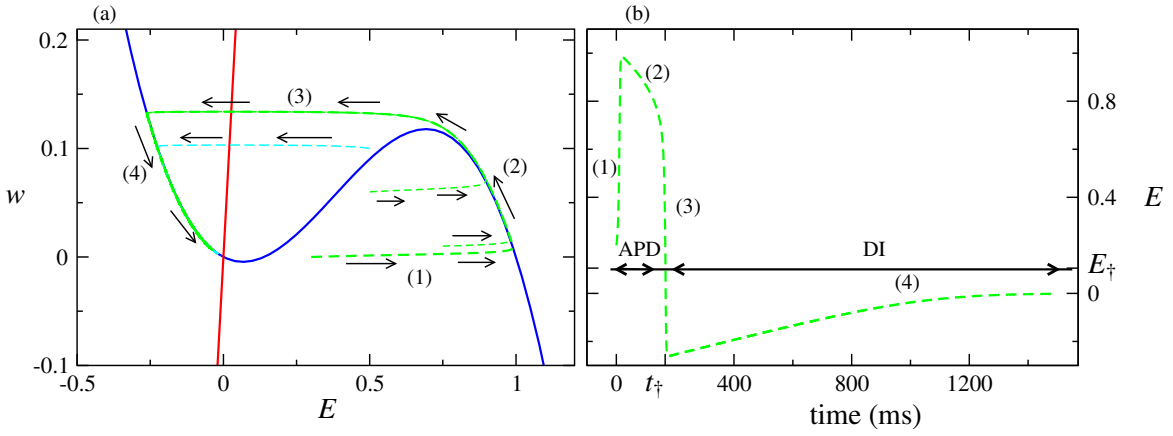

Figure 3.1: A solution of the FitzHugh-Nagumo system (FitzHugh, 1961; Nagumo et al., 1962) model in the (E,w)-plane (phase portrait(a)) and the (t,E)-plane (action potential (b)). In (a) the blue cubic curve is the E-nullcline, the red line is the w-nullcline and the trajectories are shown in green for different initial conditions. In (b) one of the trajectories from (a) is plotted as a function of time. $E_\dagger$ is a threshold value which is used to define the action potential duration and diastolic interval.

In a simplified model, an action potential consists of two separated time scales: the depolarisation and repolarisation phases which are the fast parts of an action potential and the plateau and the resting phases which are the slow parts of an action potential. In general the plateau phase and the resting phase are described by $\dfrac{\mathrm{d}y}{\mathrm{d}t} = g(x,y)$ along the slow manifold $f(x,y) = 0$. Hence, as stated previously the long-time behaviour of the system evolves on a slow manifold. Consider the FitzHugh-Nagumo system (FitzHugh, 1961; Nagumo et al., 1962) model. One selected solution of the FHN system (2.5) is plotted in Figure 3.1, in the (E,w)-plane and in the (t,E)-plane and four phases of the action potential are denoted (Mitchell and Schaeffer, 2003). Action potential duration is the time taken for the solution to travel along the blue curve in phase two of the action potential. The diastolic interval is the time taken for the trajectory to return to its resting potential (i.e. equilibrium point) in phase four of the action potential. These phases of an action potential are labelled (2) and (4) in the figures 3.1(a) and 3.1(b) respectively (Mitchell and Schaeffer, 2003). Therefore by integrating the slow variable equation along these two branches we can get the *APD restitution map*, which is defined as follows

$$\mathrm{A}_{k+1} = F(\mathrm{D}_k) \tag{3.1}$$

$$= F(B - \mathrm{A}_k) \tag{3.2}$$

$$= F(\mathbf{a}, B - \mathrm{A}_k) = \Phi(\tilde{\mathbf{a}}, \mathrm{A}_k).$$

Here $\tilde{\mathbf{a}} = [\mathbf{a}, B]^T$ is a vector of model parameters and for completeness we define the *action potential duration* A_k and the *diastolic interval* D_k of the k-th AP as follows.

Definition 3.1 *Consider an action potential sequence, let the beginning of the k-th AP be at time kB, and let $t_{\dagger_k}$ be the first subsequent moment such that $E(t_{\dagger_k}) = E_\dagger$, where $E_\dagger$ is a threshold value to calculate APD and DI. We define*

$$\mathrm{A}_k = t_{\dagger_k} - (k-1)B, \qquad \mathrm{D}_k = kB - t_{\dagger_k}, \qquad k \in \mathbb{N}. \tag{3.3}$$

In direct numerical simulations and in physiological measurements 90% of the total course of repolarisation is often the value at which the "cut-off" is considered and action potential duration and diastolic interval are calculated. In Figure 3.1 the role of the "cut-off" is assigned to $E_\dagger$.

Whether postulated heuristically or derived from models of the action potentials like (3.1), we end up with a discrete iterative map of type (3.1) as a model for restitution. Based on the stability and bifurcation of these maps, different responses of the system to periodic stimulation, are categorised below. We note that based on the work presented by Chialvo et al. (1990), in the notation m:n, m is the number of stimuli, n is the number of action potentials or responses and

1:1 response A normal 1:1 response is the one where every stimulus excites an action potential and all the action potentials are similar and have equal durations. It can be represented by a superthreshold, stable fixed point $\overline{\mathrm{A}} = F(\overline{\mathrm{A}})$ of map (3.1),

$$\overline{\mathrm{A}} = F(\mathbf{a}, B - \overline{\mathrm{A}}), \tag{3.4a}$$

$$\left| \left[\partial_{\mathrm{A}} F(\mathbf{a}, B - \mathrm{A}) \right]_{\overline{\mathrm{A}}} \right| < 1, \tag{3.4b}$$

$$B > \overline{B}_{\mathrm{thr}}. \tag{3.4c}$$

The first condition (3.4a) requires that $\mathrm{A}_k = \mathrm{A}_{k+1}$ which is true for a sequence of identical action potentials. The second condition (3.4b) asserts that this fixed point must be stable to be physically realisable. Furthermore, condition (3.4c) is a "threshold" condition for excitation of such an AP sequence. This condition ensures the solutions of the map are stable and find the minimum basic cycle length at which the solution loses its stability. Thus, for any action potential with cycle length smaller than $\overline{B}_{\mathrm{thr}}$, the 1:1 solution loses its stability.

2:2 response (alternans) A 2:2 response, also known as *alternans*, is one where every stimulus excites an action potential but even and odd action potentials are different. Analogously, this can be represented by a superthreshold, stable fixed point of the composed second-generation map $\Phi^2 = \Phi \circ \Phi$,

called a 2-cycle of Φ,

$$\overline{\overline{\mathrm{A}}} = F\big(\mathbf{a}, B - F(\mathbf{a}, B - \overline{\overline{\mathrm{A}}})\big), \tag{3.5a}$$

$$\left|\left[\partial_{\mathrm{A}} F\big(\mathbf{a}, B - F(\mathbf{a}, B - \overline{\overline{\mathrm{A}}})\big)\right]_{\overline{\overline{\mathrm{A}}}}\right| < 1, \tag{3.5b}$$

$$B > \overline{\overline{B}}_{\mathrm{thr}}. \tag{3.5c}$$

The condition (3.5a) requires that $\mathrm{A}_k = \mathrm{A}_{k+2}$, the condition (3.5b) states that this fixed point must be stable and (3.5c) is a "threshold" condition for existence of stable 2:2 solution.

2:1 response A 2:1 response is the one where only every second stimulus excites an action potential and all the action potentials are identical. Since every second stimulus fails to initiate an action potential, the basic cycle length between successful action potentials is effectively doubled to $2B$ and this case can be represented by

$$\widetilde{\mathrm{A}} = F(\mathbf{a}, 2B - \widetilde{\mathrm{A}}), \tag{3.6a}$$

$$\left|\left[\partial_{\mathrm{A}} F(\mathbf{a}, 2B - \widetilde{\mathrm{A}})\right]_{\widetilde{\mathrm{A}}}\right| < 1, \tag{3.6b}$$

$$2B > \overline{B}_{\mathrm{thr}}. \tag{3.6c}$$

where (3.6a) requires $\mathrm{A}_k = \mathrm{A}_{k+2}$ such that AP_{k+1} is not initiated in the first place. The condition (3.6b) indicates the stability of this fixed point and (3.6c) is a "threshold" condition for excitation of action potential after one unsuccessful stimulus.

Further instabilities Other periodic responses can be described in a similar way. For instance $\mathrm{A}_{n+N} = \Phi^N(\mathrm{A}_n)$ is the key to understand the beginning of the period N-cycle. A fixed point $\overline{\mathrm{A}} = \Phi^N(\overline{\mathrm{A}})$ represents a N-periodic cycle. Furthermore, the slope of $\Phi^N(\mathrm{A}_n)$ at the fixed point $\overline{\mathrm{A}}$, determines the stability of the response (i.e. for a stable fixed point the slope is less than 1) (Strogatz, 2001)

Conditions such as (3.4), (3.5) and (3.6) can be used to partition the parameter space $\tilde{\mathbf{a}}$ of the action potential duration map (3.1), thus they provide a direct correspondence between the model parameters and types of response. Action potential duration maps act as a guide to determine the important parameters in inducing instabilities. The results obtained from a one-dimensional map must be comparable to the full excitable models (Mitchell and Schaeffer, 2003; Schaeffer et al., 2007; Tolkacheva et al., 2002).

3.3 Boundary Value Problem formulation

In this section, we formulate a set of boundary value problems for generic excitable models. Our proposed formulation can be used to derive analytically or compute numerically various branches of the action potential duration restitution maps in the full excitable systems.

The experimental protocols for measuring restitution encounter a number of difficulties including that of distinguishing the ultimate periodic regime from transient behaviour. By formulating boundary value problems with periodic boundary conditions, we consider an idealised version of the dynamic restitution protocol i.e. we consider strictly periodic wave solutions. In this case, the dependence between the basic cycle length and action potential duration is well defined mathematically via solvability of the corresponding boundary-value problem with periodic boundary conditions. We consider the following general model

$$\frac{\mathrm{d}E}{\mathrm{d}t} = f(E,\ \mathbf{y},\ r,\ \varepsilon), \tag{3.7a}$$

$$\frac{\mathrm{d}\mathbf{y}}{\mathrm{d}t} = g(E,\ \mathbf{y},\ r,\ \varepsilon), \tag{3.7b}$$

where E is voltage, the variables $\mathbf{y}$ are generalised gating variable, r are generalised parameters of the model and ε are asymptotic embedding parameters. This is subject to an idealised stimulation protocol given by

$$E(kB) = E_{\text{stim}}, \qquad k \in \mathbb{N}, \tag{3.7c}$$

where B is the basic cycle length. The equations are completed by the following initial conditions

$$E(0) = E_{\text{stim}}, \qquad \mathbf{y}(0) = \mathbf{y}_{\text{equilibrium}}, \tag{3.7d}$$

The equations (3.7) represent the general form of the models of the action potential in excitable systems as discussed in Section 2.2.2. Therefore, the functions f and g have certain properties as stated in the Section 2.2.2. The vector of parameters $\mathbf{r}$ may be the time-scaling function of a particular gating variable. For example in the McKean (1970) which is studied in Chapter 4 of this thesis, the parameter r determines the time scale at which the slow recovery gating variable evolves. In the Caricature Noble (Biktashev et al., 2008) model, the parameter$r$ defines the amplitude of the K^+ current and this will be discussed in Chapter 5. Moreover, in the Courtemanche et al. (1998) model, the parameter r defines the slow inactivation in the L-type Ca^{+2} current.

The boundary value problem should be well posed such that given the input to the problem, there exists a unique solution which depends continuously on the input. Possible periodic solutions, known as orbits, can be found by imposing the following boundary conditions on one basic cycle length.

1-cycle solution (1:1 response, normal) Boundary conditions that can be imposed on the system of equation (3.7) to obtain the normal response is as follows:

$$E\left(kB,\ r,\ \varepsilon\right) = E\left((k+1)B,\ r,\ \varepsilon\right), \tag{3.8a}$$

$$\mathbf{y}\left(kB,\ r,\ \varepsilon\right) = \mathbf{y}\left((k+1)B,\ r,\ \varepsilon\right), \tag{3.8b}$$

where $k \in \mathbb{N}$, B is the basic cycle length and E_{stim} is a threshold value of excitation for voltage. The normal response with the imposed boundary condition is well illustrated in Figure 3.2.

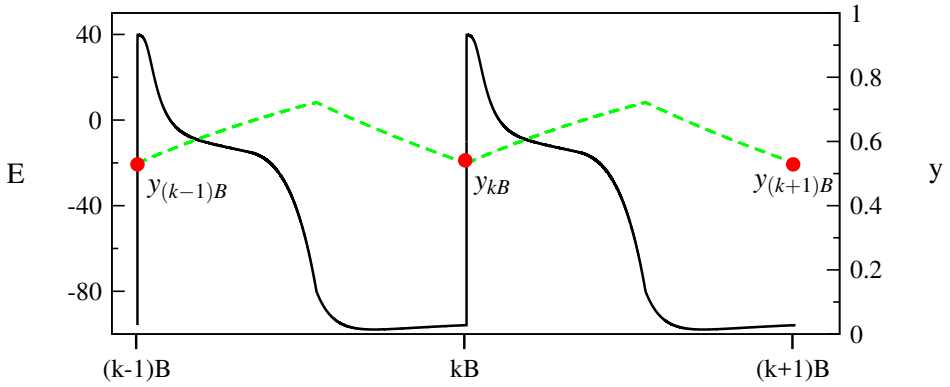

Figure 3.2: A normal response where the black curve is voltage and the green curve is a gating variable $\mathbf{y}$. The gating variable reaches its initial value after one basic cycle length which is shown in red circles. This is a solution of the Caricature Noble model (Biktashev et al., 2008) for $B = 290$ (ms).

2-cycle solution (2:2 response, alternans) Imposing the following boundary conditions on the system (3.7), results in a 2-cycle solution for the system.

$$E\left(kB,\ r,\ \varepsilon\right) = E_{\text{stim}}, \tag{3.9a}$$

$$E\left((k+1)B,\ r,\ \varepsilon\right) = E_{\text{stim}}, \tag{3.9b}$$

$$\mathbf{y}\left(kB,\ r,\ \varepsilon\right) = \mathbf{y}\left((k+2)B,\ r,\ \varepsilon\right), \tag{3.9c}$$

$$\mathbf{y}\left((k+1)B,\ r,\ \varepsilon\right) = \mathbf{y}\left((k+3)B,\ r,\ \varepsilon\right), \tag{3.9d}$$

where, again $k \in \mathbb{N}$ and the case $\mathbf{y}\left(kB,\ r,\ \varepsilon\right) = \mathbf{y}\left((k+2)B,\ r,\ \varepsilon\right)$ describes alternans. An example of this response is shown in Figure 3.3 where the beginning of the odd solutions (the end of the even

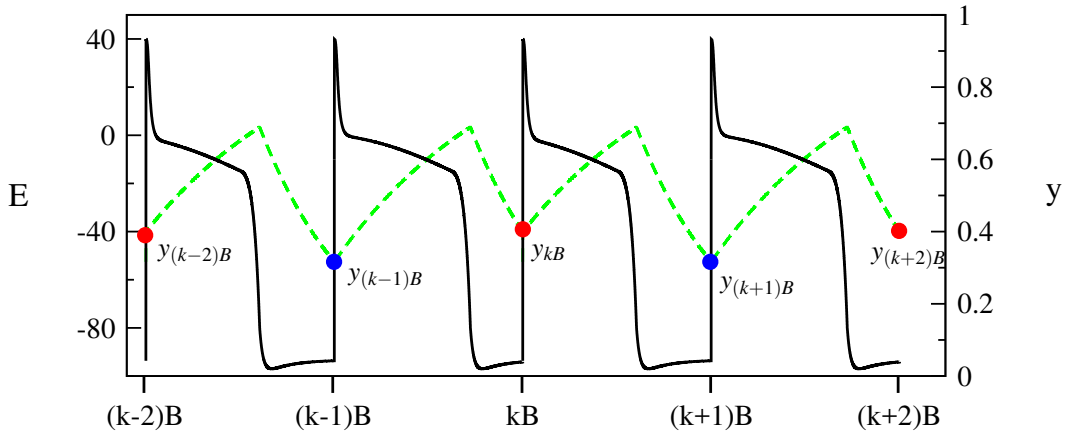

Figure 3.3: A typical 2:2 response where the action potential is illustrated in black and the gating variable **y** is shown in green. The blue and the red circles indicate the points in which the gating variable **y** rests at the end of each AP. This is a solution of the Caricature Noble Biktashev et al. (2008) model for $B = 250$ (ms).

solutions) are indicated by blue circles and the beginning of the even solutions (the end of the odd solutions) are shown in red circles.

P-cycle solution (P:P-response) The P-cycle solution may be obtained by imposing the following The 3-,4-, .. P-cycles can be obtained by constructing boundary value problem with boundary conditions similar to (3.9).

∞-cycle solution (∞ : ∞-response, chaos) If the solution of the system (3.7) does not satisfy the above mentioned periodic boundary conditions, the system may expect a chaotic solution.

3.3.1 Enlarged 2:2 Boundary Value Problems

Looking at the conditions in (3.9), can be seen that the time $t = (k+1)B$ is in the middle of the (3.9a) and the $t = (k+2)B$ is in the middle of the (3.9b), hence, the boundary is imposed on the middle of the time interval and not at the end of it. Therefore, in order to apply these conditions on the system of equations, we need to convert them to a standard boundary value problem.

Let E_1, $\mathbf{y}_1$ and E_2, $\mathbf{y}_2$ be the solutions of the system (3.7) for the first and the second action potential respectively. We are interested in the situation when all transients have died out, then $t = kB$ can be replaced by $t = 0$ as this is just a translation in time. Hence, the equations for E_1, $\mathbf{y}_1$ and E_2, $\mathbf{y}_2$ are solved on the same time interval $t \in [0, B]$. The boundary conditions at 0 and B are as in (3.9),

hence the resulting enlarged 2:2 boundary value problem for $t \in [0, B]$ is formulated as:

$$\frac{\mathrm{d}E_1}{\mathrm{d}t} = f\left(E_1,\, \mathbf{y}_1,\, r,\, \varepsilon\right), \tag{3.10a}$$

$$\frac{\mathrm{d}\mathbf{y}_1}{\mathrm{d}t} = g\left(E_1,\, \mathbf{y}_1,\, r,\, \varepsilon\right), \tag{3.10b}$$

$$\frac{\mathrm{d}E_2}{\mathrm{d}t} = f\left(E_2,\, \mathbf{y}_2,\, r,\, \varepsilon\right), \tag{3.10c}$$

$$\frac{\mathrm{d}\mathbf{y}_2}{\mathrm{d}t} = g\left(E_2,\, \mathbf{y}_2,\, r,\, \varepsilon\right), \tag{3.10d}$$

$$E_1(0, ...) = E_{\text{stim}}, \tag{3.10e}$$

$$E_2(0, ...) = E_{\text{stim}}, \tag{3.10f}$$

$$\mathbf{y}_1(0, ...) = \mathbf{y}_2(B, ...), \tag{3.10g}$$

$$\mathbf{y}_2(0, ...) = \mathbf{y}_1(B, ...). \tag{3.10h}$$

The above equation is well illustrated in Figure 3.3 where red circles denote $\mathbf{y}_1(0) = \mathbf{y}_2(B)$ and the blue circles show $\mathbf{y}_2(0, ...) = \mathbf{y}_1(B, ...)$, when $k = 0$.

3.3.2 Solutions and construction of the action potential duration restitution curve

In order to construct the action potential duration restitution curve, the equations (3.10) are solved simultaneously using the solution of the initial value problem as an initial guess. The action potential solution $E(t)$ is dependent on the basic cycle length B, the model parameters r, ε and constants of the model.

In order to obtain the action potential duration restitution curve as a function of the basic cycle length, the parameters of the model are fixed and duration of each action potential is calculated for different basic cycle length.

The action potential duration restitution curve is constructed from the solution such that the duration of action potential is calculated for each basic cycle length, while other parameters r and ε are fixed. In the following chapters the action potential duration restitution curve for each model is constructed as a function of basic cycle length.

We remark that in order to measure restitution, it is possible to use quantities other than the action potential duration. For example $\mathbf{y}_2(t = 0, B)$ for different values of B provides an equivalent representation of the action potential duration restitution curve.

In the next chapter, the above methods are applied to the McKean (1970) model which is a caricature version of the FitzHugh-Nagumo system (FitzHugh, 1961; Nagumo et al., 1962).

Chapter 4

Restitution and alternans in the McKean model

4.1 Introduction

In this chapter, the methodology that was described in Chapter 3 is assessed by applying it to a simplified model of spiking neurons proposed by McKean (1970). The McKean model is a piecewise-linear version of the FitzHugh-Nagumo model (FitzHugh, 1961; Nagumo et al., 1962) and despite being simple, the essential features of the FitzHugh-Nagumo model are preserved. We study this model since its simplicity enables us to find the exact solution of the system and to do explicit calculations. Furthermore, this two dimensional model is a simple example of a slow-fast system and has a well-defined geometrical construction in the phase plane. Hence, with analyzing this system, we aim to gain more insight into systems in which two time scales are involved.

4.2 Formulation

The McKean model has two dynamical variables $E(t)$ and $w(t)$ representing voltage and a recovery gating variable, respectively. The model equations are as follows:

$$\frac{\mathrm{d}E}{\mathrm{d}t} = g(E,w) = \frac{1}{b}(f(E) - w), \tag{4.1}$$

$$\frac{\mathrm{d}w}{\mathrm{d}t} = h(E,w) = E - Cw, \tag{4.2}$$

where

$$f(E) = -E + H(E-a),$$

H is a Heaviside function, $0 < a < 1$ and b and C are positive real numbers. The McKean (1970) model will be used to study the restitution properties in an excitable model, hence the following adjustments are made to the system:

(i) Parameter embedding based on the work of Biktashev and Suckley (2004); Biktashev et al. (2008), is used to introduce a small parameter $\varepsilon > 0$ to the model. The parameter b is replaced by εb so that the original problem corresponds to $\varepsilon = 1$.

(ii) The results offered by Mitchell and Schaeffer (2003), suggested that variation of the voltage-dependent time function in the slow gating variable, induces instabilities in the system. In order to investigate the role of the voltage-dependent time function in the McKean model, we modified the constant C in (4.2) with a function of voltage and a dimensionless parameter $r > 0$ as follows:

$$C(E,r) = c_{\mathrm{w}}\left(rH(a-E) + H(E-a)\right),$$

where c_{w} is a constant and the parameter r changes the speed at which the slow gating variable $w(t)$ evolves during the diastolic phase of an action potential. As shown in Figure 4.1, the amplitude of $C(E,r)$ for $E < a$ (i.e. during diostolic interval), is dependent on r. Moreover, r determines the time required for $w(t)$ to reach its resting value.

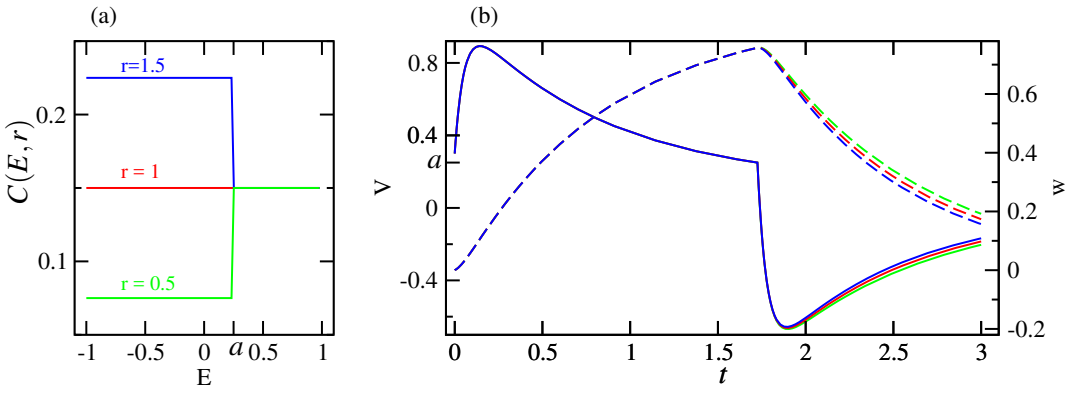

Figure 4.1: The effects of parameter r on the solution of the McKean model. In (a), $C(E,r)$ is plotted as a function of E for different values of r. (b) illustrates the effects of r on the solution of the gating variable w and consequently on the voltage E.

The modified version of the McKean model is:

$$\frac{\mathrm{d}E}{\mathrm{d}t} = g(E,w) = \frac{1}{\varepsilon b}\big(f(E) - w\big) \tag{4.3a}$$

$$\frac{\mathrm{d}w}{\mathrm{d}t} = h(E,w) = E - C(E,r)w. \tag{4.3b}$$

with the following periodic forcing:

$$E(kB) = E_{\text{stim}}, \quad w(kB) = w_0, \quad \forall k \in \mathbb{N} \tag{4.4}$$

where E_{stim} is the threshold value for the membrane voltage to become depolarized and action potential is formed.

4.3 Phase portrait and parameter ranges

The McKean model is a two-dimensional model and can be studied in the (E,w) phase plane. The nullclines of the model are given by

$$-E + H(E-a) - w = 0 \tag{4.5a}$$

$$E - C(E,r)w = 0. \tag{4.5b}$$

The E-nullcline has two branches, the left branch is $E + w = 0$, and the right branch is $w + E - 1 = 0$. The left and the right branches are stable and are separated at $E = a$, where $a \in (0, 0.5)$ and in this case is considered as $a = 0.25$. The discontinuity at $E = a$ can be considered as a threshold region, where the firing state is separated from the resting state.

The nullclines (4.5) always have a "stable" intersection at the origin of the $E - w$ plane. They may intersect elsewhere as well depending on the values of r and c_{w}, as can be seen in Figures 4.2(c) and 4.2(d). Since the interest of this research is on analyzing excitable models, therefore the desired parameter space for c_{w} and r are the regions where the origin is the only intersection between the two nullclines. Thus, c_{w} and r are found such that there is only one equilibrium point located on the left branch of the E-nullcline. This is well illustrated as region γ in Figure 4.2(a) where the red line is the E-nullcline and the green lines are the w-nullcline for different values of c_{w}.

In Figure 4.2(a), (α) and (β) are regions where w-nullcline crosses the right branch of E-nullcline. Hence, parameters c_{w} and r should be chosen such that the cases (α) and (β) are avoided. These cases are depicted in Figures 4.2(c) and 4.2(d) and are described below:

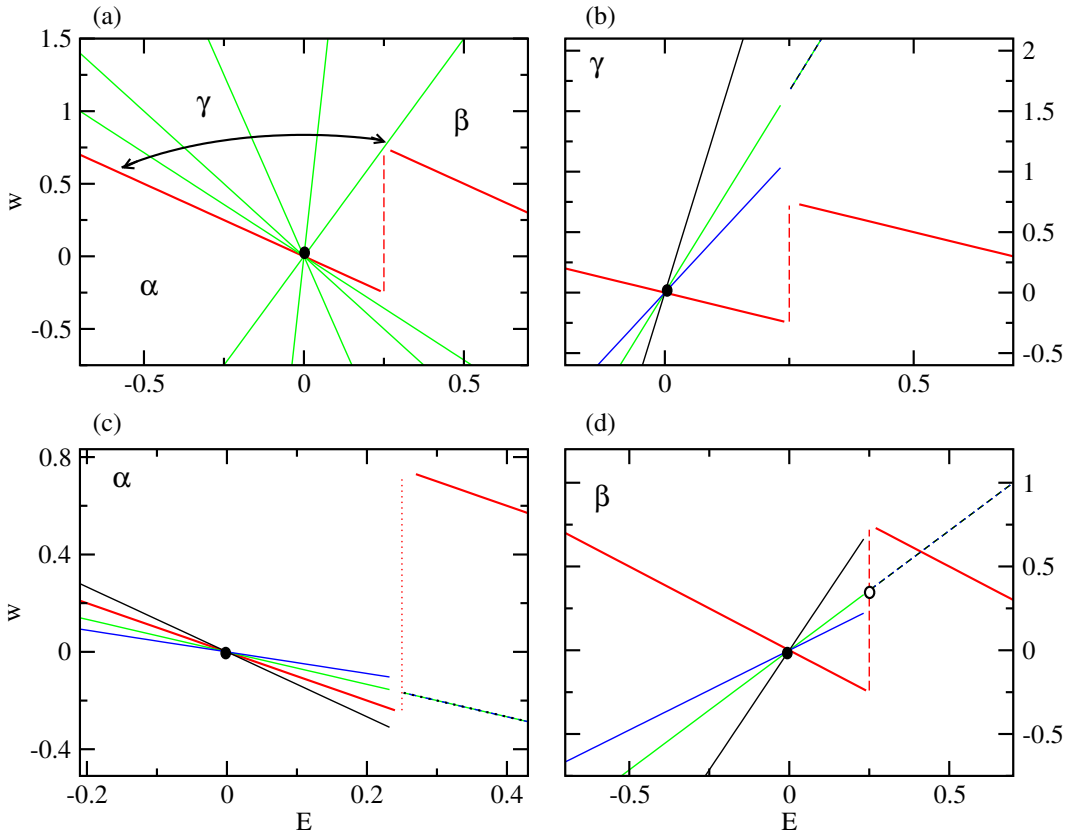

Figure 4.2: Phase space of the McKean (1970) model, when $a = 0.25$ and for different values of c_w. In (a) the red curve is the E-nullcline and the green lines are w-nullclines for $c_w \in (-1, \frac{a}{1-a})$ and $r = 1$. (b) shows the region (γ), where for $c_w = 0.15$ and $r = 0.5, 1, 1.5$, two nullcline have one intersection at the origin. In panel (c), c_w is chosen from the region (α), i.e. $c_w = -1.5$. For figure in panel (d), c_w is selected in region (β), i.e. $c_w = 0.7$.

(i) For $E < a$, the slope of w-nullcline should be more than the the slope of the E-nullcline. Otherwise two lines coincide and have many intersections. Therefore, two nullclines lie on the top of each other if $rc_w = -1$. Hence, in order to avoid this situation, c_w is chosen such that $\frac{1}{rc_w} > -1$.

(ii) For $E > a$, E-nullcline and w-nullcline intersect at $\left(\frac{c_w}{1+c_w}, \frac{1}{1+c_w}\right)$ if $-1 < \frac{1}{c_w} \leq \frac{1-a}{a}$. To avoid intersections, c_w must be $\frac{1}{c_w} < -1$ or $\frac{1}{c_w} > \frac{1-a}{a}$. This yields to $-1 < c_w < 0$ and $c_w < \frac{a}{1-a}$.

Combining the above conditions and considering $r > 0$, c_{w} must be chosen as follows:

$$c_{\mathrm{w}} \in \left(\max(\frac{-1}{r}, -1), \frac{a}{1-a} \right)$$

Based on the above limitations, the McKean model (4.3) as an excitable system with a resting state and a firing state is studied.

Figure 4.3(a) outlines the nullclines of the system and the trajectories with attached arrows describing their directions. E-nullcline is shown in red and the w-nullcline for $r = 1$ is illustrated in blue. w-nullclines for different values of $r > 0$ are outlined in different colours to show the role of the parameter r in the phase portrait of the system. $E(t)$ and $w(t)$ are also shown in red and blue respectively in Figure 4.3(b). The other parameters of the model in Figure 4.3, are $c_{\mathrm{w}} = -0.15$, $a = 0.25$, $b = 0.05$ and $\varepsilon = 1$.

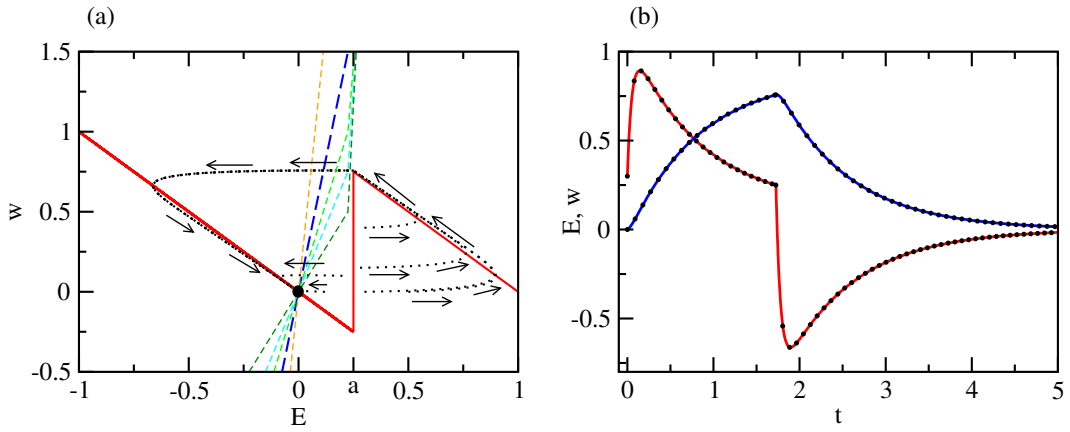

Figure 4.3: A solution of the McKean (1970) model in (E,w)- and (t,E)-planes. Parameter values are $a = 0.25$, $b = 0.05$, $\varepsilon = 1$, $c_{\mathrm{w}} = 0.15$ and $r = 1$. Panel (a) is the phase portrait of the system (4.3), E-nullcline is plotted in solid red and the dashed lines are w-nullclines for different values of $r > 0$. The dotted black curves with attached arrows, represent trajectories with various initial conditions (4.4). (b) shows the $E(t)$ and $w(t)$ in red and blue respectively. The Initial condition is $E(0) = E_{\mathrm{stim}} = 0.3$ and $w(0) = 0$. The black dotted curves in panel (b) correspond to the exact solution of the $E(t)$ and $w(t)$ (4.23) and is presented in Section 4.5.

As stated before and illustrated in Figure 4.3(a) the "diastolic" branch or resting state is when $E \in (-\infty, a]$ and the "systolic" branch or excited state is $E \in [a, +\infty]$. The threshold state which is the middle branch of the E-nullcline, is discontinuity at $E = a$. Thus, there is no threshold region in this

version of the McKean model. The concept of threshold region and its dependency on the voltage, will be discussed in the following chapters in more details.

A sufficiently large perturbation from the steady state $(E_{ss}, w_{ss}) = (0,0)$, produces action potential. A trajectory starting from the region $E > a$ is attracted by the right branch of the E-nullcline, thus making a relatively large excursion, then travels slowly along the systolic branch and at w_* jumps to the diastolic branch. (E_*, w_*) is called a turning point where the recovery gating variable w takes it maximal value at $E_* = a$ as given by the below equation:

$$w_* = 1 - E_*. \tag{4.6}$$

The trajectory then has another slow movement along the diastolic branch and approaches the steady state, where the motion will stops. The cycle is repeated if there is sufficiently large perturbation from the steady state.

In the next section, we apply asymptotic reduction method to the model, we derive the asymptotic action potential duration restitution map.

4.4 Asymptotic action potential duration restitution map

Asymptotic reduction The variables of the McKean model (4.3) have two different time scales, in the limit $\varepsilon \to 0$ the variable E is much faster than w, hence E is the fast variable and the recovery variable w is the slow variable. The system is a typical fast-slow system and its asymptotic properties are studied as below:

The slow system: In the limit $\varepsilon \to 0$, the variable E is fast and the slow recovery gating variable w is slow. Therefore in the equation (4.3).

$$0 = \frac{1}{b}\big(H(E-a) - w - E\big), \tag{4.7a}$$

$$\frac{\mathrm{d}w}{\mathrm{d}t} = E - C(E,r)w. \tag{4.7b}$$

The slow manifold of the McKean system is defined by

$$w = \mathcal{W}(E) = H(E-a) - E. \tag{4.8}$$

and in $t \sim 1$ equation (4.7b) describes the motion along this manifold and the essential dynamical variable w describes the plateau and the recovery stages of the action potential.

The fast system is obtained by rescaling time in equation (4.3). Setting

$$\tau = t/\varepsilon \quad \text{we get} \quad d\tau = \frac{dt}{\varepsilon}, \quad \frac{\mathrm{d}}{\mathrm{d}t} = \frac{\mathrm{d}}{\mathrm{d}\tau}\frac{\mathrm{d}\tau}{\mathrm{d}t} = \frac{1}{\varepsilon}\frac{\mathrm{d}}{\mathrm{d}\tau},$$

and so

$$\begin{aligned} \frac{\mathrm{d}E}{\mathrm{d}\tau} &= \frac{1}{b}\big(H(E-a) - w - E\big) \\ \frac{\mathrm{d}w}{\mathrm{d}\tau} &= \varepsilon\big(E - C(E,r)w\big). \end{aligned} \tag{4.9}$$

Taking $\varepsilon \to 0$ the system becomes a fast system with only one equation for membrane potential, as follows:

$$\begin{aligned} \frac{\mathrm{d}E}{\mathrm{d}\tau} &= \frac{1}{b}\big(H(E-a) - w - E\big) \\ \frac{\mathrm{d}w}{\mathrm{d}\tau} &= 0. \end{aligned} \tag{4.10}$$

The fast system (4.10) describes the front and the back of the action potential.

Map The action potential duration restitution map is now derived for the slow system (4.7) on the domain of the problem in general is $t \in [kB, (k+1)B]$ and the boundary conditions are (4.4).

Remark 1 *As explained in Chapter 3, the domain $t \in [kB, (k+1)B]$ is just a translation in time of the interval $t \in [0, B]$.*

Using maps of type (3.1), i.e. $\mathrm{A}_{k+1} = \Phi(\mathrm{A}_k)$, where A_k is the action potential duration of the k-th action potential, the asymptotic restitution map is derived as follows:

Lemma 4.1 *For an action potential sequence generated in problem* (4.3)

$$\mathrm{A}_k = a(w_{k-1}), \qquad a(x) \equiv \frac{1}{1+c_\mathrm{w}} \ln\left|\frac{1-(1+c_\mathrm{w})x}{1-(1+c_\mathrm{w})w_*}\right|, \tag{4.11a}$$

$$\mathrm{D}_k = \mathrm{d}(w_k), \qquad \mathrm{d}(x) \equiv \frac{1}{1+rc_\mathrm{w}} \ln\left|\frac{w_*}{x}\right|, \tag{4.11b}$$

$$w_k \equiv w(kB), \quad k \in \mathbb{N}.$$

where $w_k = w(kB)$ denotes the value of the gating variable w at the beginning of the $(k+1)$-st action potential and $k \in \mathbb{N}$.

Proof The action potential duration is defined to be the time during which the voltage is greater than a. According to the Figure 4.2, the voltage exceeds a during phase two of the action potential and during parts of phases one and three. However, phases one and three are very fast and negligible. Thus, the action potential duration is approximately equal to the length of phase two which is the time required for w to increase from its resting value at the end of the preceding action potential $w((k-1)B)$ to w_*. And the diastolic interval is equal to the length of phase four which is the time required for w to decrease from w_* to its resting value at the end of the action potential which is $w(kB)$. The result follows by integration of (4.7) along the two branches of the slow manifold (4.8):

$$\mathrm{A}_k = \int_{(k-1)B}^{(k-1)B+\mathrm{A}_k} \mathrm{d}t = \int_{w((k-1)B)}^{w_*} \frac{\mathrm{d}w}{1-(1+c_\mathrm{w})w} = \frac{1}{1+c_\mathrm{w}} \ln\left|\frac{1-(1+c_\mathrm{w})w_{k-1}}{1-(1+c_\mathrm{w})w_*}\right|, \quad E > a, \tag{4.12}$$

$$\text{where} \quad w_{k-1} = w((k-1)B), \tag{4.13}$$

$$\mathrm{D}_k = \int_{(k-1)B+\mathrm{A}_k}^{kB} \mathrm{d}t = -\frac{1}{(1+rc_\mathrm{w})} \int_{w_*}^{w(kB)} \frac{\mathrm{d}w}{w} = \frac{1}{1+rc_\mathrm{w}} \ln\left|\frac{w_*}{w_k}\right|, \quad E < a \tag{4.14}$$

$w_* = 1-a$ is the point where the gating variable w is at its turning point (the maximal value on the systolic branch of the slow manifold (4.7a)), e.g. $w((k-1)B+\mathrm{A}_k) = w(kB+\mathrm{A}_{k+1}) = w_*$ for any $k \in \mathbb{N}$. We also note that the end of a plateau phase coincides with the beginning of the next recovery stage and this can be seen by the phase portrait in Figure 4.2(a). ∎

Proposition 4.1 *An action potential duration restitution map relating* A_{k+1} *to* A_k *is given by*

$$\mathrm{A}_{k+1} = \Phi(\mathrm{A}_k),$$

$$\Phi(\mathrm{A}_k) = F(\tilde{\mathbf{a}}, B-\mathrm{A}_k) = \frac{1}{1+c_\mathrm{w}} \ln\left|\frac{1-(1+c_\mathrm{w})w_* \exp\big(-(1+rc_\mathrm{w})\,(B-\mathrm{A}_k)\big)}{1-(1+c_\mathrm{w})w_*}\right|, \tag{4.15}$$

where $\tilde{\mathbf{a}}$ *is a vector of parameters in this model* $\tilde{\mathbf{a}} = [c_\mathrm{w}, r]^T$.

Proof The result is obtained by eliminating w_k between expression (4.11a) written for A_{k+1} and expression (4.11b) written for $\mathrm{D}_k = B - \mathrm{A}_k$. ∎

Lemma 4.1 provides a parametric form of the action potential duration restitution map and the Proposition gives an equivalent explicit representation.

Fixed points Lemma 4.1 is the general solution of the equations (4.7) on the domain $t \in [0, B]$ before imposing the boundary condition $w(0) = w(B)$. When this boundary condition is imposed, the particular solution of interest is obtained as it will be explained in the following Proposition.

Proposition 4.2 *The equation* $\overline{\mathrm{A}} = \Phi(\overline{\mathrm{A}})$ *has a unique solution branch given in parametric form by*

$$\overline{\mathrm{A}} = a(\overline{w}), \qquad \overline{\mathrm{D}} = \mathrm{d}(\overline{w}), \tag{4.16}$$

so that $a(\overline{w}) = B - \mathrm{d}(\overline{w})$ *and a parameter* $\overline{w} \in [0,1]$.

Proof In order to solve $\overline{\mathrm{A}} = \Phi(\overline{\mathrm{A}})$ we use the equivalent parametric representation of Lemma 4.1. In a 1:1 response

$$\mathrm{A}_k = \mathrm{A}_{k+1} \quad \text{and} \quad \mathrm{D}_k = \mathrm{D}_{k+1},$$

which is equivalent by (4.11) to

$$a(w_{k-1}) = a(w_k) \quad \text{and} \quad \mathrm{d}(w_k) = \mathrm{d}(w_{k+1}),$$

respectively.

By the bijectivity of the logarithmic function, solutions are $w_{k-1} = w_k \equiv \overline{w}$ and $w_k = w_{k+1} \equiv \overline{w}$, respectively. It follows that in a 1:1 response all the action potentials start from identical values of the w gate, $\overline{w}$ thus expressions (4.16) hold. The parameter $\overline{w}$ is a gating variable hence $\overline{w}$ must be in the range $[0,1]$. ∎

The fixed points of Φ^2 corresponds to a case when asymptotic action potential duration restitution map exhibits a 2:2 response. This is demonstrated below.

Proposition 4.3 *The equation* $\overline{\overline{\mathrm{A}}} = \Phi \circ \Phi(\overline{\overline{\mathrm{A}}})$ *has three solution branches: the first one is identical to* (4.16)*, and the other two are given in parametric form by*

$$\overline{\overline{\mathrm{A}}}_{\text{even}} = a(w_{\mathrm{o}}), \qquad \overline{\overline{\mathrm{D}}}_{\text{even}} = d(w_{\mathrm{e}}) = d(\alpha w_{\mathrm{o}}), \tag{4.17a}$$

$$\overline{\overline{\mathrm{A}}}_{\text{odd}} = a(\alpha w_{\mathrm{o}}), \qquad \overline{\overline{\mathrm{D}}}_{\text{odd}} = d(w_{\mathrm{o}}), \tag{4.17b}$$

where

$$w_{\mathrm{o}} = \frac{\alpha^{\left(\frac{1+c_{\mathrm{w}}}{1+rc_{\mathrm{w}}}\right)} - 1}{(1+c_{\mathrm{w}})\left(\alpha^{\left(\frac{1+c_{\mathrm{w}}}{1+rc_{\mathrm{w}}}\right)^{+1}} - 1\right)} \tag{4.17c}$$

with a parameter $\alpha \in (0,\infty)$.

Proof In order to prove this proposition, similar to the previous proof, rather than solving the transcendental equation $\overline{\overline{\mathrm{A}}} = \Phi \circ \Phi(\overline{\overline{\mathrm{A}}})$ directly, we use the equivalent parametric representation of Lemma 4.1. In a 2:2 response,

$$\mathrm{A}_{2k} = \mathrm{A}_{2k+2} \quad \text{and} \quad \mathrm{A}_{2k+1} = \mathrm{A}_{2k+3}, \quad \forall k \in \mathbb{N}$$

as well as

$$\mathrm{D}_{2k} = \mathrm{D}_{2k+2} \quad \text{and} \quad \mathrm{D}_{2k+1} = \mathrm{D}_{2k+3}, \quad \forall k \in \mathbb{N}.$$

Applying expressions (4.11), we find $w_{2k-1} = w_{2k+1} \equiv w_{\mathrm{o}}$ and $w_{2k} = w_{2k+2} \equiv w_{\mathrm{e}}$. Since the basic cycle length B is fixed, it is also required

$$B = \mathrm{A}_{2k} + \mathrm{D}_{2k} = \mathrm{A}_{2k+1} + \mathrm{D}_{2k+1} \;\Leftrightarrow\; a(w_{\mathrm{o}}) + d(w_{\mathrm{e}}) = a(w_{\mathrm{e}}) + d(w_{\mathrm{o}}), \tag{4.18}$$

and explicitly

$$\frac{1}{1+c_{\mathrm{w}}} \ln \left| \frac{1-(1+c_{\mathrm{w}})w_{\mathrm{o}}}{1-(1+c_{\mathrm{w}})w_{\mathrm{e}}} \right| = \frac{1}{1+rc_{\mathrm{w}}} \ln \left| \frac{w_{\mathrm{e}}}{w_{\mathrm{o}}} \right|.$$

By the bijectivity of the logarithm and after the change of variable $w_{\mathrm{e}} = \alpha w_{\mathrm{o}}$ this equation reduces to

$$(1+c_{\mathrm{w}})w_{\mathrm{o}} \left(\alpha \left(\frac{1+c_{\mathrm{w}}}{1+rc_{\mathrm{w}}} \right)^{+1} - 1 \right) - \alpha \left(\frac{1+c_{\mathrm{w}}}{1+rc_{\mathrm{w}}} \right) + 1 = 0. \tag{4.19}$$

Equation (4.19) can be solved for w_{o} and its exact solution is (4.17c), where w_{o} is a function of α and model's parameters. Equations (4.17a) and (4.17b) then follow, since equation (4.18) is invariant with respect to exchanging w_{e} and w_{o}. In addition, since w_{e} and w_{o} are positive, the range of α is established as $\dfrac{w_{\mathrm{e}}}{w_{\mathrm{o}}} = \alpha \in (0,\infty)$. If $w_{\mathrm{e}} \geq w_{\mathrm{o}}$ then $\alpha \in [1,\infty)$ and if $w_{\mathrm{e}} < w_{\mathrm{o}}$ then $\alpha \in (0,1)$. In order to compute the two branches of $\overline{\overline{\mathrm{A}}} = \Phi \circ \Phi(\overline{\overline{\mathrm{A}}})$, a more straight forward approach is considered such that the equation (4.19) is solved for α when w_{o} varies from 0 to 1. This is followed by calculating $w_{\mathrm{e}} = \alpha w_{\mathrm{o}}$ and consequently the even and odd branches (4.17a) and (4.17b), respectively.

Finally, a fixed point of Φ is also a fixed point of $\Phi \circ \Phi$, hence (4.16) is a third solution branch of $\overline{\overline{\mathrm{A}}} = \Phi \circ \Phi(\overline{\overline{\mathrm{A}}})$. The solutions (4.16) and (4.17) can be verified by back-substitution into $\overline{\mathrm{A}} = \Phi(\overline{\mathrm{A}})$ and $\overline{\overline{\mathrm{A}}} = \Phi \circ \Phi(\overline{\overline{\mathrm{A}}})$, respectively.

Remark 2 *This is a general procedure that makes it possible to derive exact parametric solutions for the fixed points of the higher-generation compositions of* Φ.

■

Stability and bifurcations of equilibria We now impose conditions (3.4b) and (3.5b) to establish the stability properties of 1:1 and 2:2 responses.

Proposition 4.4 *The equilibrium* (4.16) *of the action potential duration restitution map* (4.15) *loses stability in a flip (period-doubling) bifurcation at*

$$w_{\mathrm{bif}} = \frac{1}{2 + c_{\mathrm{w}}(1+r)} \tag{4.20a}$$

or in terms of the BCL, alternatively at

$$B_{\mathrm{bif}} = a(w_{\mathrm{bif}}) + \mathrm{d}(w_{\mathrm{bif}}) = \ln \left| \left(\frac{1-(1+c_{\mathrm{w}})w_{\mathrm{bif}}}{1-(1+c_{\mathrm{w}})w_*} \right)^{\left(\frac{1}{1+c_{\mathrm{w}}}\right)} \left(\frac{w_*}{w_{\mathrm{bif}}} \right)^{\left(\frac{1}{1+rc_{\mathrm{w}}}\right)} \right| \tag{4.20b}$$

B_{bif} *as a function of r is the region where 2:2-response bifurcates from the 1:1-response and is shown in Figure 4.4.*

Proof The expression (4.16) is substituted in (3.4b) and $\left|\partial_{\mathrm{A}} F(\mathbf{a}, \mathrm{A})\right|_{\overline{\mathrm{A}}} = 1$, is solved as below

$$\left| \frac{w_*(1+rc_{\mathrm{w}})\exp(-(1+rc_{\mathrm{w}})\mathrm{D}_{\mathrm{bif}}}{1-(1+c_{\mathrm{w}})w_*\exp(-(1+rc_{\mathrm{w}})\mathrm{D}_{\mathrm{bif}}} \right| = 1, \tag{4.21}$$

we write $w_{\mathrm{bif}} = w_*\exp(-(1+rc_{\mathrm{w}})\mathrm{D}_{\mathrm{bif}})$, since at this value w recovers during the time $\mathrm{D}_{\mathrm{bif}}$. By rewriting (4.21) in terms of w_{bif}, we obtain

$$\frac{w_{\mathrm{bif}}(1+rc_{\mathrm{w}})}{1-(1+c_{\mathrm{w}})w_{\mathrm{bif}}} = 1$$

which provides an expression for w_{bif} in terms of models parameters:

$$\overline{w} = w_{\mathrm{bif}} = \frac{1}{2+c_{\mathrm{w}}(1+r)}.$$

Evaluating (4.16) at w_{bif} we then find

$$\mathrm{A}_{\mathrm{bif}} = a(w_{\mathrm{bif}}) = \frac{1}{1+c_{\mathrm{w}}} \ln \left| \frac{1-(1+c_{\mathrm{w}})w_{\mathrm{bif}}}{1-(1+c_{\mathrm{w}})w_*} \right|, \tag{4.22a}$$

$$\mathrm{D}_{\mathrm{bif}} = \mathrm{d}(w_{\mathrm{bif}}) = \frac{1}{1+rc_{\mathrm{w}}} \ln \left| \frac{w_*}{w_{\mathrm{bif}}} \right|, \tag{4.22b}$$

$$B_{\mathrm{bif}} = a(w_{\mathrm{bif}}) + \mathrm{d}(w_{\mathrm{bif}}) = \ln \left| \left(\frac{1-(1+c_{\mathrm{w}})w_{\mathrm{bif}}}{1-(1+c_{\mathrm{w}})w_*} \right)^{\left(\frac{1}{1+c_{\mathrm{w}}}\right)} \left(\frac{w_*}{w_{\mathrm{bif}}} \right)^{\left(\frac{1}{1+rc_{\mathrm{w}}}\right)} \right| \tag{4.22c}$$

■

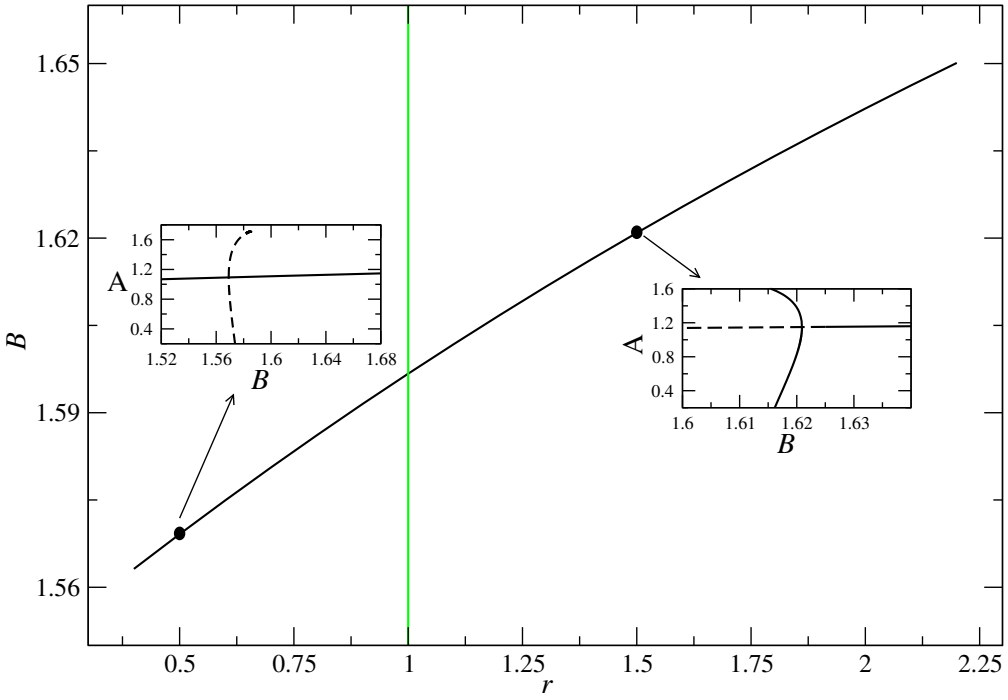

Figure 4.4: Bifurcation set in the r-B parameter space. The black curve is B_{bif} (4.20b) as a function of r, this is the region where 2:2 response bifurcates from the 1:1 response. The green line is $r = 1$ which separates stable from unstable 2:2 responses. For $r > 1$, 2:2 solution is stable and for $r = 0.5$, 2:2 solution is unstable. Restitution curves, illustrating bifurcation regions, are plotted for the two value of r.

Proposition 4.5 *The equilibria* (4.17) *of the second-generation map* $\Phi \circ \Phi$ *bifurcate from the equilibrium* (4.16) *of the action potential duration restitution map* (4.15) *at* (4.20) *and lose their stability at* $r = 1$.

Proof To confirm that equilibria (4.17) bifurcate from equilibrium (4.16) it is enough to evaluate (4.17c) at $\alpha = 1$, the value where (4.17) first emerges. Since

$$\lim_{\alpha \to 1} w_{\text{o}} = \frac{1}{2 + c_{\text{w}}(1+r)} \overset{\text{(H)}}{=} w_{\text{bif}},$$

then (4.16) and (4.17) intersect at w_{bif}.

Rather than using (3.5b) directly, we recall that a flip bifurcation for Φ is a pitchfork bifurcation for the second generation map $\Phi \circ \Phi$. A pitchfork bifurcation (and the corresponding flip bifurcation) can be either supercritical if $[\partial_{\text{A}}^3 \Phi \circ \Phi]_{\text{A}_{\text{bif}}} < 0$ or subcritical if $[\partial_{\text{A}}^3 \Phi \circ \Phi]_{\text{A}_{\text{bif}}} > 0$. Substituting (4.22)

into $[\partial_{\mathrm{A}}^3 \Phi \circ \Phi]_{\mathrm{A_{bif}}} = 0$ and solving this equation for r we find that $r = 1$ is the boundary between the subcritical and the supercritical cases. The subcritical case is characterised by one stable branch on one side and no stable branches on the other side of the bifurcation point. The supercritical case is characterised by one stable branch on one side and two stable and one unstable branches on the other side of the bifurcation point. ■

4.5 Exact solution of the restitution boundary value problem

The equations of the system (4.3) are piecewise-linear meaning that they take a slightly different form on different intervals. Also, on each interval the equations are first-order linear and at the time intervals $t \in [0, t_a]$ and $t \in [t_a, \infty)$, $E(t_a) = a$ and $w(t_a) = a$. Therefore, the system can be solved analytically as it is explained below.

General solution The general solution of the system (4.3) is given by

$$w(t) = \begin{cases} \overset{1}{w}(t) = M_1 \exp(\alpha_1 t) + N_1 \exp(\beta_1 t) + \dfrac{1}{1+c_{\mathrm{w}}} & t \in [0, t_a] \\ \overset{2}{w}(t) = M_2 \exp(\alpha_2 t) + N_2 \exp(\beta_2 t) & t \in [t_a, \infty) \end{cases} \tag{4.23a}$$

$$E(t) = \begin{cases} \overset{1}{E}(t) = M_1(\alpha_1 + c_{\mathrm{w}}) \exp(\alpha_1 t) + N_1(\beta_1 + c_{\mathrm{w}}) \exp(\beta_1 t) + \dfrac{c_{\mathrm{w}}}{1+c_{\mathrm{w}}} & t \in [0, t_a] \\ \overset{2}{E}(t) = M_2(\alpha_2 + r c_{\mathrm{w}}) \exp(\alpha_2 t) + N_2(\beta_2 + r c_{\mathrm{w}}) \exp(\beta_2 t) & t \in [t_a, \infty) \end{cases} \tag{4.23b}$$

where $M_1,\ M_2,\ N_1$ and N_2 are functions of the model's parameters $c_{\mathrm{w}}, \varepsilon, _{\_}$ and. Furthermore, α_1, α_2, β_1 and β_2 are real eigenvalues and are found as below:

$$\alpha_1,\ \beta_1 = \Big(-(c_{\mathrm{w}} + \frac{1}{\varepsilon b}) \pm \sqrt{\Delta_1} \Big)/2$$

and

$$\alpha_2,\ \beta_2 = \Big(-(r c_{\mathrm{w}} + \frac{1}{\varepsilon b}) \pm \sqrt{\Delta_2} \Big)/2$$

provided that $\Delta_1 = (c_{\mathrm{w}} + \frac{1}{\varepsilon b})^2 - 4(\frac{1+c_{\mathrm{w}}}{\varepsilon b}) > 0$ and $\Delta_2 = (r c_{\mathrm{w}} + \frac{1}{\varepsilon b})^2 - 4(\frac{r c_{\mathrm{w}} + 1}{\varepsilon b}) > 0$.

Particular solution of the initial value problem As is shown in (4.24), the functions $M_1,\ M_2,\ N_1$ and N_2 can be found using the initial conditions:

$$E(0) = E_{\mathrm{stim}}, \quad w(0) = w_0,$$

and also

$$\overset{1}{E}(t_a) = \overset{2}{E}(t_a), \quad \overset{1}{w}(t_a) = \overset{2}{w}(t_a)$$

$$\begin{aligned}
M_1 &= w_0 - N_1 - \frac{1}{c_\mathrm{w}+1}, \\
N_1 &= \frac{(\alpha_1 w_0 + c_\mathrm{w} w_0 - E_\mathrm{stim})(1+c_\mathrm{w}) - \alpha_1}{(\alpha_1 - \beta_1 - c_\mathrm{w})(1+c_\mathrm{w})}, \\
M_2 &= \frac{M_1 \exp(\alpha_1 t_a) + N_1 \exp(\beta_1 t_a) + \frac{1}{1+cn} - N_2 \exp(\beta_2 t_a)}{\exp(\alpha_2 t_a)}, \\
N_2 &= \frac{M_1(\alpha_1 + c_\mathrm{w})\exp(\alpha_1 t_a) + N_1(\beta_1 + c_\mathrm{w})\exp(\beta_1 t_a) + \dfrac{c_\mathrm{w}}{c_\mathrm{w}+1} - M_2(\alpha_2 + r c_\mathrm{w})\exp(\alpha_2 t_a)}{\exp(\beta_2 t_a)(\beta_2 + r c_\mathrm{w})},
\end{aligned} \tag{4.24}$$

The exact solution is plotted in Figure 4.3(b) for $E(0) = 0.3,\ w(0) = 0,\ b = 0.05,\ c_\mathrm{w} = 0.15,\ r = 1,\ a = 0.25,\ \varepsilon = 1$. The parameter t_a can be found numerically as the solution of either of the equations

$$\overset{1}{E}(t_a) = a, \quad \overset{2}{E}(t_a) = a.$$

Particular solution of the periodic 1:1-restitution boundary value problem Applying the periodic forcing condition given in (4.4), the functions $M_1,\ M_2,\ N_1$ and N_2 in the solutions (4.23) can be found as functions of basic cycle length.

The expressions $M_1,\ M_2,\ N_1$ and N_2 can be found numerically as solutions of transcendental equations. Therefore, in the next section, we impose the boundary value formulations (3.8) and (3.10), and construct the restitution curves for 1:1 and 2:2 response, respectively.

4.5.1 Constructing restitution curves

Constructing 1:1 solution In order to produce the 1:1-response restitution curve, the condition (3.8) must be satisfied $\forall k \in \mathbb{N}$:

$$\begin{cases} E(kB,\ r,\ \varepsilon) = E((k+1)B,\ r,\ \varepsilon) = E_\mathrm{stim}, \\ w(kB,\ r,\ \varepsilon) = w((k+1)B,\ r,\ \varepsilon). \end{cases} \tag{4.25}$$

Hence, by imposing the above condition for $k = 0$, the functions $M_1,\ M_2,\ N_1$ and N_2 are found.

$$w(0,\ r,\ \varepsilon) = w(B,\ r,\ \varepsilon), \tag{4.26}$$

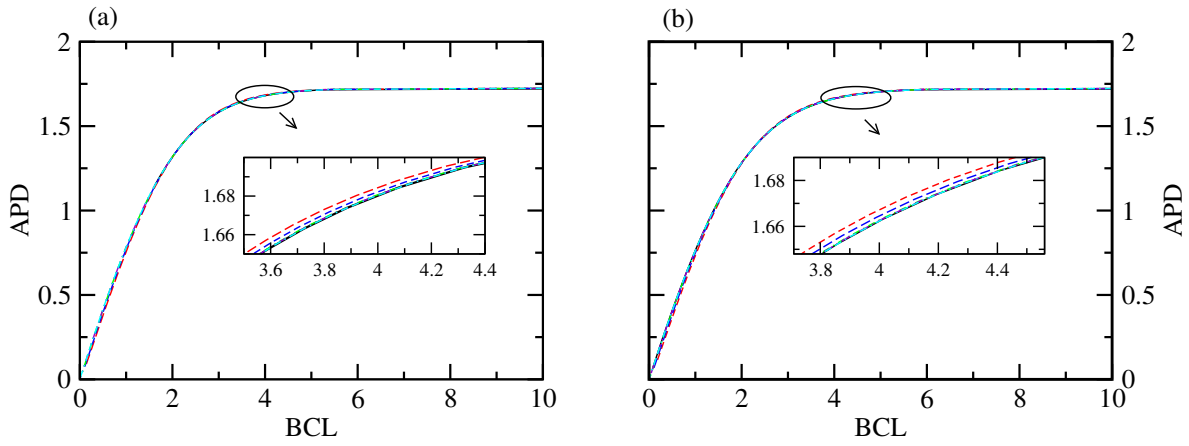

Figure 4.5: The 1:1 restitution curve for the McKean system of equations (4.3). The parameters of the model are $a = 0.25,\ b = 0.05,\ c_{\mathrm{w}} = 0.15.$ and $r = 1.5$in Figure (a) whilst $r = 0.5$ in Figure (b). In both figures, as $\varepsilon \to 0$ the numerical solutions via the BVP formulation approach the asymptotic map.

By finding the value of t_a for each B, the action potential duration restitution curve is constructed. It can be seen from Figure 4.5 that as ε decreases, the exact analytical solution approaches the asymptotic map (4.11) which corresponds to $\varepsilon = 0$.

Constructing 2:2 solution As stated in Chapter 3, in order to construct the 2:2 restitution curve, the condition (3.10) must be satisfied. This is given as below where numbers (1) and (2) denote the first and the second action potentials.

$$E_1(0,\ r,\ \varepsilon) = E_{\mathrm{stim}}, \tag{4.27}$$

$$E_2(0,\ r,\ \varepsilon) = E_{\mathrm{stim}}, \tag{4.28}$$

$$w_1(0,\ r,\ \varepsilon) = w_2(B,\ r,\ \varepsilon), \tag{4.29}$$

$$w_2(0,\ r,\ \varepsilon) = w_1(B,\ r,\ \varepsilon). \tag{4.30}$$

The value of t_a can be found now for each basic cycle length and the action potential duration restitution can be constructed for the 2:2 response. The parameters are selected using the information from Figure 4.4 so that the different situations can be found in the parameter space. As can be seen in Figure 4.6, for $r > 1$ there is a supercritical bifurcation, i.e. persistent alternans. When $r < 1$ there is a subcritical bifurcation, i.e. transient alternans. As $\varepsilon \to 0$ the curves constructed by the BVP formulation approach the asymptotic map (4.11).

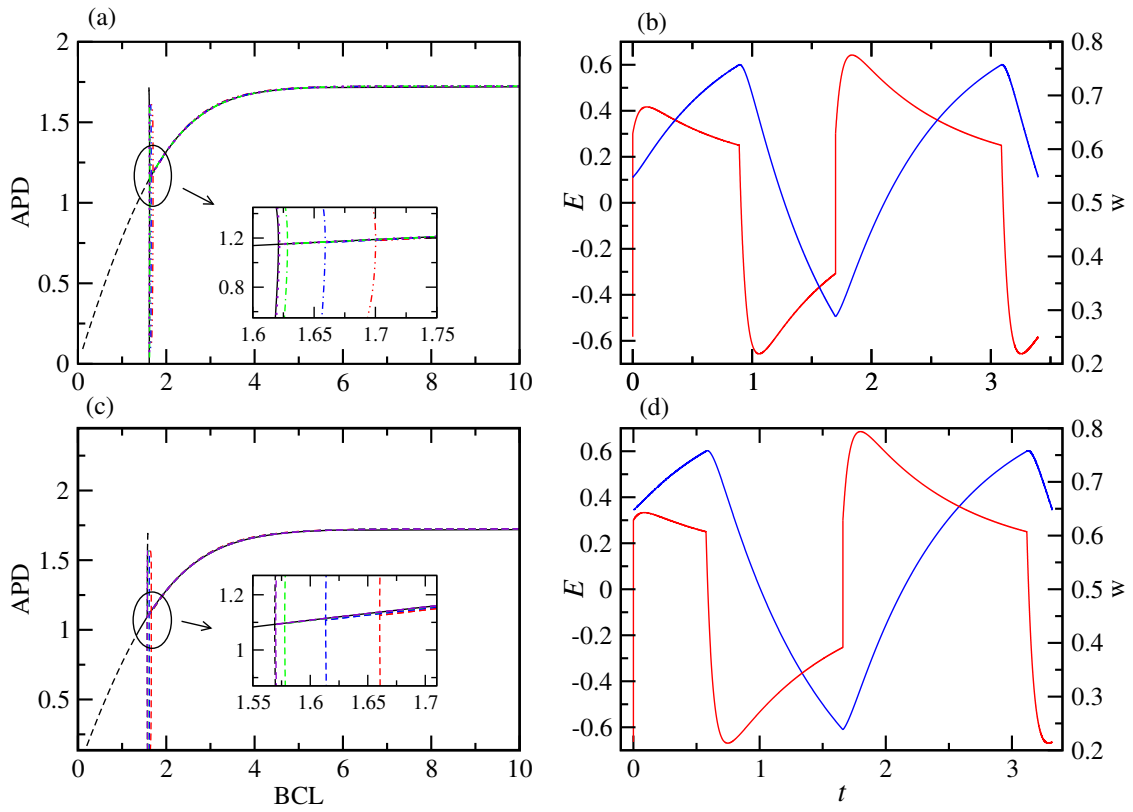

Figure 4.6: Restitution curves and selected solutions of the McKean model (4.3). The parameters are $a = 0.25,\ b = 0.05,\ c_{\rm w} = 0.15,\ E_{\rm stim} = 0.3$. Plots (a) and (c) illustrate the restitution curves for super-critical alternans at $r = 1.5$ and subcritical alternans at $r = 0.5$, respectively. When $\varepsilon \to 0$ and the numerical curves approach the asymptotic maps. In plots (b) and (d) $\varepsilon = 1$, the red curve is action potential $E(t)$ and the blue curve is the recovery gating variable $w(t)$. Plot (b) shows persistent alternans for $B = 1.6989$ when $r = 1.5$ and (d) illustrates transient alternans for $B = 1.66$ when $r = 0.5$.

4.6 Summary

In this Chapter, we have modified the recovery gating variable $w(t)$ (4.3b) by replacing its constant C with a heaviside function of voltage E and a parameter r. We have derived a one-dimensional memoryless map using asymptotic reduction methods and studied the stability of the map. We have outlined the region of parameters where the system loses its stability and alternans occurs. Moreover, we have shown that the asymptotic solution is in agreement with the McKean ODEs predictions.
The reason behind the above mentioned modification is that $w(t)$ plays an important role during the relaxation of an action potential. We have introduced a parameter r such that its role is to change the speed of evolution of $w(t)$ in the diastolic interval phase. The parameter r describes the ratio of the two branches of the w-nullcline.

We have studied the stability of the model based on changes in r. As r increases, the motion along the slow manifold (4.8) in the diastolic part, $E < a$, decreases quickly and $w(t)$ reaches its resting value very as shown in Figure 4.6(b). Therefore, the next action potential starts while the gating variable $w(t)$ has not recovered fully. As a result, it reaches its maximum value very quickly, hence the next action potential has a short duration. This is followed by a longer diastolic interval and consequently a longer action potential duration and so on so forth.

As it is illustrated in Figures 4.4, $r = 1$ is the boundary between stable alternans for $r > 1$ and unstable alternans for $r < 1$. Having described the above stages, we confirm that the evolution of the slow gating variable during the diastole phase of an action potential, determines the existence of alternans.

However, a key limitation of the McKean model is that it does not address the role of E_{stim} in inducing and maintaining instabilities. This is due to simplicity of the model and its piecewise linear functions. The threshold of excitation, E_{stim}, is an important factor in the cardiac cell functioning, therefore, studies on the effect of voltage threshold in alternans, is still lacking.

To address this issue, in the next chapter, we will study a caricature model of a cardiac action potential, proposed by (Biktashev et al., 2008). That caricature Noble model is more complex mathematically than the McKean model but solvable analytically. It parameters and variables are physiologically meaningful and the effect of threshold of excitation (E_{stim}) in inducing instabilities in the model, can be studied.

Chapter 5

Restitution and alternans in the Caricature Noble model

5.1 Introduction

In this chapter a simple model of a cardiac action potential proposed by Biktashev et al. (2008) is studied. The model is an accurate approximation of the classical Noble (1962) model of cardiac Purkinje fibers and is called the Caricature Noble model (Biktashev et al., 2008). The Noble (1962) is the first mathematical model of cardiac action potentials which is a development from the Hodgkin and Huxley (1952) model and is the prototype of all contemporary voltage-gated cardiac models. The Noble (1962) model has three currents: an inward I_{Na}, an outward I_{K} and a leak or background current. Its system consists of four ordinary differential equations describing the transmembrane voltage E, a slow potassium activation gate n, a sodium activation gate m and a sodium inactivation gate h.

The Noble (1962) model is used by Biktashev et al. (2008) as an initial step to construct the Caricature model by applying a well-justified asymptotic embedding method. The procedure of embedding artificial small parameters are discussed in a series of publications by Biktashev et al. (2008); Biktasheva et al. (2006); Simitev and Biktashev (2011). As a result, the modified version of the Noble (1962) model presented by Biktashev et al. (2008) can be considered as a detailed ionic model where the generic properties of cardiac excitability are preserved while the model is amenable to analytical study. Another advantage of the Caricature Noble model over realistic cardiac models, is the presence of small parameters in its system, therefore it can be reduced asymptotically. The realistic cardiac

models do not have explicit small parameters already present in them or they have so many parameters that it is not a straightforward task to determine which of them to use for asymptotic reduction. The main features of the caricature system, which make it an appropriate model to study and analyse, are as follows:

(a) It reproduces exactly the asymptotic structure of the authentic Noble (1962), which is guaranteed by the embedding of the artificial small parameters.

(b) It has the simplest possible functional form consistent with property (a) and allows analytical solutions to be obtained.

(c) It has all the essential features of contemporary ionic models of cardiac excitation and, unlike the FitzhHugh-Nagumo type systems, it reproduces all the stages of a cardiac action potential, including the following:

   (i) *Slow repolarisation* In cardiac action potentials the depolarisation phase, known as the "upstroke", is very fast while other phases including repolarisation, known as "downstroke", are much slower. A FitzHugh-Nagumo type system will have a fast upstroke and a fast downstroke of the action potential. Therefore these types of models, although simplified, do not reproduce the actual shape of a cardiac action potential. The Caricature model has small parameters in such a way that the downstroke of an action potential is slower than the fast upstroke but faster than the other phases of that action potential.

   (ii) *Slow sub-threshold response* When a sub-threshold stimulus is applied to an excitable system it returns immediately to its resting state. In FitzHugh-Nagumo type systems sub-threshold return and super-threshold upstroke are very fast. However, the sub-threshold return in real cells and realistic models is slower than the upstroke stage and its speed is comparable to the slow stages of the action potential.

   (iii) *Fast accommodation* Accommodation occurs when a cell is depolarised by a slowly rising stimulus current such that, if the threshold of excitation increases, the system fails to generate an action potential. In real cells and realistic models, accommodation is observed for a very fast stimulus which can be compared to the upstroke duration of an action potential. Whereas, in the FitzHugh-Nagumo type systems accommodation is observed for the stimulus which has a time scale of the duration of the whole action potential.

The Caricature Noble model as a system of three ordinary differential equations, is introduced in Section 5.2. This is followed by Section 5.3 where the model is asymptotically reduced and the phase portrait of the reduced model is studied. In Section 5.4 an asymptotic action potential duration restitution function is derived from the ordinary differential equations and the responses of the model under repeated stimulations, are described as a bifurcation problem (Guevara et al., 1984; Mitchell and Schaeffer, 2003). Following applying the methods described in the Chapter 3, the stability of the restitution function is studied and the regions of the model's parameters where different responses occur, are identified. This is followed by Section 5.5 where by applying the methods in Chapter 3, the Caricature Noble model is solved and different branches of the action potential duration restitution map, are derived analytically. The results are presented in this section, where it is shown that the asymptotic action potential duration restitution curve and the full boundary value formulated restitution curves agree closely.

Since the variables and parameters in the Caricature Noble model, have physiological roots, studying this model provides insight into realistic model. Section 5.6 summarises the results of this work, outlines the connection between this model and the physiology of the atrial cells and draws conclusions.

5.2 Formulation

The Caricature Noble model (Biktashev et al., 2008) contains three functions of time, the transmembrane voltage $E(t)$, a gating variable $h(t)$ which mimics the sodium inactivation gate and gating variable $n(t)$ that acts as the slow potassium activation gate $n(t)$. The system is governed by the following set of ordinary differential equations:

$$\frac{\mathrm{d}E}{\mathrm{d}t} = \frac{1}{\varepsilon_1\varepsilon_2} G_{Na}\,(E_{\mathrm{Na}} - E)\,H(E - E_*)\,h + \frac{1}{\varepsilon_2}\Big(\tilde{g_2}(E)\,n^4 + \widetilde{G}(E)\Big), \tag{5.1a}$$

$$\frac{\mathrm{d}h}{\mathrm{d}t} = \frac{1}{\varepsilon_1\varepsilon_2} F_h\,\big(H(E_\dagger - E) - h\big), \tag{5.1b}$$

$$\frac{\mathrm{d}n}{\mathrm{d}t} = \varepsilon_2 F_n\,\big(H(E - E_\dagger) - n\big), \tag{5.1c}$$

where the functions of the model are given by:

$$\tilde{g_2}(E) = g_{21}H(E_\dagger - E) + g_{22}H(E - E_\dagger), \qquad g_{21} = -2, g_{22} = -9,$$

$$\widetilde{G}(E) = \begin{cases} k_1(E_1 - E), & E \in (-\infty, E_\dagger), \\ k_2(E - E_2), & E \in [E_\dagger, E_*), \\ k_3(E_3 - E), & E \in [E_*, +\infty), \end{cases} \tag{5.1d}$$

$$k_1 = 3/40, \quad k_2 = 1/25, \quad k_3 = 1/10,$$

$$E_1 = -280/3, \quad E_2 = (k_1/k_2 + 1)E_\dagger - E_1 k_1/k_2 = -55, \quad E_3 = (k_2/k_3 + 1)E_* - E_2 k_2/k_3 = 1,$$

$$F_h = 1/2, \quad F_n = 1/270,$$

$$E_{\mathrm{Na}} = 40, \quad E_\dagger = -80, \quad E_* = -15, \quad G_{Na} = 100/3.$$

Here $H(\cdot)$ is the Heaviside step function and E_{Na}, E_1, E_2, E_3, E_*, $E_\dagger$ are constant voltages measured in mV. Time t is measured in ms, the units for $\tilde{g_2}$, g_{21}, g_{22} are Vs^{-1} and the units of G_{Na}, F_h and F_n are ms^{-1}. Note that in the general excitable system F_h and F_n can be represented as $1/\tau_n$ and $1/\tau_h$. The constant F_n in (5.1c) is changed to voltage-dependent function $F_n(E)$ as follows:

$$F_n(E) = f_n\left(rH(E_\dagger - E) + H(E - E_\dagger)\right),$$

hence (5.1c) becomes

$$\frac{\mathrm{d}n}{\mathrm{d}t} = F_n(E)\left(H(E - E_\dagger) - n\right), \tag{5.1e}$$

This modification is done in order to investigate the role of voltage-dependent time function in the slow gating variable (Mitchell and Schaeffer, 2003).The reason this change is applied to F_n rather than F_h, lies in the fact that $h(t)$ is a fast gating variable as it will be seen in the section 5.3. Therefore, it does not play a crucial role during the repolarisation phase of an action potential.

Note that in the above modified system when $\varepsilon_1 = \varepsilon_2 = 1$, $r = 1$ and $f_n = 1/270$ the original Caricature Noble model (Biktashev et al., 2008) is recovered. The modified Caricature Noble system is complemented by the following initial conditions

$$E(0) = E_{\mathrm{stim}}, \quad h(0) = h_0, \quad n(0) = n_0. \tag{5.2a}$$

and a "pacing" condition with basic cycle length B

$$E(kB) = E_{\mathrm{stim}}, \qquad \forall k \in \mathbb{N}. \tag{5.2b}$$

5.3 Asymptotic reduction

Consider the system of (5.1), in the limits $\varepsilon_1, \varepsilon_2 \to 0^+$ the model simplifies to a hierarchy of asymptotically reduced systems. The fast transient corresponding to the action potential upstroke and slow sub system corresponding to the repolarization and resting state of the action potential are described below.

Super-fast subsystem: The "super-fast" subsystem can now be obtained by changing the independent time variable t to a stretched time parameter $T = t/(\varepsilon_1\varepsilon_2)$. Since

$$\frac{\mathrm{d}}{\mathrm{d}t} = \frac{\mathrm{d}T}{\mathrm{d}t}\frac{\mathrm{d}}{\mathrm{d}T} = \frac{1}{\varepsilon_1\varepsilon_2}\frac{\mathrm{d}}{\mathrm{d}T},$$

equations (5.1) become

$$\frac{\mathrm{d}E}{\mathrm{d}T} = G_{Na}\left(E_{\mathrm{Na}} - E\right)H(E - E_*)\,h + \varepsilon_1\left(\tilde{g_2}(E)\,n^4 + \widetilde{G}(E)\right), \tag{5.3a}$$

$$\frac{\mathrm{d}h}{\mathrm{d}T} = F_h\left(H(E_\dagger - E) - h\right), \tag{5.3b}$$

$$\frac{\mathrm{d}n}{\mathrm{d}T} = \varepsilon_1\varepsilon_2 F_n(E)\left(H(E - E_\dagger) - n\right). \tag{5.3c}$$

Taking the limit $\varepsilon_1 \to 0^+$, yields the super-fast subsystem,

$$\frac{\mathrm{d}E}{\mathrm{d}T} = G_{Na}\left(E_{\mathrm{Na}} - E\right)H(E - E_*)\,h, \tag{5.4a}$$

$$\frac{\mathrm{d}h}{\mathrm{d}T} = F_h\left(H(E_\dagger - E) - h\right), \tag{5.4b}$$

$$\frac{\mathrm{d}n}{\mathrm{d}T} = 0. \tag{5.4c}$$

The system of equations (5.4) describes the upstroke stage of the action potential where E and h are the essential dynamical variables as can be seen in Figure 5.1(a). The gating variable n is constant and its variations during the upstroke stage is negligible.

Slow subsystem: The "slow" subsystem is obtained from equations (5.1) by rescaling time t to $\tau = t/\varepsilon_2$:

$$\frac{\mathrm{d}}{\mathrm{d}t} = \frac{\mathrm{d}\tau}{\mathrm{d}t}\frac{\mathrm{d}}{\mathrm{d}\tau} = \frac{1}{\varepsilon_2}\frac{\mathrm{d}}{\mathrm{d}\tau},$$

this yields:

$$\frac{\mathrm{d}E}{\mathrm{d}\tau} = \frac{1}{\varepsilon_1}G_{Na}\left(E_{\mathrm{Na}} - E\right)H(E - E_*)\,h + \tilde{g_2}(E)\,n^4 + \widetilde{G}(E), \tag{5.5a}$$

$$\frac{\mathrm{d}h}{\mathrm{d}\tau} = \frac{1}{\varepsilon_1}F_h\left(H(E_\dagger - E) - h\right), \tag{5.5b}$$

$$\frac{\mathrm{d}n}{\mathrm{d}\tau} = \varepsilon_2 F_n(E)\left(H(E - E_\dagger) - n\right). \tag{5.5c}$$

Taking the limit $\varepsilon_1 \to 0^+$, (5.5b) becomes:

$$F_h\left(H(E_\dagger - E) - h = 0\right) \qquad \text{which holds if and only if} \qquad h = H(E_\dagger - E).$$

When $h = H(E_\dagger - E)$ the first term in (5.5a) vanishes as $H(E-E_*)H(E_\dagger - E) \equiv 0$ despite the large factor ${\varepsilon_1}^{-1}$ in front of it i.e. when $E < E_\dagger = -80$ then $E < E_* = -15$ therefore $H(E-E_*) = 0$. When $E > E_\dagger$ but $E < E_*$, $H(E-E_*) = H(E_\dagger - E) = 0$, finally when $E > E_\dagger$ but $E > E_*$, then $H(E_\dagger - E) = 0$. The evolution of the essential dynamical variables E and n are then governed by

$$\frac{\mathrm{d}E}{\mathrm{d}\tau} = \tilde{g_2}(E)\,n^4 + \widetilde{G}(E), \tag{5.6a}$$

$$h = H(E_\dagger - E), \tag{5.6b}$$

$$\frac{\mathrm{d}n}{\mathrm{d}\tau} = \varepsilon_2 F_n(E)\left(H(E-E_\dagger) - n\right). \tag{5.6c}$$

This system describes the post-overshoot drop, the plateau, repolarization and recovery stages of the action potential. As can be seen from the equation (5.6) the slow subsystem still has a small parameter ε_2. Therefore the evolution of the system can be studied in the limits of $\varepsilon_2 \to 0^+$ and the slow subsystem, as shown in Figure 5.1(b)-(d), can be studied as "fast-" and "slow-" slow subsystems as follows:

- **Fast-slow subsystem:**In the limit $\varepsilon_2 \to 0^+$ the Equations (5.6) become:

$$\frac{\mathrm{d}E}{\mathrm{d}\tau} = \tilde{g_2}(E)\,n^4 + \widetilde{G}(E), \tag{5.7a}$$

$$h = H(E_\dagger - E), \tag{5.7b}$$

$$\frac{\mathrm{d}n}{\mathrm{d}\tau} = 0. \tag{5.7c}$$

  This essential dynamical variable is E and the system describes the post-overshoot drop and the repolarisation stages of the action potential where the variable n is a parameter and its variation is negligible. This is illustrated in Figure 5.1(c).

- **Slow-slow subsystem:**This system is obtained by rescaling back to $t_2 = \varepsilon_2\tau$ in (5.6). Since

$$\frac{\mathrm{d}}{\mathrm{d}t_2} = \frac{1}{\varepsilon_2}\frac{\mathrm{d}}{\mathrm{d}\tau},$$

  equations (5.6) become:

$$\frac{\mathrm{d}E}{\mathrm{d}t_2} = \frac{1}{\varepsilon_2}\left(\tilde{g_2}(E)\,n^4 + \widetilde{G}(E)\right), \tag{5.8a}$$

$$h = H(E_\dagger - E), \tag{5.8b}$$

$$\frac{\mathrm{d}n}{\mathrm{d}t_2} = F_n(E)\left(H(E-E_\dagger) - n\right). \tag{5.8c}$$

Taking the limit $\varepsilon_2 \to 0^+$, equations (5.8) become:

$$0 = \tilde{g_2}(E)\, n^4 + \widetilde{G}(E), \tag{5.9a}$$

$$h = H(E_\dagger - E), \tag{5.9b}$$

$$\frac{\mathrm{d}n}{\mathrm{d}t_2} = F_n(E)\left(H(E - E_\dagger) - n\right). \tag{5.9c}$$

The algebraic equation (5.9a) defines the super-slow branch and the equation (5.9c) describes the motion along this branch. This system describes the plateau (Figure 5.1(b)) and the recovery (Figure 5.1(d)) of the action potential.

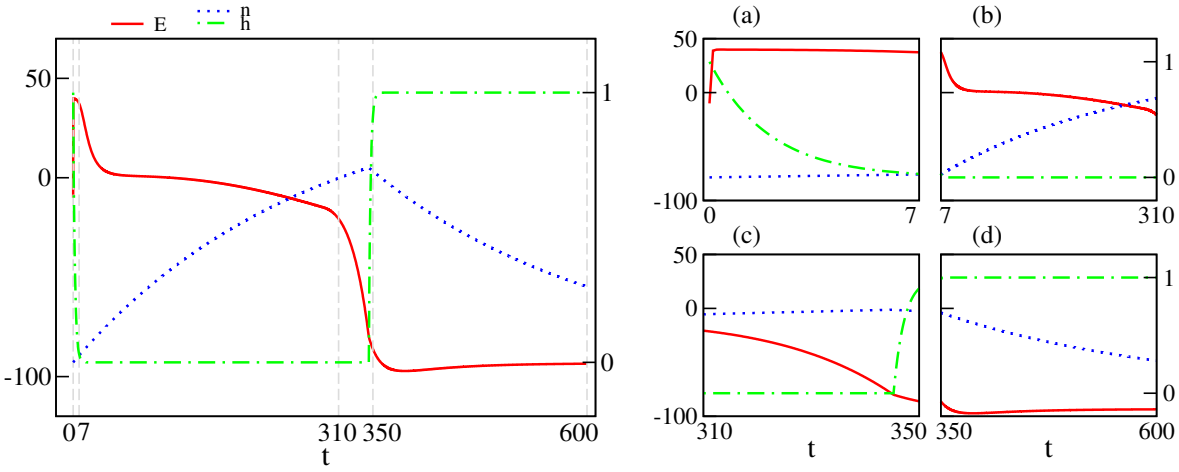

Figure 5.1: Action potential solutions of the Caricature Model (5.1) and its different regimes. (a) in the super-fast time $T = t/(\varepsilon_1\varepsilon_2) \in [0,7]$, described by system (5.4). (b), (c) and (d) in the slow-time scale $\tau = t/\varepsilon_2 \in [7,600]$, described by system (5.6). (c) illustrates the fast-slow subsystem (5.7) with E as the fast variable of the slow-subsystem, describing post-overshoot drop and the repolarisation stages in $t \in [310,350]$. (b) and (d) in the slow timescales $t_2 = \varepsilon_2\tau \in [7,310]$ and $t \in [350,600]$, described by the slow-slow subsystem (5.9c) describing plateau and the recovery stages of the action potential.

5.3.1 Phase portraits

Phase portrait of the supper-fast subsystem The system (5.4) demonstrate the evolution of the two fast variables E and h. The h-nullcline and E-nullcline are shown in Figure 5.2(a). E_* acts as a threshold of excitation, therefore, if $E_{\text{stim}} > E_*$ leads to excitation of the super-fast upstroke. If

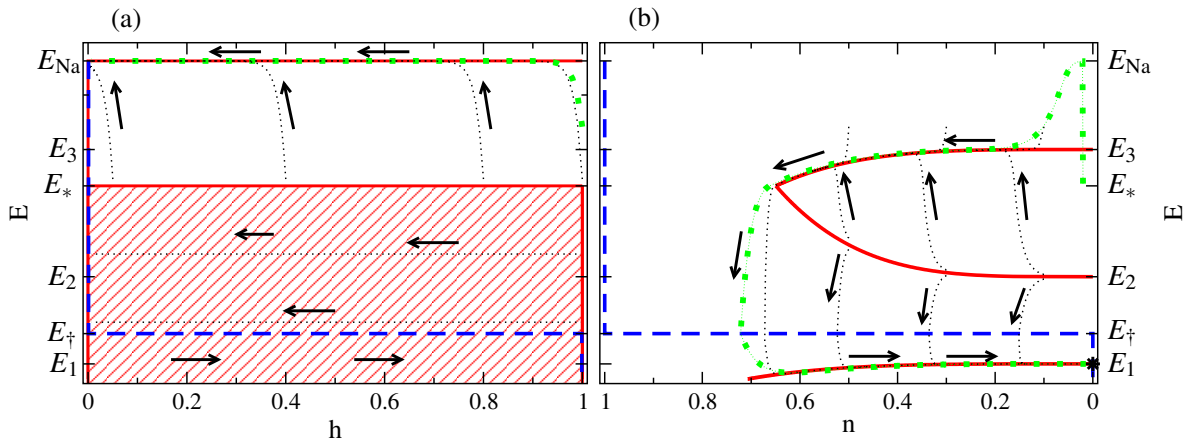

Figure 5.2: Phase portrait of the super-fast subsystem (5.4) and slow subsystem (5.6) are plotted in (a) and in (b), respectively. The red curve is nullclines $\frac{\mathrm{d}E}{\mathrm{d}t} = 0$ and black lines with attached arrows represent trajectories. One selected trajectory corresponding to initial conditions (5.47) is plotted in green. The blue lines represent nullclines $\frac{\mathrm{d}h}{\mathrm{d}t} = 0$ in (a) and $\frac{\mathrm{d}n}{\mathrm{d}t} = 0$ in (b).

$E_{\mathrm{stim}} < E_*$ the super-fast subsystem is not activated, hence the action potential will be generated by the slow-time subsystem alone Biktashev et al. (2008).

Phase portrait of the slow subsystem The phase portrait of the slow subsystem (5.6) is shown in Figure 5.2(b). The super-slow manifold is a curve, given implicitly by equation (5.9a) as follows:

$$n = \mathcal{N}(E) = \left(-\widetilde{G}(E)/\tilde{g}_2(E)\right)^{1/4}, \tag{5.10a}$$

and for $t \sim 1$ equation (5.9c) describes the motion along this manifold. As illustrated in Figure 5.2(b) the super-slow manifold is split into two parts by the condition $n^4 \geq 0$, namely the "diastolic" branch $E \in (-\infty, E_1]$ and the "systolic" branch for $E \in [E_2, E_3]$. The stability of the fast-slow equilibrium is determined by the sign of $\partial\dot{E}/\partial E$: the stable branches of the super-slow manifold correspond to regions in the (n,E) plane where its graph has a negative slope. These are the regions of the entire diastolic branch and the upper part of the systolic branch, in the range $E \in (E_*, E_3]$. Here E_* is a cusp point since $\mathcal{N}'(E_*) \neq 0$ and $\mathcal{N}'(E)$ changes its sign at the neighbourhood of the point E_*. The super-slow gating variable n takes its maximal value in the interval $E \in [E_2, E_3]$, at (n_*, E_*):

$$n_* = \left(k_3(E_3 - E_*)/g_{22}\right)^{1/4}. \tag{5.10b}$$

These considerations determine the excitability properties in terms of the slow-slow-time subsystem (5.9). As seen in Figure 5.2(b), a trajectory starting from $E_{\text{stim}} > E_2$ will be repelled by the lower systolic branch and attracted to the upper one, thus making a relatively large excursion if the following conditions are satisfied:

When $E_{\text{stim}} \in [E_2, E_*]$, $n(E_{\text{stim}})$ is defined via threshold branch of n. Therefore, for $E_{\text{stim}} \in [E_2, E_*)$, $n(0)$ must be chosen in $[0, n_{\text{thr}}(E_{\text{stim}})]$ to have an action potential. For $E_{\text{stim}} \in [E_*, \infty]$, $n(E_{\text{stim}})$ is defined by the excitable branch of the n-nullcline and $n(0) \in [0, n_*]$. Figure 5.3 illustrates these two regions of the phase portrait where the threshold branch as a function of stimulus voltage, plays an important role in forming the action potential. For a particular voltage stimulus, there is a threshold value for the gate variable n. For $n(0) > n_{\text{thr}}$ an action potential is formed, this is shown as the red regions in Figure 5.3. If $n(0) < n_{\text{thr}}$ decay back towards zero.

$$n(t_0) > n_{\text{thr}} \equiv \left(k_2(E_2 - E_{\text{stim}})/g_{22}\right)^{1/4}, \qquad n_{\text{thr}} \in [0, n_*). \tag{5.11}$$

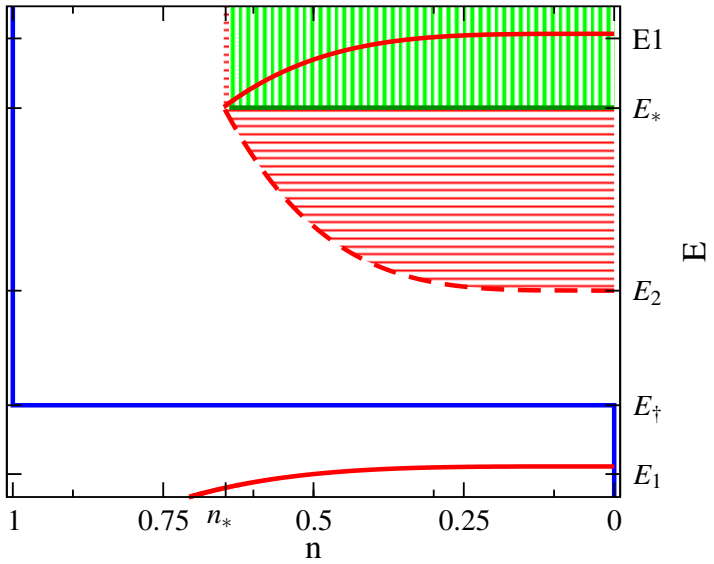

Figure 5.3: Phase portrait of the slow subsystem (5.6). The red curve is nullclines $\frac{dE}{dt} = 0$ and the blue lines represent n-nullcline. The green hatched area represent the region in which $E_{\text{stim}} \in [E_*, \infty]$ and $n(0) \in [0, n_*]$. The red hatched area, describes the role of the threshold branch (red dashed curve). For $E_{\text{stim}} \in [E_2, E_*]$, $n(0) \in [0, n_{\text{thr}}(E_{\text{stim}})]$.

This will be followed by a slow movement along the upper systolic branch. Then a jump to the

diastolic branch at (n_*, E_*) and then another slow movement along the diastolic branch approaching the global equilibrium, $(E_{ss},\ n_{ss}) = (E_1, 0)$, where the motion will eventually stop unless another super-threshold external stimulus is applied, in which case the entire cycle is repeated.

5.4 Asymptotic action potential duration restitution map

Similar to the previous chapter and following the description of the *action potential duration restitution map* in (3.1), the restitution map for the slow subsystem of the Caricature Noble model (5.6) is derived. The stability of the map is studied and the regions of the model parameters for the occurrence of a normal responses and alternans responses are outlined.

A simple action potential duration restitution map from the slow subsystem The simplest action potential duration restitution map of (5.6) is obtained in the limits $\varepsilon_1, \varepsilon_2 \to 0^+$ as follows.

Lemma 5.1 *For an action potential sequence generated as in problem* (5.6) *with* (5.2)*, we have:*

$$\mathrm{A}_k = a(n_{k-1}), \qquad a(x) \equiv {f_n}^{-1} \ln \left| \frac{1-x}{1-n_*} \right|, \tag{5.12a}$$

$$\mathrm{D}_k = d(n_k), \qquad d(x) \equiv (r f_n)^{-1} \ln \left| \frac{n_*}{x} \right|, \tag{5.12b}$$

$$n_k \equiv n(kB), \quad k \in \mathbb{N},$$

where $n_k = n(kB)$ denotes the value of the gating variable n at the beginning of the $(k+1)$-st action potential for $k \in \mathbb{N}$.

Proof The time during which the voltage in greater than E_* is the action potential duration as can be seen in Figure 5.2. Although the voltage during parts of the phase (3) exceeds E_*, as stated previously, the motion away from the slow manifold is very fast and this phase like the phase (1) of the action potential is very brief. As a result, the time required for the n gating variable to travel from its preceding value to n_* is considered to be the duration of phase (2) and is obtained by integration of $\dfrac{\mathrm{d}n}{\mathrm{d}t}$ along the systolic branch $E \in [E_*, +\infty]$. The time required for the motion at the phase four of the action potential is diastolic interval D_k and is obtained by integration of Equation (5.9c) along the diastolic branches of the super-slow manifold. Thus the following equations are obtained:

$$\mathrm{A}_k = \int_{(k-1)B}^{(k-1)B+\mathrm{A}_k} \mathrm{d}t = {f_n}^{-1} \int_{n((k-1)B)}^{n_*} \frac{\mathrm{d}n}{1-n} = {f_n}^{-1} \ln \left| \frac{1-n_{k-1}}{1-n_*} \right|, \qquad E > E_\dagger, \tag{5.13a}$$

$$\mathrm{D}_k = \int_{(k-1)B+\mathrm{A}_k}^{kB} \mathrm{d}t = -\frac{1}{rf_n}\int_{n_*}^{n(kB)} \frac{\mathrm{d}n}{n} = \frac{1}{rf_n}\ln\left|\frac{n_*}{n_k}\right|, \qquad E < E_\dagger. \tag{5.13b}$$

The crucial observation in deriving expressions (5.12) is that in this limit the end of any plateau phase coincides with the beginning of the next recovery stage when the slow gating variable n takes its maximal value $n_{\max}$ on the systolic branch of the super-slow manifold (5.10a), that is

$$n\left((k-1)B+\mathrm{A}_k\right) = n\left(kB+\mathrm{A}_{k+1}\right) = n_*, \qquad \text{for any} \qquad k \in \mathbb{N}.$$

This is well illustrated by the phase portrait in Figure 5.2(b). ∎

Proposition 5.1 *An action potential duration restitution map relating* A_{k+1} *to* A_k *is given by*

$$\begin{aligned} \mathrm{A}_{k+1} &= \Phi(\mathrm{A}_k), \\ \Phi(\mathrm{A}) = F(\tilde{\mathbf{a}},\mathrm{D}) = F(\mathbf{a},B-\mathrm{A}) &= \frac{1}{f_n}\log\left(\frac{1-n_*\exp\left(-rf_n\left(B-\mathrm{A}\right)\right)}{1-n_*}\right), \end{aligned} \tag{5.14}$$

where $\tilde{\mathbf{a}}$ *is a vector of the Caricature Noble model's parameters, i.e.* $\tilde{\mathbf{a}} = [\mathbf{a},B]^T = [r,f_n,n_*,B]^T$.

Proof The result is obtained by eliminating n_k between expression (5.12a) written for A_{k+1} and expression (5.12b) written for $\mathrm{D}_k = B - \mathrm{A}_k$. ∎

Lemma 5.1 gives a parametric representation of the action potential duration restitution map and Proposition (5.1) gives an equivalent explicit representation.

Fixed points We now find the fixed points of Φ and $\overline{\overline{\mathrm{A}}} = \Phi\circ\Phi(\overline{\overline{\mathrm{A}}})$ corresponding the 1:1- and 2:2-responses

Proposition 5.2 *The equation* $\overline{\mathrm{A}} = \Phi(\overline{\mathrm{A}})$ *has a unique solution branch given in parametric form by*

$$\overline{\mathrm{A}} = a(\overline{n}), \qquad \overline{\mathrm{D}} = \mathrm{d}(\overline{n}), \tag{5.15}$$

for a parameter $\overline{n} \in [0, n_{\mathrm{thr}}]$.

Proof In order or obtain the solution of the equation $\overline{\mathrm{A}} = \Phi(\overline{\mathrm{A}})$, the equivalent parametric representation of Lemma 5.1 is used. In a 1:1 response $\mathrm{A}_k = \mathrm{A}_{k+1}$ and $\mathrm{D}_k = \mathrm{D}_{k+1}$, equivalent by (5.12) to $a(n_{k-1}) = a(n_k)$ and $d(n_k) = d(n_{k+1})$, respectively. By the bijectivity of the logarithm function, solutions are $n_{k-1} = n_k \equiv \overline{n}$ and $n_k = n_{k+1} \equiv \overline{n}$, respectively. Note that in a 1:1 response all action potentials start from identical values of the n gate, $\overline{n}$, therefore expressions (5.15) hold. As the parameter $\overline{n}$ is a gating variable it must be in the range $[0,1]$. Furthermore, no action potential can be excited above n_{thr} so $\overline{n} \in [0, n_{\mathrm{thr}}]$. ∎

Perturbation solution of $\overline{\mathrm{A}} = \Phi(\overline{\mathrm{A}})$ It is also possible to find an explicit approximation to the solution of $\overline{\mathrm{A}} = \Phi(\overline{\mathrm{A}})$ by using a regular perturbation approach. Note that equation (5.14) is exactly solvable in the case $r = 1$. Expanding the unknown $\overline{\mathrm{A}}$ in a Taylor series near $r = 1$ yields

$$\overline{\mathrm{A}} = \sum_{m=0}^{\infty} (1-r)^m \mathrm{A}_m.$$

Upon substitution of the expansion in equation (5.14), collecting powers of the small quantity $(1-r)$, and solving for the expansion coefficients A_m, the fixed point $\overline{\mathrm{A}}$ is obtained as follows

$$\overline{\mathrm{A}} = \mathrm{A}_0 + (1-r)\mathrm{A}_1 + O\big((1-r)^2\big), \tag{5.16}$$

where

$$\begin{aligned}
\mathrm{A}_0 &= B - \frac{1}{f_n}\ln(\gamma), \\
\mathrm{A}_1 &= -\frac{1}{f_n}\ln(\gamma)\left(1 + \frac{n_*}{\gamma}(1-r)\right), \\
\gamma &= (1-\exp(Bf_n))\, n_* + \exp(Bf_n).
\end{aligned}$$

Proposition 5.3 *The equation* $\overline{\overline{\mathrm{A}}} = \Phi \circ \Phi(\overline{\overline{\mathrm{A}}})$ *has three solution branches: the first branch is obtained by the Proposition* (5.15) *and the other two are given in parametric form by*

$$\overline{\overline{\mathrm{A}}}_{\mathrm{even}} = a(\alpha n_{\mathrm{e}}), \qquad \overline{\overline{\mathrm{D}}}_{\mathrm{even}} = d(n_{\mathrm{e}}), \tag{5.17a}$$

$$\overline{\overline{\mathrm{A}}}_{\mathrm{odd}} = a(n_{\mathrm{e}}), \qquad \overline{\overline{\mathrm{D}}}_{\mathrm{odd}} = d(\alpha n_{\mathrm{e}}), \tag{5.17b}$$

$$n_{\mathrm{e}} = \frac{\alpha^{1/r} - 1}{\alpha^{(r+1)/r} - 1}, \tag{5.17c}$$

with a parameter $\alpha \in (0, \infty)$.

Proof Similar to the proof of the Proposition (5.15), the transcendental equation $\overline{\overline{\mathrm{A}}} = \Phi \circ \Phi(\overline{\overline{\mathrm{A}}})$ is not solved directly and the equivalent parametric representation of Lemma 5.1 is used. In a 2:2 response

$$\mathrm{A}_{2k} = \mathrm{A}_{2k+2} \qquad \text{and} \qquad \mathrm{A}_{2k+1} = \mathrm{A}_{2k+3}, \qquad \forall k \in \mathbb{N}$$

as well as

$$\mathrm{D}_{2k} = \mathrm{D}_{2k+2} \qquad \text{and} \qquad \mathrm{D}_{2k+1} = \mathrm{D}_{2k+3}, \qquad \forall k \in \mathbb{N}.$$

Thus, by applying the expressions (5.12), the following equations are obtained:

$$n_{2k-1} = n_{2k+1} \equiv n_{\mathrm{o}} \qquad \text{and} \qquad n_{2k} = n_{2k+2} \equiv n_{\mathrm{e}}.$$

The basic cycle length B is assumed to be fixed, therefore it is required that

$$B = \mathrm{A}_{2k} + \mathrm{D}_{2k} = \mathrm{A}_{2k+1} + \mathrm{D}_{2k+1} \iff a(n_\mathrm{o}) + d(n_\mathrm{e}) = a(n_\mathrm{e}) + d(n_\mathrm{o}), \tag{5.18}$$

and explicitly $\ln\big((1-n_\mathrm{o})/(1-n_\mathrm{e})\big) = r^{-1}\ln\big(n_\mathrm{e}/n_\mathrm{o}\big)$. By the bijectivity of the logarithm function and after the change of variable $n_\mathrm{o} = \alpha n_\mathrm{e}$ this equation reduces to $\alpha(1-\alpha n_\mathrm{e})^r = (1-n_\mathrm{e})^r$ with exact solution (5.17). Equations (5.17a) and (5.17b) follow immediately. To establish the range of α note that (5.18) is invariant with respect to exchanging n_o and n_e, so without loss of generality the case $n_\mathrm{o} \geq n_\mathrm{e}$ is considered and since n_o and n_e are positive it follows that $n_\mathrm{o}/n_\mathrm{e} = \alpha \in (1,\infty)$. Finally, a fixed point of Φ is also a fixed point of $\Phi\circ\Phi$, hence (5.15) is a third solution branch of $\overline{\overline{\mathrm{A}}} = \Phi\circ\Phi(\overline{\overline{\mathrm{A}}})$.

Remark 3 *The solutions* (5.15) *and* (5.17) *can be verified by back-substitution into* $\overline{\mathrm{A}} = \Phi(\overline{\mathrm{A}})$ *and* $\overline{\overline{\mathrm{A}}} = \Phi\circ\Phi(\overline{\overline{\mathrm{A}}})$*, respectively.*

■

Stability and bifurcations of equilibria We now impose conditions (3.4b) and (3.5b) to establish the stability properties of 1:1 and 2:2 responses.

Proposition 5.4 *The equilibrium* (5.15) *of the action potential duration restitution map* (5.14) *loses stability in a flip (period-doubling) bifurcation at*

$$n_\mathrm{bif} = 1/(1+r) \tag{5.19a}$$

or in terms of the basic cycle length, alternatively at

$$B_\mathrm{bif} = \frac{1}{f_n}\log\left(\frac{r{n_*}^{1/r}(1+r)^{(1-r)/r}}{(1-n_*)}\right). \tag{5.19b}$$

Equation (5.19b) *defines a surface where 2:2 response bifurcates from the 1:1 response and is denoted as* S_1 *in figure 5.4.*

Proof Inserting (5.15) into (3.4b), the border of stability is obtained as

$$\overline{n} = n_\mathrm{bif} = 1/(1+r) \in (0,1) \quad \text{if} \quad \Big[\partial_\mathrm{A}\Phi(\mathbf{a},\mathrm{A})\Big]_{\overline{\mathrm{A}}} = -1$$

or

$$\overline{n} = n_\mathrm{bif} = 1/(1-r) \in (-\infty,0)\cup(1,\infty) \quad \text{if} \quad \Big[\partial_\mathrm{A}\Phi(\mathbf{a},\mathrm{A})\Big]_{\overline{\mathrm{A}}} = 1.$$

Since the gating variables are defined in the interval $[0,1]$, the second solution which is outside this interval, is rejected. The first solution is valid and since it is obtained at

$$[\partial_{\mathrm{A}}\Phi(\mathbf{a},\mathrm{A})]_{\overline{\mathrm{A}}} = -1 \tag{5.20}$$

At the end of the the k-st action potential, $n_k = 1-(1-n_*)\exp f_n(B-\mathrm{D})$ and when $\mathrm{D}=\mathrm{D}_{\mathrm{bif}}$ then $n_{\mathrm{bif}} = 1-(1-n_*)\exp f_n(B_{\mathrm{bif}}-\mathrm{A}_{\mathrm{bif}})$. Rewriting the expression in (5.20) in terms of n_{bif}, we obtain the point at which stability is lost in a flip bifurcation of the action potential duration restitution map (5.14). Evaluating (5.15) at $n_{\mathrm{bif}} = 1/(1+r)$ we then find

$$\mathrm{A}_{\mathrm{bif}} = a(n_{\mathrm{bif}}) = {f_n}^{-1}\ln\left(\frac{n_{\mathrm{bif}}-1}{n_*-1}\right), \tag{5.21a}$$

$$\mathrm{D}_{\mathrm{bif}} = d(n_{\mathrm{bif}}) = (rf_n)^{-1}\ln\left(\frac{n_*}{n_{\mathrm{bif}}}\right), \tag{5.21b}$$

$$B_{\mathrm{bif}} = a(n_{\mathrm{bif}})+d(n_{\mathrm{bif}}) = {f_n}^{-1}\ln\left(\frac{r{n_*}^{1/r}(1+r)^{(1-r)/r}}{(1-n_*)}\right). \tag{5.21c}$$

■

Proposition 5.5 *The equilibria* (5.17) *of the second-generation map* $\Phi\circ\Phi$ *bifurcate from the equilibrium* (5.15) *of the action potential duration restitution map* (5.14) *at* (5.19) *and lose their stability at* $r=1$.

Proof To confirm that the equilibria (5.17) bifurcate from the equilibrium (5.15), we evaluate (5.17c) at $\alpha=1$, which is the value where $n_{\mathrm{e}} = n_0$. Since

$$n_{\mathrm{e}}(\alpha) = n_{\mathrm{e}}(1) = 1/(1+r) = n_{\mathrm{bif}}$$

then (5.15) and (5.17), intersect at n_{bif}, where (5.17) first emerges. Recall that a flip bifurcation for Φ is a pitchfork bifurcation for the second generation map $\Phi\circ\Phi$ (Strogatz, 2001). A pitchfork bifurcation can be either supercritical if $[\partial^3_{\mathrm{A}}\Phi\circ\Phi]_{\mathrm{A}_{\mathrm{bif}}} < 0$ or subcritical if $[\partial^3_{\mathrm{A}}\Phi\circ\Phi]_{\mathrm{A}_{\mathrm{bif}}} > 0$. Substituting (5.21) into $[\partial^3_{\mathrm{A}}\Phi\circ\Phi]_{\mathrm{A}_{\mathrm{bif}}} = 0$ and solving it for r, we find that $r=1$ is the boundary between the subcritical and the supercritical cases. The subcritical case is as it was explained before, has one stable branch on one side and no branches on the other side of the bifurcation point. The supercritical case has one stable branch on one side and two stable branches and one unstable branch on the other side of the bifurcation point. ■

Thresholds As stated in the previous chapter, the 1:1 responses are stable when condition (3.4c) is satisfied where $\overline{B}_{\text{thr}} < B$ is the threshold value of basic cycle length for excitation of a 1:1 response. The 2:2 responses are stable for $B > \overline{\overline{B}}_{\text{thr}}$ which is the condition (3.5c) such that $\overline{\overline{B}}_{\text{thr}}$ is the threshold value for excitation of 2:2 response. These conditions are explained in propositions and respectively.

Proposition 5.6 *The threshold value of basic cycle length B for excitation of a 1:1 response is*

$$\overline{\text{A}}_{\text{thr}} = a(n_{\text{thr}}) = {f_n}^{-1} \log\left((1-n_{\text{thr}})/(1-n_*)\right), \tag{5.22a}$$

$$\overline{\text{D}}_{\text{thr}} = d(n_{\text{thr}}) = (r f_n)^{-1} \log(n_*/n_{\text{thr}}), \tag{5.22b}$$

$$\overline{B}_{\text{thr}} = \overline{\text{A}}_{\text{thr}} + \overline{\text{D}}_{\text{thr}}. \tag{5.22c}$$

The surface given by the equation (5.22c) *is the threshold for existence of the 1:1 response. It is illustrated as a blue surface in Figure 5.4 and denoted by* S_2.

Proof The k-th action potential can only be excited by a super-threshold stimulus that rises the voltage sufficiently to pass the nullcline i.e. $E_{\text{stim}} > E_2$ for which $n_{k-1} < n_{\text{thr}}$ where n_{thr} is a function of E_{stim} and it is given by (5.11). The result then follows by evaluation of (5.15) at $\overline{n} = n_{\text{thr}}$. Since $n_{\text{thr}} = n_{\text{thr}}(E_{\text{stim}})$, then

$$\overline{\text{A}}_{\text{thr}} = \overline{\text{A}}_{\text{thr}}(n_{\text{thr}}) = \overline{\text{A}}_{\text{thr}}(E_{\text{stim}}, r)$$

$$\overline{\text{D}}_{\text{thr}} = \overline{\text{D}}_{\text{thr}}(n_{\text{thr}}) = \overline{\text{D}}_{\text{thr}}(E_{\text{stim}}, r)$$

$$\overline{B}_{\text{thr}} = \overline{B}_{\text{thr}}(n_{\text{thr}}).$$

Hence (5.22c) a function of E_{stim} and r. ∎

Proposition 5.7 *The threshold value of basic cycle length for the excitation of a 2:2 response is*

$$\overline{\overline{B}}_{\text{thr}} = a(n_{\text{thr}}) + d(\alpha(n_{\text{thr}})n_{\text{thr}}) = a(\alpha(n_{\text{thr}})n_{\text{thr}}) + d(n_{\text{thr}}), \tag{5.23a}$$

where $\alpha(n_{\text{thr}})$ *is the solution of the equation*

$$n_{\text{thr}} = \left(\alpha^{1/r} - 1\right) / \left(\alpha^{(r+1)/r} - 1\right). \tag{5.23b}$$

Equation (5.23a) *is the threshold for existence of the 2:2 response and is a function of* E_{stim} *and r. This surface is shown in a black transparent surface in Figure 5.4 and is denoted by* S_3.

Proof Similar to the proof of the Proposition (5.6), E_{stim} must be greater than E_2 for which n_{k-1} is smaller than n_{thr} given by (5.11). Evaluating (5.17) at $n_{\text{e}} = n_{\text{thr}}$ and treating n_{thr} as a parameter, equation (5.17c) is inverted. ■

The surfaces B_{bif}, $\overline{B}_{\text{thr}}$ and $\overline{\overline{B}}_{\text{thr}}$ are plotted in Figure 5.4 as red, blue and black surfaces. The parameter regions where 1:1 and 2:2 response occur, are well illustrated in Figure 5.4 where the dimensionless parameter r changes from 0 to 3.5 and E_{stim} changes from -55 (mV) to -15 (mV). Boundary between normal response and 2:2 response is the surface $r = 1$ and is plotted as a green surface in Figure 5.4. When $r < 1$ the responses of the system is a norm 1:1 response. For $r > 1$ the system exhibits instability in 1:1 response.

Remark 4 *The range of E_{stim} is chosen based on the phase portrait of the slow subsystem in Figure 5.2.*

In order to gain a better understanding of Figure 5.4 various 2 dimensional slices of the figure are depicted in Figure 5.5. Column (a) of Figure 5.5 shows the cross sections given by $B = 250$ (ms) and $B = 300$ (ms) respectively. In the first diagram alternans occurs in the gray region where $r \approx 1.8$. As the basic cycle length increases the gray region of occurrence of alternans shrinks and has completely disappeared by the time $B = 300$ (ms), as is visible in the lower diagram. Column (b) shows the cross sections given by $E_{\text{stim}} = -20$ (mV) and $E_{\text{stim}} = -50$ (mV) respectively. In each case the gray region between B_{bif} and $\overline{B}_{\text{thr}}$ is where alternans occurs. This region shrinks as E_{stim} decreases. As stated previously, the value of E_{stim} determines whether an action potential can be formed or there is no action potential. Column (c) shows the cross sections in E_{stim}-B space, given by $r = 2.5$ and $r = 0.5$ respectively. As r decreases from 2.5, the gray region of alternans becomes smaller and has completely disappears by $r = 0.5$. We now have the solution of the system (5.9), in the next section, we analyse the slow-system (5.6)

5.5 Exact solution of the restitution boundary value problem

In this section the slow subsystem and the full system are solved analytically, their general solutions are obtained and by imposing boundary conditions described in the Chapter 3, particular solutions for different responses are derived. In addition, the restitution curves for 1:1 response and 2:2 response are constructed.

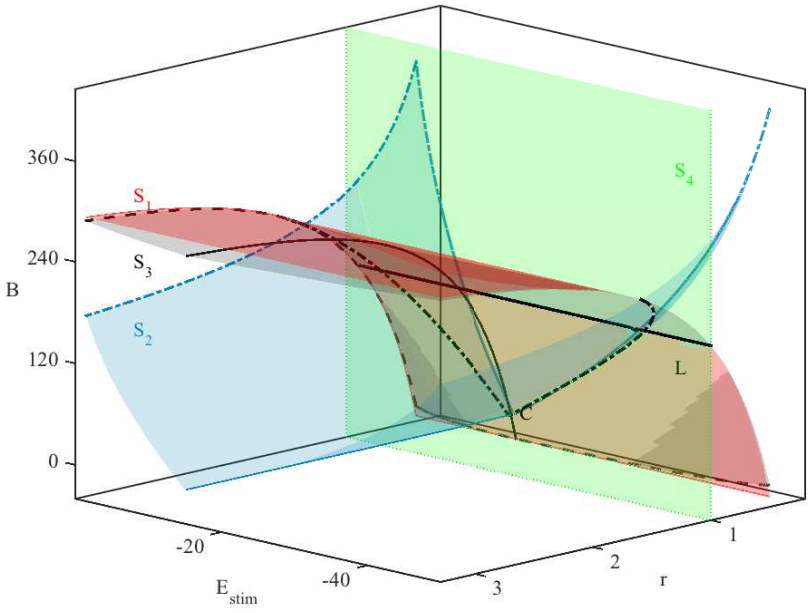

Figure 5.4: Bifurcation set in the E_{stim}-r-B parameter space. The red surface S_1 is defined by (5.19b) and illustrates the region where 2:2 response bifurcates from the 1:1 response. The blue surface S_2 is defined by (5.22c) and indicates the threshold for existence of the 1:1 response. The transparent black surface S_3 given by (5.23a) is the threshold for existence of the 2:2 response. The green surface S_4 with equation $r = 1$ separates region of alternans $(r > 1)$ from healthy response $(r < 1)$

Remark 5 *Depending on the initial value of the transmembrane voltage, Simitev and Biktashev (2011) described three types of solutions for the slow subsystem* (5.6) *and the full system* (5.6)*. The cases are well illustrated in Figure 5.2 and described below:*

Case 1 *The initial value of the voltage is greater than the threshold of the beginning of the fast system* (5.4)*, that is* $E_0 > E_*$*. In this case, the fast current is activated and a normal fast-upstroke action potential is initiated.*

Case 2 *The initial value of the voltage* E_0 *is greater than the threshold value of* E_2 *of the beginning of the slow subsystem* (5.6) *but less than the threshold of the beginning of the fast system* (5.4)*. Then the fast current is not involved and the slow subsystem is sufficient enough to describe the action potential.*

Case 3. *If the initial value of the voltage* E_0 *is less than the threshold value* E_2 *of the slow subsystem*

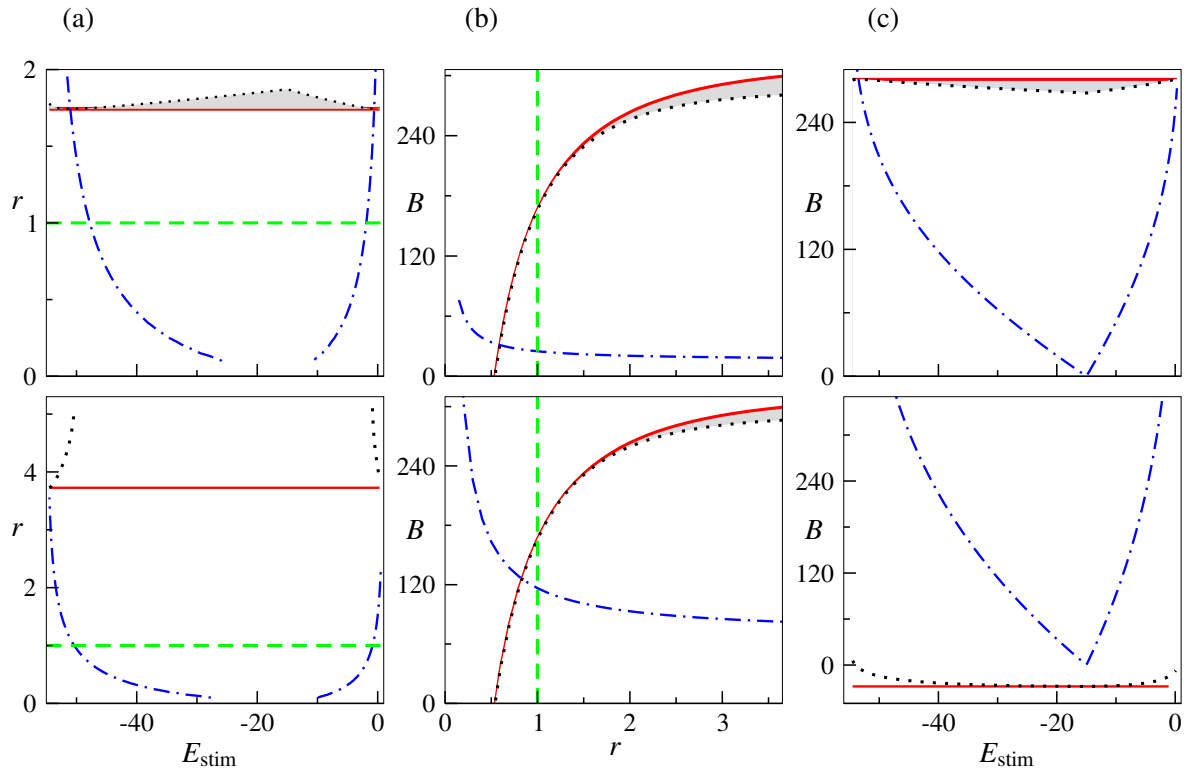

Figure 5.5: Projections of the 3 dimensional figure are shown in 2 dimensional visualisations. The colour code is the same as in Figure 5.4. Reading each column from top to bottom, the projections are (a) $B = 250$ (ms), $B = 300$ (ms), (b) $E_{\text{stim}} = -20$ (mV), $E_{\text{stim}} = -50$ (mV), (c) $r = 2.5$, $r = 0.5$, respectively. The region in which alternans occurs is shaded in gray in each plot.

(5.6). *Then the voltage decays and no action potential is excited.*

Cases 1 and 2, which are description of action potentials for different initial values of voltage, are solved analytically in this chapter. Case 3 does not exhibit an action potential, therefore we do not study this case.

5.5.1 The slow subsystem

It is possible to solve the slow system of the caricature model (5.6) analytically and obtain an exact solution. Equation (5.6c) is linear and simple enough to be easily solved. After its solutions are substituted into the voltage equation (5.6a), the equation also becomes a first-order linear ODE which can be solved analytically.

5.5.1.1 Case 1. Normal fast-upstroke action potential

In this case, since we do not have the fast system here, the voltage increases but does not reach E_{Na}. The action potential is formed but it does not have an upstroke.

$$E(0) = E_0 > E_*, \quad n(0) = n_0. \tag{5.24}$$

Solution of the initial value problem The system (5.6) has the following solutions for the time intervals $t \in [0, t_*]$, $[t_*, t_\dagger]$ and $[t_\dagger, \infty)$.

$$n(t) = \begin{cases} 1 - (1 - n_0)\exp(-f_n t), & t \in [0, t_\dagger] \\ \left(1 - (1 - n_0)\exp(-f_n t_\dagger)\right)\exp\left(f_n r(t_\dagger - t)\right), & t \in [t_\dagger, \infty) \end{cases} \tag{5.25a}$$

$$E(t) = \begin{cases} \overset{1}{E}(t) = (N(t) - N(0) + E_0)\exp(\frac{-k_3}{\varepsilon_2}t), & t \in [0, t_*] \\ \overset{2}{E}(t) = w(t) + (E_* - w(t_*))\exp(\frac{k_2(t-t_*)}{\varepsilon_2}), & t \in [t_*, t_\dagger] \\ \overset{3}{E}(t) = m(t) + (E_\dagger - m(t_\dagger))\exp\left(\frac{k_1}{\varepsilon_2}(t_\dagger - t)\right), & t \in [t_\dagger, \infty) \end{cases} \tag{5.25b}$$

where

$$N(t) \equiv E_3 \exp(\frac{k_3 t}{\varepsilon_2}) + g_{22}\sum_{l=0}^{4}(n_0 - 1)^l \binom{4}{l} \frac{\exp\left((-\varepsilon_2 l f_n + k_3)t\right)}{k_3 - l\varepsilon_2 f_n},$$

$$w(t) \equiv E_2 + g_{22}\sum_{l=0}^{4}(n_0 - 1)^l \binom{4}{l} \frac{\exp\left(-l f_n t\right)}{-k_2 - l\varepsilon_2 f_n},$$

$$m(t) \equiv E_1 + \frac{g_{21}}{k_1 - 4\varepsilon_2 f_n r}\sum_{l=0}^{4}(n_0 - 1)^l \binom{4}{l} \exp\left((4 f_n r - l f_n)t_\dagger\right)\exp(-4 f_n r t),$$

This exact analytical solution is plotted in Figure 5.6 for $E(0) = -10$ (mV), $n(0) = 0$ and all other parameters as in (5.1). The parameters t_* and $t_\dagger$are found numerically to be $t_* = 292.815$ (ms) and $t_\dagger = 345.240$ (ms). They are obtained as solutions of

$$\overset{1}{E}(t_*) = \overset{2}{E}(t_*) = E_*, \qquad \overset{2}{E}(t_\dagger) = \overset{3}{E}(t_\dagger) = E_\dagger. \tag{5.26}$$

The effect of ε_2 in the repolarisation of the action potential is apparent from the figure, where in Figure 5.6(a) $\varepsilon_2 = 1$ and in Figure 5.6(b) $\varepsilon_2 = 0.1$.

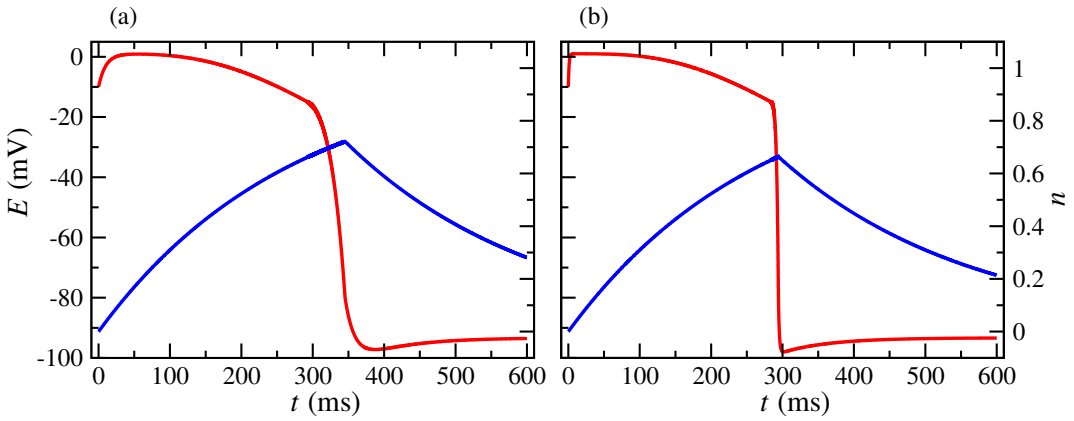

Figure 5.6: The exact solution (5.25) of the slow subsystem (5.6) for the range $t \in [0, 600]$. The red curve is voltage E and the blue curve is the evolution of n-gating variable. In (a) $\varepsilon_2 = 1$ and in (b) $\varepsilon_2 = 0.1$.

Solution of the periodic boundary value problem In this case the conditions are

$$E(0) = E_0 > E_*, \quad n(0) = n(kB) \quad \forall k \in \mathbb{N}. \tag{5.27}$$

Imposing conditions (5.27), the general solutions are as follows

$$n(t) = \begin{cases} 1 - \mathrm{C}_1 \exp(-f_n t), & t \in [0, t_\dagger] \\ \left(1 - \mathrm{C}_1 \exp(-f_n t_\dagger)\right) \exp\left(f_n r (t_\dagger - t)\right), & t \in [t_\dagger, \infty) \end{cases} \tag{5.28a}$$

$$E(t) = \begin{cases} \overset{1}{E}(t) = (N(t) - N(0) + E_0) \exp\left(\frac{-k_3}{\varepsilon_2} t\right), & t \in [0, t_*] \\ \overset{2}{E}(t) = w(t) + (E_* - w(t_*)) \exp(\frac{k_2 (t - t_*)}{\varepsilon_2}), & t \in [t_*, t_\dagger] \\ \overset{3}{E}(t) = m(t) + (E_\dagger - m(t_\dagger)) \exp\left(\frac{k_1}{\varepsilon_2}(t_\dagger - t)\right), & t \in [t_\dagger, \infty) \end{cases} \tag{5.28b}$$

where

$$N(t) \equiv E_3 \exp(\frac{k_3 t}{\varepsilon_2}) + g_{22} \sum_{l=0}^{4} (-\mathrm{C}_1)^l \binom{4}{l} \frac{\exp\left((-\varepsilon_2 l f_n + k_3) t\right)}{k_3 - l \varepsilon_2 f_n},$$

$$w(t) \equiv E_2 + g_{22} \sum_{l=0}^{4} (-\mathrm{C}_1)^l \binom{4}{l} \frac{\exp\left(-l f_n t\right)}{-k_2 - l \varepsilon_2 f_n},$$

$$m(t) \equiv E_1 + \frac{g_{21}}{k_1 - 4\varepsilon_2 f_n r} \sum_{l=0}^{4} (-\mathrm{C}_1)^l \binom{4}{l} \exp\left((4 f_n r - l f_n) t_\dagger\right) \exp(-4 f_n r t),$$

Constructing the restitution curves

1:1 restitution curve In order to construct the 1:1 restitution curve, the condition (3.8) must be satisfied $\forall k \in \mathbb{N}$, i.e. we require that

$$\begin{aligned} E(0,\ r,\ \varepsilon_2) &= E(B,\ r,\ \varepsilon_2) = E_{\text{stim}}, \\ n(0,\ r\ \varepsilon_2) &= n(B,\ r,\ \varepsilon_2), \end{aligned} \tag{5.29}$$

By imposing the condition (5.29) for $k = 0$, the constant C_1 as a function of B and $t_\dagger$ is found.

$$\begin{aligned} \overset{1}{n}(0) &= \overset{2}{n}(B), \\ 1 - \mathrm{C}_1 &= (1 - \mathrm{C}_1 \exp(-f_n t_\dagger)) \exp\left(f_n r (t_\dagger - B)\right). \end{aligned}$$

Thus the following expression for the constant function C_1 is obtained

$$\mathrm{C}_1 = \frac{1 - \exp\left(f_n r (t_\dagger - B)\right)}{1 - \exp\left((-f_n t_\dagger) - f_n r (B - t_\dagger)\right)}. \tag{5.30}$$

Substituting the function (5.30) into the voltage (5.28b) gives an expression for $E(t)$ as a function of B and $t_\dagger$. In order to construct the restitution curve, the value of $t_\dagger$ is found numerically. Figure 5.7 illustrates $t_\dagger$ against basic cycle length B for different values of ε_2. As ε_2 decreases from 1 to 0, the 1:1 restitution curves approach the asymptotic map (5.14). The value of $t_\dagger$ in Figures 5.7(a) and 5.7(b) differs slightly since the is understandable from the formula (6.9). It can be seen in the Figure 5.7 that as r increases, the action potential duration also increases. Note that although the 1:1 restitution curve is constructed for a wide range of basic cycle length, this solution is not stable for all the values of B and it loses its stability at some basic cycle length $B = \overline{B}_{\text{thr}}$. The occurrence of the "unstable" solution is explained as below.

2:2 restitution curves We now apply condition (3.10) to the solutions of (5.28) and the 2-cycle solution corresponding to the 2:2 response is derived. The following condition must be satisfied

$$E_{\text{even}}(0,\ r,\ \varepsilon_2) = E_{\text{stim}}, \tag{5.31a}$$

$$E_{\text{odd}}(0,\ r,\ \varepsilon_2) = E_{\text{stim}}, \tag{5.31b}$$

$$n_{\text{even}}(0,\ r,\ \varepsilon_2) = n_{\text{odd}}(B,\ r,\ \varepsilon_2), \tag{5.31c}$$

$$n_{\text{odd}}(0,\ r,\ \varepsilon_2) = n_{\text{even}}(B,\ r,\ \varepsilon_2), \tag{5.31d}$$

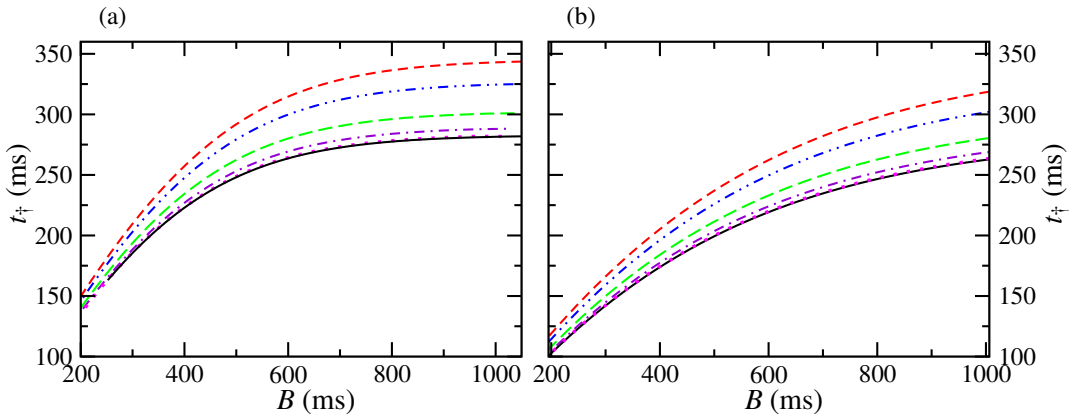

Figure 5.7: Action potential duration restitution curves for 1:1 response in comparison with the asymptotic restitution curve. The red, blue, green, violet and magenta curves are for ε_2 values of 1, 0.6, 0.2,0.05 and 0.001, respectively. The black solid curve is the asymptotic action potential duration restitution map (5.14). In (a) $r = 1.8$ and in (b) $r = 0.8$.

where "even" and "odd" refer to two succeeding action potentials with different durations. Now the conditions (5.31) are applied on the exact solution of the n-gating variable. Recall the exact solution for (5.28a), hence it yields:

$$\begin{cases} {}^{1}n_{\text{even}}(0) = {}^{2}n_{\text{odd}}(B), \\ {}^{2}n_{\text{even}}(B) = {}^{1}n_{\text{odd}}(0), \end{cases} \tag{5.32}$$

The equations (5.32) are solved simultaneously using the solution of the initial value problem as an initial guess. Thus, similar to the previous part, we formulate the $E(t)$ solution as a function of B and $t_\dagger$. By decreasing the value of B and finding the $t_\dagger$ for each basic cycle length, the restitution curves for different ε_2 are constructed. For $r > 1$ the bifurcation is Supercritical and stable alternans occur. The restitution curves for this condition are illustrated in Figure 5.8(a) and when $r < 1$ the bifurcation is subcritical and alternans is unstable as can from Figure 5.8(c). Different action potential duration-restitution curves from the exact analytical solutions are plotted in figure 5.8(a). As $\varepsilon_2 \to 0$ the exact solution reaches the asymptotic solution (5.14).

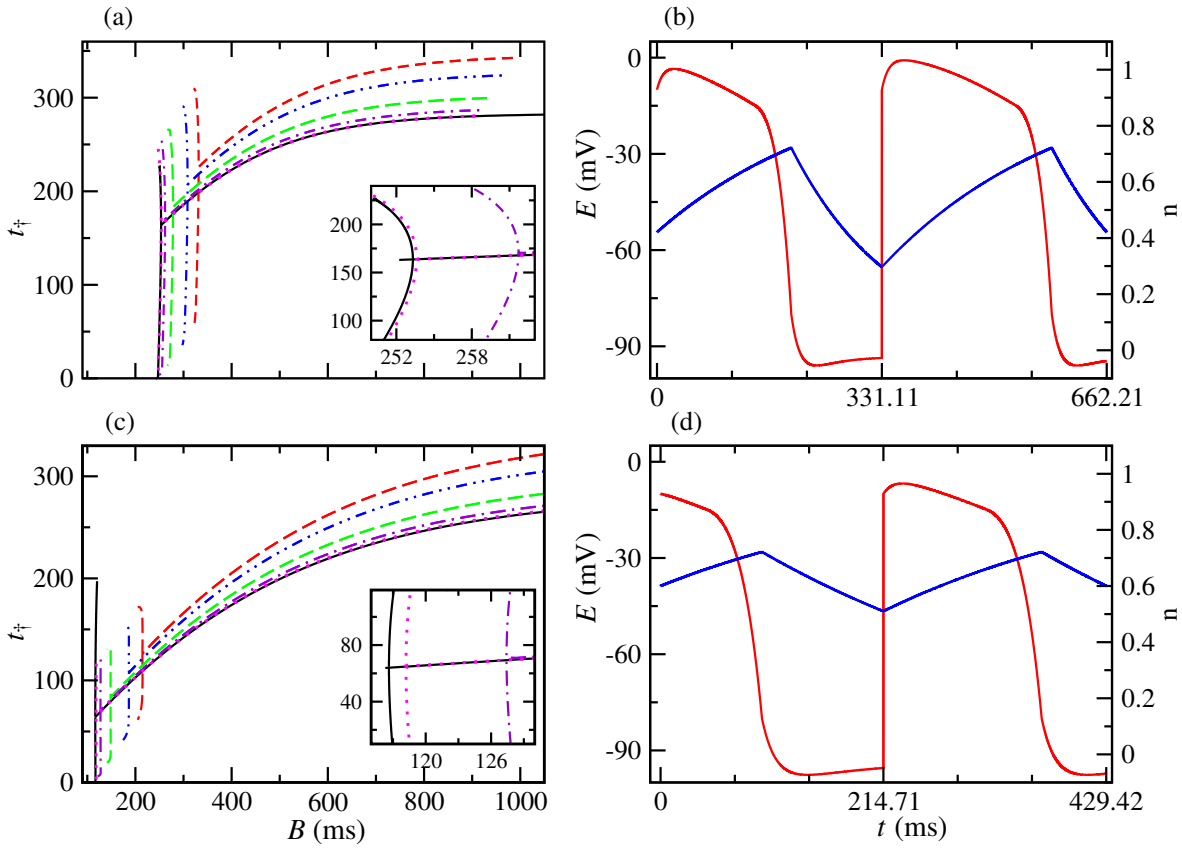

Figure 5.8: The restitution curves from the exact analytical solution are compared with the asymptotic map. The red, blue, green, purple and magenta correspond to $\varepsilon_2 = 1, 0.6, 0.2, 0.05, 0.005$, respectively and the black curve is the asymptotic map corresponding to $\varepsilon_2 = 0$. In (a) $r = 1.8$ and in (b) stable alternans at $B = 331$ (ms) is illustrated. In (c) $r = 0.8$ and in (d) an unstable alternans at $B = 214$ (ms).

5.5.1.2 Case 2. Slow over-threshold response

The slow over-threshold response is when the initial value of the voltage is less than the threshold of the beginning of the fast system and the following initial conditions are considered:

$$E(0) = E_2 < E_0 < E_*, \quad n(0) = n_0, \tag{5.33}$$

Solution of the initial value problem The system (5.6) has the following solutions for the time intervals $t \in [0, t_{*1}]$, $t \in [t_{*1}, t_{*2}]$, $[t_{*2}, t_\dagger]$ and $[t_\dagger, \infty)$.

$$n(t) = \begin{cases} 1 - (1-n_0)\exp(-f_n t), & t \in [0, t_\dagger] \\ \big(1 - (1-n_0)\exp(-f_n t_\dagger)\big)\exp\big(f_n r(t_\dagger - t)\big), & t \in [t_\dagger, \infty) \end{cases} \tag{5.34a}$$

$$E(t) = \begin{cases} \overset{1}{E}(t) = w(t) + (E_0 - w(0))\exp\left(\frac{k_2}{\varepsilon_2} t\right), & t \in [0, t_{*1}] \\ \overset{2}{E}(t) = N(t) + (E_* - N(t_{*1}))\exp\left(\frac{k_3}{\varepsilon_2}(t - t_{*1})\right), & t \in [t_{*1}, t_{*2}] \\ \overset{3}{E}(t) = w(t) + (E_* - w(t_{*2}))\exp\left(\frac{k_2}{\varepsilon_2}(t - t_{*2})\right), & t \in [t_{*2}, t_\dagger] \\ \overset{4}{E}(t) = m(t) + (E_\dagger - m(t_\dagger))\exp\left(\frac{k_1}{\varepsilon_2}(t_\dagger - t)\right), & t \in [t_\dagger, \infty) \end{cases} \tag{5.34b}$$

where

$$N(t) \equiv E_3 \exp(\frac{k_3 t}{\varepsilon_2}) + g_{22} \sum_{l=0}^{4} (n_0 - 1)^l \binom{4}{l} \frac{\exp\left((-\varepsilon_2 l f_n + k_3)t\right)}{k_3 - l\,\varepsilon_2 f_n},$$
$$w(t) \equiv E_2 + g_{22} \sum_{l=0}^{4} (n_0 - 1)^l \binom{4}{l} \frac{\exp\left(-l f_n t\right)}{-k_2 - l\,\varepsilon_2 f_n},$$
$$m(t) \equiv E_1 + \frac{g_{21}}{k_1 - 4\varepsilon_2 f_n r} \sum_{l=0}^{4} (n_0 - 1)^l \binom{4}{l} \exp\big((4 f_n r - l f_n) t_\dagger\big) \exp(-4 f_n r t).$$

The exact analytical solution is plotted in Figure 5.9 for $E(0) = -30$ (mV), $n(0) = 0$, $\varepsilon_2 = 1$ and all other parameters as in (5.1). The parameters t_{*1}, t_{*2} and $t_\dagger$ are determined numerically to be $t_{*1} = 11.750$ (ms), $t_{*2} = 292.815$ (ms) and $t_\dagger = 345.240$ (ms), as solutions of

$$\overset{1}{E}(t_{*1}) = \overset{2}{E}(t_{*1}) = E_*, \qquad \overset{2}{E}(t_{*2}) = \overset{3}{E}(t_{*2}) = E_*, \qquad \overset{3}{E}(t_\dagger) = \overset{3}{E}(t_\dagger) = E_\dagger. \tag{5.35}$$

Solution of the periodic boundary value problem In this case the conditions are:

$$E(0) = E_* < E_0 < E_2, \quad n(0) = n(kB) \forall k \in \mathbb{N}, \tag{5.36}$$

$$n(t) = \begin{cases} 1 - \mathrm{C}_2 \exp(-f_n t), & t \in [0, t_\dagger] \\ \big(1 - \mathrm{C}_2 \exp(-f_n t_\dagger)\big)\exp\big(f_n r(t_\dagger - t)\big), & t \in [t_\dagger, \infty) \end{cases} \tag{5.37a}$$

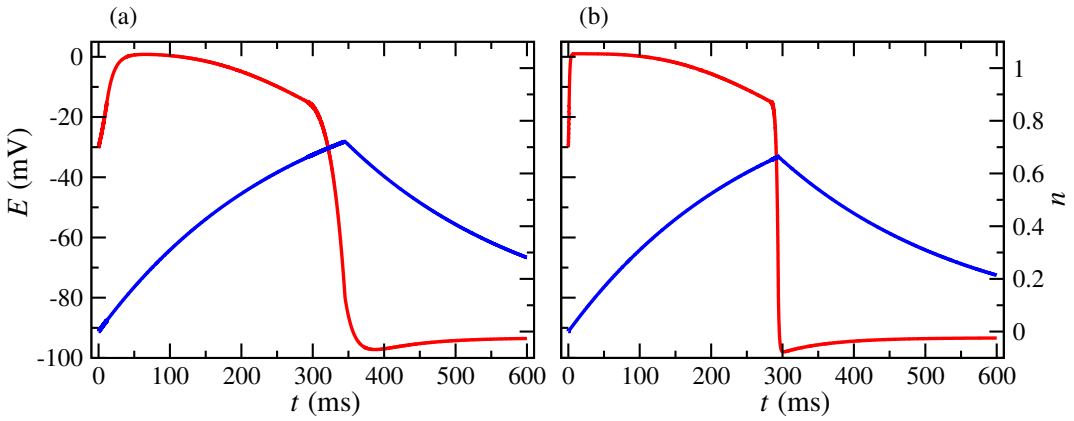

Figure 5.9: The exact solution (5.34) of the slow subsystem (5.6) for the range $t \in [0, 600]$. The red curve is voltage $E(t)$ and the blue curve is the evolution of n-gating variable. In (a) $\varepsilon_2 = 1$ and in (b) $\varepsilon_2 = 0.1$.

$$E(t) = \begin{cases} \overset{1}{E}(t) = (E_0 - w(0))\exp(\frac{k_2}{\varepsilon_2}t) + w(t), & t \in [0, t_{*1}] \\ \overset{2}{E}(t) = (E_* - N(t_{*1}))\exp\left(\frac{k_3}{\varepsilon_2}(t - t_{*1})\right) + N(t), & t \in [t_{*2}, t_\dagger] \\ \overset{3}{E}(t) = (E_* - w(t_{*2}))\exp\left(\frac{k_2}{\varepsilon_2}(t - t_{*2})\right) + w(t), & t \in [t_{*2}, t_\dagger] \\ \overset{4}{E}(t) = (E_\dagger - m(t_\dagger))\exp\left(\frac{k_1}{\varepsilon_2}(t_\dagger - t)\right) + m(t), & t \in [t_\dagger, \infty) \end{cases} \tag{5.37b}$$

where

$$N(t) \equiv E_3 \exp\left(\frac{k_3 t}{\varepsilon_2}\right) + g_{22} \sum_{l=0}^{4} (-C_2)^l \binom{4}{l} \frac{\exp\left((-\varepsilon_2 l f_n + k_3)t\right)}{k_3 - l\varepsilon_2 f_n},$$

$$w(t) \equiv E_2 + g_{22} \sum_{l=0}^{4} (-C_2)^l \binom{4}{l} \frac{\exp(-l f_n t)}{-k_2 - l\varepsilon_2 f_n},$$

$$m(t) \equiv E_1 + \frac{g_{21}}{k_1 - 4\varepsilon_2 f_n r} \sum_{l=0}^{4} (-C_2)^l \binom{4}{l} \exp\left((4 f_n r - l f_n)t_\dagger\right) \exp(-4 f_n r t),$$

Having obtained the exact analytical solution for the slow system in case two, similar to the previous part, we can now impose the boundary conditions and demonstrate restitution curves.

Constructing the restitution curves Similar to the previous Case, the conditions (5.29) and (5.31)are applied to the solutions (5.37). Note that the exact solution for n-gating variable is identical for cases 1 and 2 therefore, the constant function C_2 is identical to C_1. Consequently the 1:1 restitution curves in Figure 5.10 and 2:2 restitution curves in Figure 5.11 are similar to the case 1.

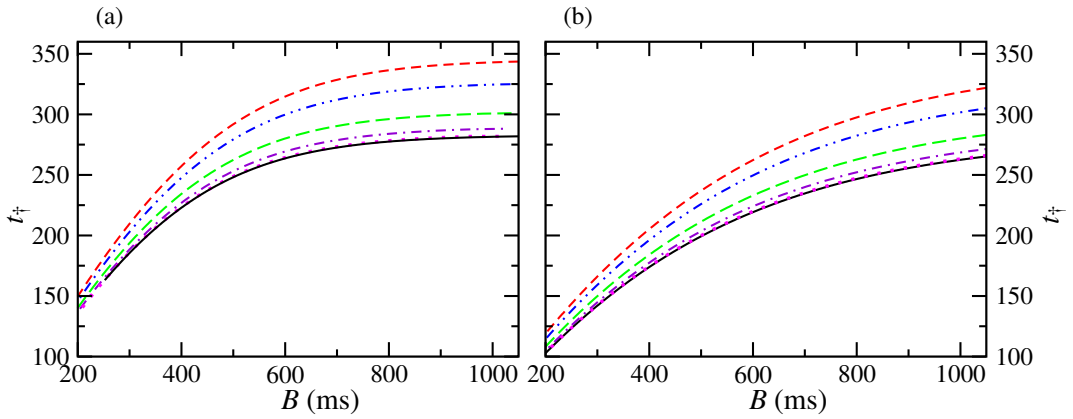

Figure 5.10: Action potential duration restitution curves with boundary conditions (5.29) imposed on the solutions (5.37). The red, blue, green, violet and magenta curves are for ε_2 values of 1, 0.6, 0.2, 0.05 and 0.001, respectively. The black solid curve is the asymptotic action potential duration restitution map (5.14). In (a) $r = 1.8$ and in (b) $r = 0.8$.

1:1 restitution curve The 1:1 restitution curve for this case is illustrated in figure 5.10. Similar to the case 1, as ε_2 decreases, the exact analytical solution approaches the asymptotic map (5.14).

2:2 restitution curves The 2:2 restitution curves are shown in Figure 5.11, where similar to the previous part, the restitution curves for different ε_2 are constructed. For $r > 1$ the bifurcation is Supercritical and stable alternans occur. The restitution curves for this condition are illustrated in Figure 5.11(a) and action potentials illustrating alternans are plotted in Figure 5.11(b) for $B = 330$ ms. When $r < 1$ the bifurcation is subcritical and alternans is unstable as can be seen in Figure 5.11(c) and action potentials are plotted in Figure 5.11(d) for $B = 317$ ms. As $\varepsilon_2 \to 0$ the exact solution reaches the asymptotic solution (5.14).

Figures 5.8(a) and 5.11(a) are illustrations of the top row of Figure 5.5(c). When r is greater than 1, there is alternans at $B = 250$ (ms) for the asymptotic solution and for exact solutions with $\varepsilon_2 = 0.001$. These solutions depicted by black curve and magneta curves respectively in Figures 5.8(a) and 5.11(a).

As ε_2 increases from 0 to 1, the position of the bifurcation value of B gets deformed. The deformation of B_{bif} is illustrated in red curve in Figure 5.12(a) as a function of ε_2 and the following formula for B_{bif} is derived by fitting the data to a curve:

$$B_{\text{bif}} = 368.32 - 114.08\exp(-1.1\varepsilon_2). \tag{5.38}$$

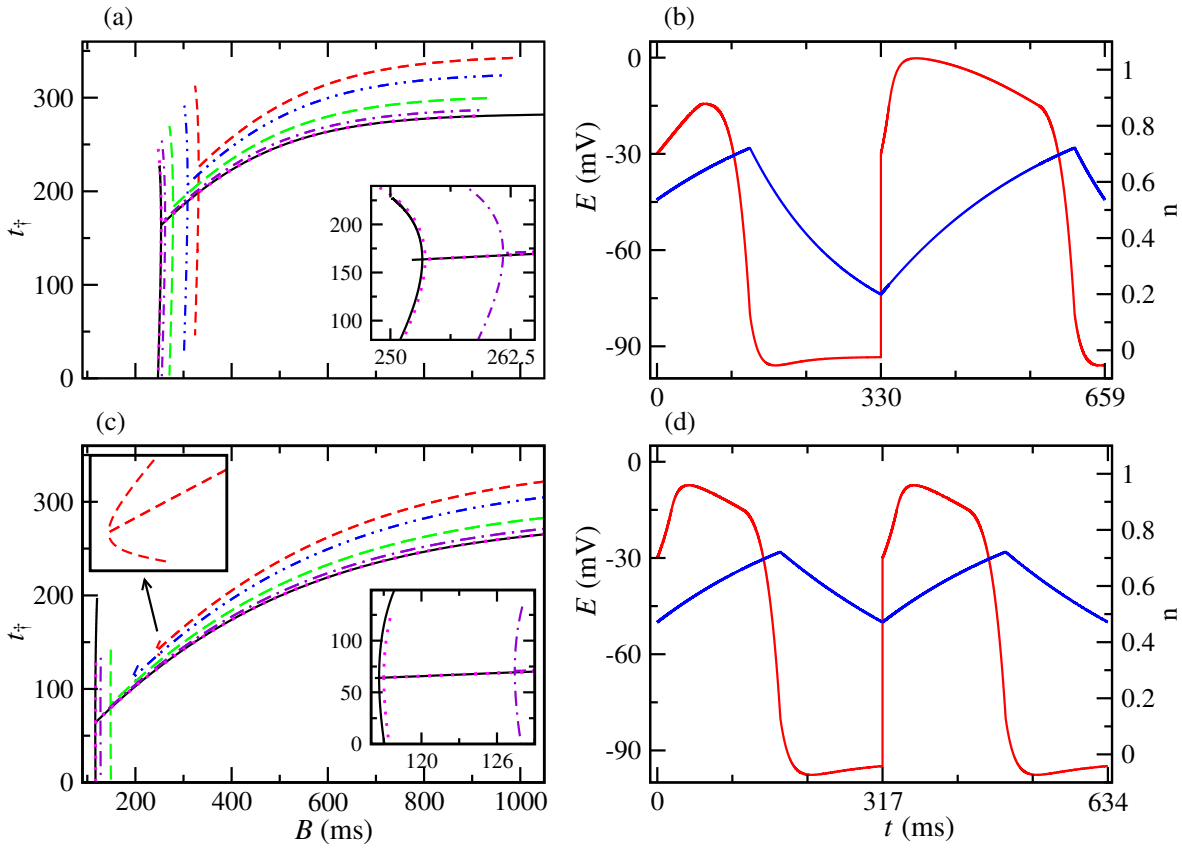

Figure 5.11: The restitution curves from the exact analytical solution are compared with the asymptotic map. The blue, red, green and magenta correspond to $\varepsilon_2 = 1$, 0.6, 0.2, 0.05, 0.005, respectively and the black curve is the asymptotic map corresponding to $\varepsilon_2 = 0$. In (a) $r = 1.8$ and in (b) stable alternans at $B = 330$ (ms) is illustrated. In (c) $r = 0.8$ and in (d) an unstable alternans at $B = 317$ (ms).

According to Figure 5.12 the bifurcation occurs at $B_{\text{bif}} = 330$ when $\varepsilon_2 = 1$. This finding is confirmed with action potentials in Figures 5.8(b) and 5.11(b), in which bifurcation occurs at $B = 331$ (ms) for case 1 and $B = 329$ (ms) for case 2.

The threshold $\overline{\overline{B}}_{\text{thr}}$ for the existence of the 1:1 response also changes its position as ε_2 increases from 0 to 1. This displacement is shown as blue curve in Figure 5.12(a) and the following formula for $\overline{\overline{B}}_{\text{thr}}$ as a function of ε_2 is derived:

$$\overline{\overline{B}}_{\text{thr}} = 397.71 - 148.2\exp(-0.67\varepsilon_2). \tag{5.39}$$

Figures 5.8(c) and 5.11(c) are illustrations of the bottom row of Figure 5.5(c). When r is less

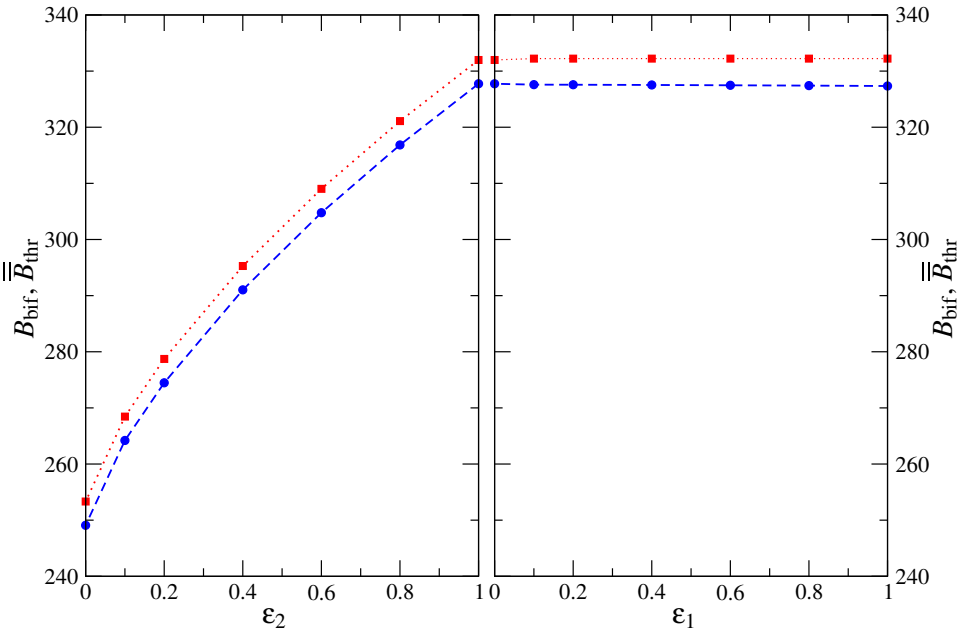

Figure 5.12: Several data points for B_{bif} and $\overline{\overline{B}}_{\text{thr}}$ together with their approximating curves. The red squares are data points for B_{bif} and the blue circles are the data points for $\overline{\overline{B}}_{\text{thr}}$. The region between these two curves is the region where stable alternans occurs. In plot (a) B_{bif} and $\overline{\overline{B}}_{\text{thr}}$ are functions of ε_2 as (5.38) and (5.39), respectively. Plot(b) shows B_{bif} and $\overline{\overline{B}}_{\text{thr}}$ as functions of ε_1.

than 1 alternans does not occur. The system undergoes an unstable pitchfork bifurcation over a very small interval $r \in [0.7, 1)$. The bifurcation is compared for different values of ε_2 in Figures 5.11(c) and 5.11(c). The restitution curve as a function of r for the slow subsystem is plotted in Figure 5.13. The Basic cycle length and E_{stim} are fixed and the curve is obtained for different values of r. When $B = 250$ (ms) and $E_{\text{stim}} = -10$ (mV) there is a bifurcation at $r = 1.8$. This is in agreement with Figure 5.5(a) and 5.5(c). As basic cycle length increases from 250 (ms) to 320 (ms) the value of r at which bifurcation occurs increases. At large basic cycle length, even if r increases, there is no bifurcation as can be seen in Figure 5.13 where for $B \geq 350$ there is no alternation of action potential duration.

5.5.2 The full system of the Caricature Noble model

In this section the approach presented in Section 5.5.1 is used and the full Caricature Noble system (5.1) is analysed. Two cases based on the initial value of voltage E_0 are considered and the full

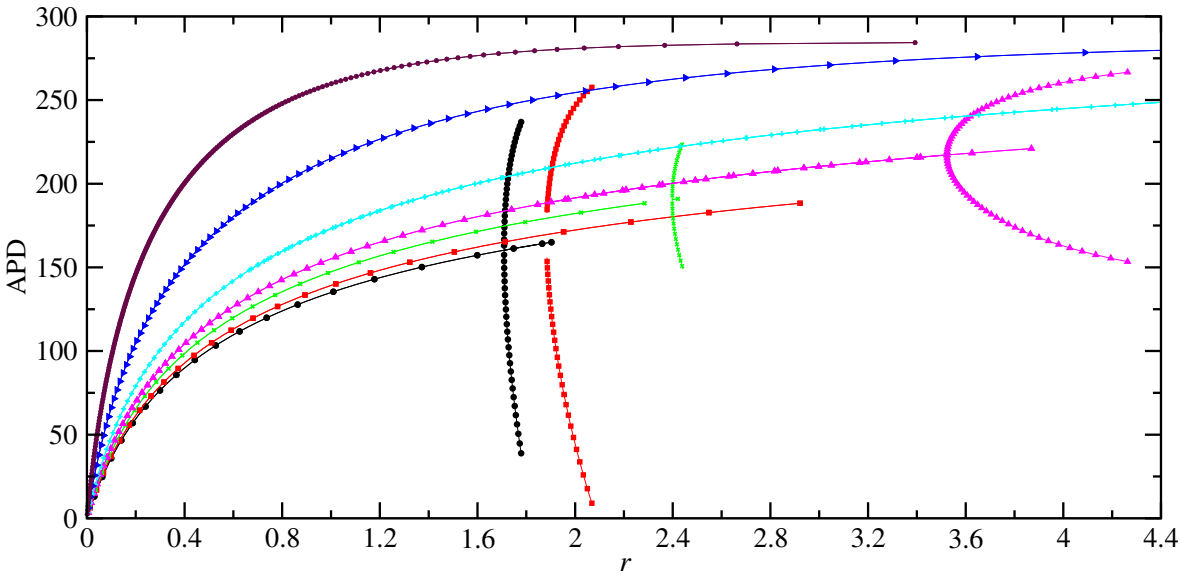

Figure 5.13: The action potential duration restitution curve as a function of r. $E_{\text{stim}} = -10$ (mV) and from the top to bottom the values of basic cycle length are 800, 500, 350, 300, 280, 260, 250 (ms).

system is solved analytically. Since the fast gating variable h is included in the full system, hence the role of the fast current and the fast subsystem is also studied in this section.

5.5.2.1 Case 1. Normal fast-upstroke action potential

Solution of the initial value problem In this case the following initial conditions are applied to the full Caricature system (5.1):

$$E(0) = E_0 > E_*, \quad h(0) = h_0, \quad n(0) = n_0, \tag{5.40}$$

Equations (5.1b) and (5.1c) are separable and can be easily solved. After their solutions are substituted into the voltage equation (5.1a) it becomes a first order ordinary differential equation and the system (5.1) has the following exact analytical solutions for the time intervals $t \in [0, t_*]$, $t \in [t_*, t_\dagger]$ and $t \in [t_\dagger, \infty)$.

$$n(t) = \begin{cases} 1 - (1 - n_0)\exp(-f_n t), & t \in [0, t_\dagger] \\ \left(1 - (1 - n_0)\exp(-f_n t_\dagger)\right)\exp\left(f_n r(t_\dagger - t)\right), & t \in [t_\dagger, \infty) \end{cases} \tag{5.41a}$$

$$h(t) = \begin{cases} h_0 \exp\big(-F_h t/(\varepsilon_1\varepsilon_2)\big), & t \in [0, t_\dagger] \\ 1 - (\exp(F_h t_\dagger/(\varepsilon_1\varepsilon_2)) - h_0)\exp(-F_h t/(\varepsilon_1\varepsilon_2)), & t \in [t_\dagger, \infty) \end{cases} \tag{5.41b}$$

$$E(t) = \begin{cases} \overset{1}{E}(t) = \exp\left(\dfrac{G_{Na}h_0}{F_h}\exp\left(-\dfrac{F_h t}{\varepsilon_1\varepsilon_2}\right) - \dfrac{k_3 t}{\varepsilon_2}\right) \times \\ \qquad \left[E_0 \exp\left(-\dfrac{G_{Na}h_0}{F_h}\right) - k_3 E_3\, u(-k_3\varepsilon_1, t)\right. \\ \qquad -g_{22}\displaystyle\sum_{l=0}^{4}\binom{4}{l}(n_0-1)^l\; u(-k_3\varepsilon_1 + \varepsilon_1\varepsilon_2 l f_n, t) \\ \qquad \left. -\dfrac{G_{Na}h_0 E_{\mathrm{Na}}}{\varepsilon_1}\, u(-k_3\varepsilon_1 + F_h, t)\right], & t \in [0, t_*] \\ \overset{2}{E}(t) = w(t) + (E_* - w(t_*))\exp\left(\frac{k_2}{\varepsilon_2}(t - t_*)\right), & t \in [t_*, t_\dagger] \\ \overset{3}{E}(t) = m(t) + (E_\dagger - m(t_\dagger))\exp\left(\frac{k_1}{\varepsilon_2}(t_\dagger - t)\right), & t \in [t_\dagger, \infty) \end{cases} \tag{5.41c}$$

where

$$u(\varkappa, t) \equiv \frac{\varepsilon_1}{F_h}\left(\frac{F_h}{G_{Na}h_0}\right)^{\frac{\varkappa}{F_h}}\left[\Gamma\left(\frac{\varkappa}{F_h}, \frac{G_{Na}h_0}{F_h}\right) - \Gamma\left(\frac{\varkappa}{F_h}, \frac{G_{Na}h_0}{F_h}\exp\left(-\frac{F_h t}{\varepsilon_1\varepsilon_2}\right)\right)\right],$$

$$w(t) \equiv E_2 + g_{22}\sum_{l=0}^{4}(n_0-1)^l\binom{4}{l}\frac{\exp(-l f_n t)}{-k_2 - l\varepsilon_2 f_n},$$

$$m(t) \equiv E_1 + \frac{g_{21}}{k_1 - 4\varepsilon_2 f_n r}\sum_{l=0}^{4}(n_0-1)^l\binom{4}{l}\exp\big((4f_n r - l f_n)t_\dagger\big)\exp(-4f_n r t),$$

and $\Gamma(a,x)$ is the upper incomplete Gamma function,$\Gamma(a,x) \equiv \int_x^\infty z^{a-1}e^{-z}\mathrm{d}z$ for $\Re(a) > 0$ and $\Gamma(a+1,x) = a\Gamma(a,x) + x^a e^{-x}$ as defined in Abramowitz and Stegun (1965). The exact analytical solution of the Caricature model is plotted in Figure 5.14 for $E_0 = -10$ (mV), $h_0 = 1$ and $n_0 = 0$. The parameters t_* and $t_\dagger$ are found numerically according to the equations

$$\overset{1}{E}(t_*) = E_*, \qquad \overset{2}{E}(t_\dagger) = E_\dagger. \tag{5.42}$$

For $t \in [0, 600]$, the parameters are found as $t_* \approx 292.81$ (ms) and $t_\dagger \approx 345.24$ (ms).

Solution of the periodic boundary value problem Applying the following periodic boundary conditions

$$E(0) = E_0 > E_*, \quad h(0) = h(B), \quad n(0) = n(B), \tag{5.43}$$

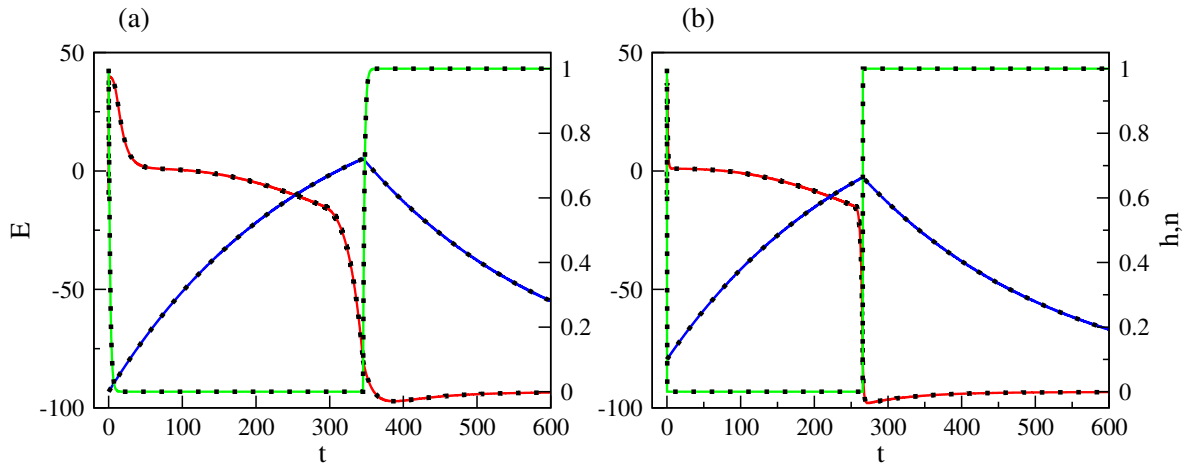

Figure 5.14: The numerical solution of the Caricature Model (5.1) in comparison with its analytical solution (5.41) for $t \in [0, 600]$. The red, green and blue curves correspond to the numerical solution of $E(t)$, $h(t)$ and $n(t)$ respectively and the black dotted lines are the analytical solutions. In (a) $\varepsilon_1 = \varepsilon_2 = 1$, and in (b) $\varepsilon_1 = \varepsilon_2 = 0.1$.

the exact solution of the full system is given by

$$n(t) = \begin{cases} 1 - \mathrm{C}_3 \exp(-f_n t), & t \in [0, t_\dagger] \\ \left(1 - \mathrm{C}_3 \exp(-f_n t_\dagger)\right) \exp\left(f_n r (t_\dagger - t)\right), & t \in [t_\dagger, \infty) \end{cases} \tag{5.44a}$$

$$h(t) = \begin{cases} \mathrm{D}_3 \exp\left(-F_h t/(\varepsilon_1 \varepsilon_2)\right), & t \in [0, t_\dagger] \\ 1 - \left(\exp(F_h t_\dagger/(\varepsilon_1 \varepsilon_2)) - \mathrm{D}_3\right) \exp(-F_h t/(\varepsilon_1 \varepsilon_2)), & t \in [t_\dagger, \infty) \end{cases} \tag{5.44b}$$

$$E(t) = \begin{cases} \overset{1}{E}(t) = \exp\left(\dfrac{G_{Na}\mathrm{D}_3}{F_h} \exp\left(-\dfrac{F_h t}{\varepsilon_1 \varepsilon_2}\right) - \dfrac{k_3 t}{\varepsilon_2}\right) \times \\ \qquad \left[E_0 \exp\left(-\dfrac{G_{Na}\mathrm{D}_3}{F_h}\right) - k_3 E_3\, u(-k_3\varepsilon_1, t)\right. \\ \qquad -g_{22} \displaystyle\sum_{l=0}^{4} \binom{4}{l} (-\mathrm{C}_3)^l\, u(-k_3\varepsilon_1 + \varepsilon_1\varepsilon_2 l f_n, t) \\ \qquad \left. -\dfrac{G_{Na}\mathrm{D}_3 E_{\mathrm{Na}}}{\varepsilon_1}\, u(-k_3\varepsilon_1 + F_h, t)\right], & t \in [0, t_*] \\ \overset{2}{E}(t) = (E_* - w(t_*)) \exp\left(\frac{k_2}{\varepsilon_2}(t - t_*)\right) + w(t), & t \in [t_*, t_\dagger] \\ \overset{3}{E}(t) = (E_\dagger - m(t_\dagger)) \exp\left(\frac{k_1}{\varepsilon_2}(t_\dagger - t)\right) + m(t), & t \in [t_\dagger, \infty) \end{cases} \tag{5.44c}$$

where

$$u(\varkappa,t) \equiv \frac{\varepsilon_1}{F_h}\left(\frac{F_h}{G_{Na}\mathrm{D}_3}\right)^{\frac{\varkappa}{F_h}}\left[\Gamma\left(\frac{\varkappa}{F_h},\frac{G_{Na}\mathrm{D}_3}{F_h}\right)-\Gamma\left(\frac{\varkappa}{F_h},\frac{G_{Na}\mathrm{D}_3}{F_h}\exp\left(-\frac{F_h t}{\varepsilon_1\varepsilon_2}\right)\right)\right],$$

$$w(t) \equiv E_2 + g_{22}\sum_{l=0}^{4}(-\mathrm{C}_3)^l\binom{4}{l}\frac{\exp(-l\,f_n t)}{-k_2 - l\,\varepsilon_2 f_n},$$

$$m(t) \equiv E_1 + \frac{g_{21}}{k_1 - 4\varepsilon_2 f_n r}\sum_{l=0}^{4}(-\mathrm{C}_3)^l\binom{4}{l}\exp\left((4f_n r - l\,f_n)t_\dagger\right)\exp(-4f_n r t),$$

Constructing restitution curves The 1:1 and 2:2 restitution curves are now derived by imposing the conditions (5.45) and (5.46) on the exact solutions (5.44) respectively.

1:1 restitution curve The condition (5.45) must be satisfied, i.e.

$$E(0,\ r,\ \varepsilon_1,\ \varepsilon_2) = E_{\text{stim}}, \tag{5.45a}$$

$$E(B,\ r,\ \varepsilon_1,\ \varepsilon_2) = E_{\text{stim}}, \tag{5.45b}$$

$$h(0,\ r,\ \varepsilon_1,\ \varepsilon_2) = h(B,\ r,\ \varepsilon_1,\ \varepsilon_2), \tag{5.45c}$$

$$n(0,\ r,\ \varepsilon_1,\ \varepsilon_2) = n(B,\ r,\ \varepsilon_1,\ \varepsilon_2). \tag{5.45d}$$

Therefore, we impose the condition (5.45) on the solution (5.44) and obtain:

$$\begin{cases} \overset{1}{n}(0) = \overset{2}{n}(B), \\ 1-\mathrm{C}_3 = (1-\mathrm{C}_3\exp(-f_n t_\dagger))\exp(f_n r(t_\dagger - B)), \end{cases}$$

$$\begin{cases} \overset{1}{h}(0) = \overset{2}{h}(B), \\ \mathrm{D}_3\exp\left(\frac{-F_h B}{\varepsilon_1\varepsilon_2}\right) = 1-\left(\exp\left(\frac{F_h t_\dagger}{\varepsilon_1\varepsilon_2}\right)-\mathrm{D}_3\right)\exp(-F_h B(\varepsilon_1\varepsilon_2)). \end{cases}$$

Hence the coefficients C_3 and D_3 as functions of B and $t_\dagger$ are found:

$$\mathrm{C}_3 = \frac{1-\exp(f_n r(t_\dagger - B))}{1-\exp((-f_n t_\dagger) - f_n r(B - t_\dagger))}$$

$$\mathrm{D}_3 = \frac{1-\exp\left(\frac{F_h(t_\dagger - B)}{\varepsilon_1\varepsilon_2}\right)}{1-\exp\left(\frac{-F_h B}{\varepsilon_1\varepsilon_2}\right)}.$$

Substituting functions C_3 and D_3 into $E(t)$, the voltage is expressed as a function of B and $t_\dagger$. The action potential duration restitution curve is illustrated in Figure 5.15 where $t_\dagger$ is plotted against basic

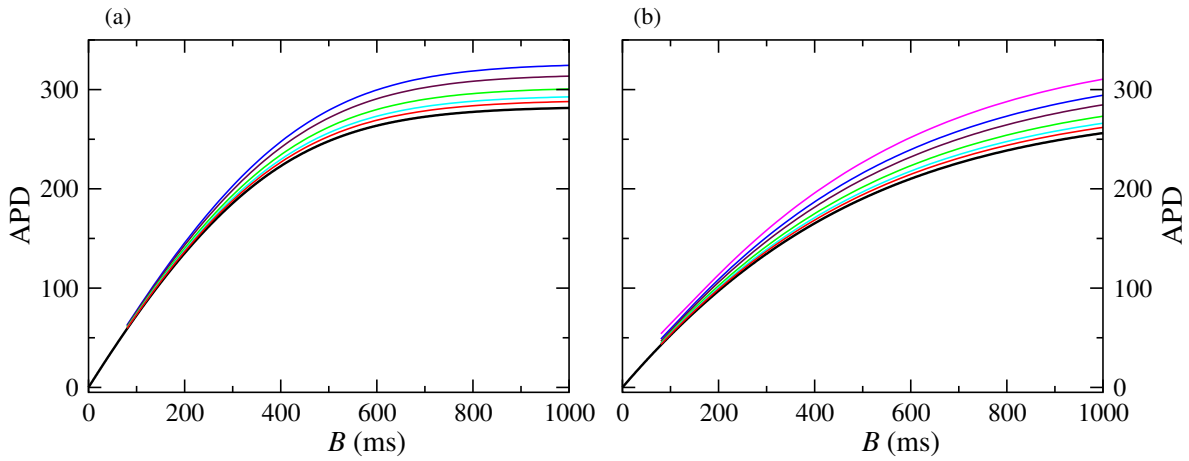

Figure 5.15: Action potential duration restitution curves exhibiting 1:1 response for the full system in case 1, in comparison with the asymptotic restitution curve (5.14). ε_2 changes from 1 to 0 from top to bottom. In (a) $r = 1.8$ and in (b) $r = 0.8$.

cycle length B. The restitution curves are plotted for $r > 1$ and $r < 1$ in Figures 5.15(a) and 5.15(b) respectively. Since ε_1 does not have an affect on the restitution curve, we set it to 1 and the curves are plotted for different values of ε_2. As can be seen from the figure, for small values of ε_2 the exact analytical solution is close to the asymptotic map (5.14).

2:2 restitution curves In order to construct the 2:2 restitution curve, condition (3.10) is applied on the solutions of (5.44):

$$E_{\text{even}}(0,\ r,\ \varepsilon_1,\ \varepsilon_2) = E_{\text{stim}}, \tag{5.46a}$$

$$E_{\text{odd}}(0,\ r,\ \varepsilon_1,\ \varepsilon_2) = E_{\text{stim}}, \tag{5.46b}$$

$$h_{\text{even}}(0,\ r,\ \varepsilon_1,\ \varepsilon_2) = h_{\text{odd}}(B,\ r,\ \varepsilon_1,\ \varepsilon_2), \tag{5.46c}$$

$$h_{\text{odd}}(0,\ r,\ \varepsilon_1,\ \varepsilon_2) = h_{\text{even}}(B,\ r,\ \varepsilon_1,\ \varepsilon_2), \tag{5.46d}$$

$$n_{\text{even}}(0,\ r,\ \varepsilon_1,\ \varepsilon_2) = n_{\text{odd}}(B,\ r,\ \varepsilon_1,\ \varepsilon_2), \tag{5.46e}$$

$$n_{\text{odd}}(0,\ r,\ \varepsilon_1,\ \varepsilon_2) = n_{\text{even}}(B,\ r,\ \varepsilon_1,\ \varepsilon_2). \tag{5.46f}$$

Thus, it yields:

$$\begin{cases} \overset{1}{n}_{\text{even}}(0) = \overset{2}{n}_{\text{odd}}(B), \\ \overset{2}{n}_{\text{even}}(B) = \overset{1}{n}_{\text{odd}}(0), \end{cases}$$

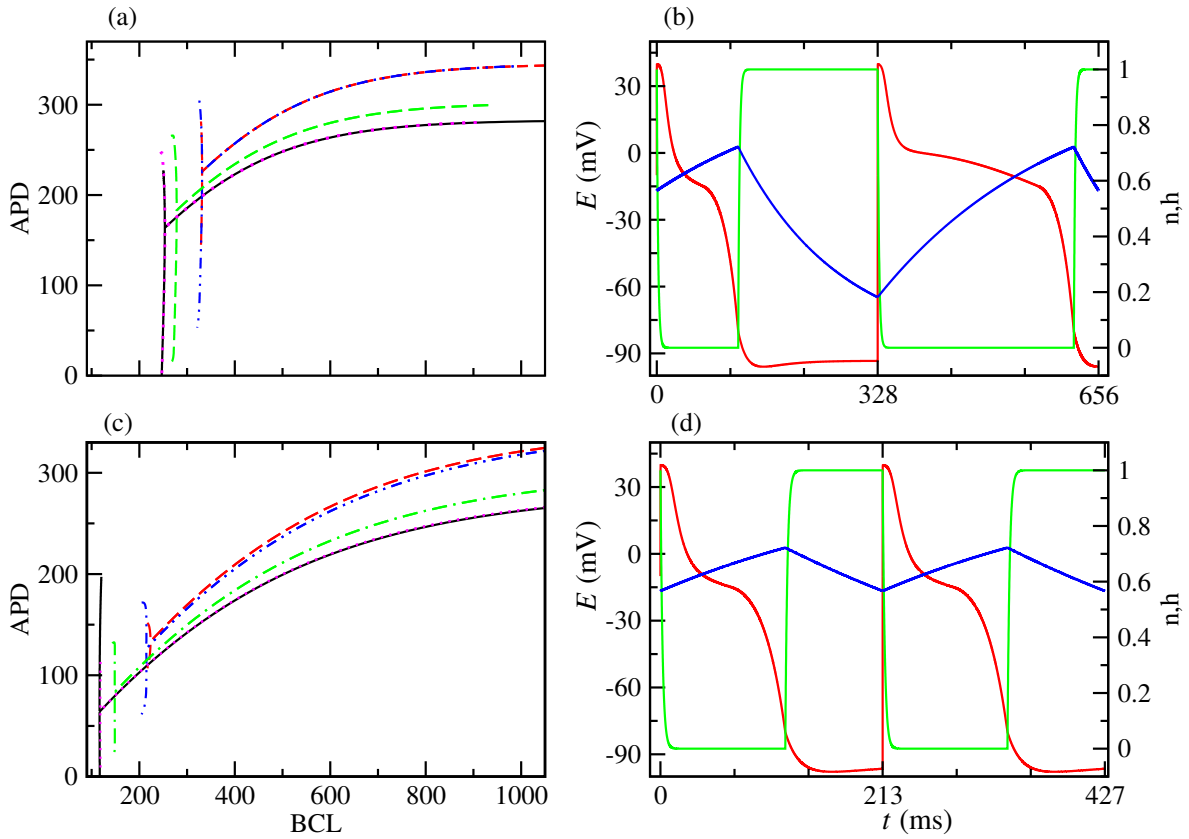

Figure 5.16: The restitution curves from the exact analytical solutions are compared with the asymptotic map (5.14) which is a solid black curve. The blue, red, green and magneta curves correspond to $\varepsilon_2 = 1, 0.4, 0.2, 0.1, 0.05$, respectively. In (a) $r = 1.8$ and in (b) stable alternans is plotted at $B = 260$ ms. In (c) $r = 0.7$ and in (d) unstable alternans at $B = 92$ ms is plotted.

$$\begin{cases} \overset{1}{h}_{\text{even}}(0) = \overset{2}{h}_{\text{odd}}(B) \\ \overset{2}{h}_{\text{even}}(B) = \overset{1}{h}_{\text{odd}}(0) \end{cases}$$

These equations are solved simultaneously using the solution of the initial value problem as an initial guess. The voltage $E(t)$ is then formulated as a function of B and $t_\dagger$. The restitution curve is constructed as $t_\dagger$ against B. By decreasing the basic cycle length the restitution curve bifurcates. For $r > 1$ the bifurcation is Supercritical as can be seen in 5.16(a) and when $r < 1$ the bifurcation is subcritical 5.16(c). Since the value of ε_1 does not have an affect on the restitution curve is it fixed at 1 and different action potential duration restitution curves from the exact analytical solutions are plotted in Figure 5.16(a). As $\varepsilon_2 \to 0$ the exact solution approaches the asymptotic solution (5.14).

5.5.2.2 Case 2. Slow over-threshold response

As described earlier, the initial value of the voltage in this case is smaller than the threshold of the fast subsystem (5.4) and greater than the threshold of the slow subsystem (5.6) i.e. $E_2 < E_0 < E_*$. We now find the solution of the full Caricature system and construct the restitution curves.

Solution of the initial value problem Assuming the following initial conditions,

$$E(0) = E_2 < E_0 < E_*, \quad h(0) = h_0, \quad n(0) = n_0, \tag{5.47}$$

the system (5.6) has the following solutions for the time intervals $t \in [0, t_{*1}]$, $[t_{*1}, t_{*2}]$, $[t_{*2}, t_\dagger]$ and $[t_\dagger, \infty)$.

$$n(t) = \begin{cases} 1 - (1-n_0)\exp(-f_n t), & t \in [0, t_\dagger] \\ \big(1 - (1-n_0)\exp(-f_n t_\dagger)\big)\exp\big(f_n r(t_\dagger - t)\big), & t \in [t_\dagger, \infty) \end{cases} \tag{5.48a}$$

$$h(t) = \begin{cases} h_0 \exp\big(-F_h t/(\varepsilon_1\varepsilon_2)\big), & t \in [0, t_\dagger] \\ 1 - (\exp(F_h t_\dagger/(\varepsilon_1\varepsilon_2)) - h_0)\exp(-F_h t/(\varepsilon_1\varepsilon_2)), & t \in [t_\dagger, \infty) \end{cases} \tag{5.48b}$$

$$E(t) = \begin{cases} \overset{1}{E}(t) = w(t) - (w(0) - E_0)\exp(\dfrac{k_2}{\varepsilon_2}t), & t \in [t \in [0, t_{*1}] \\ \overset{2}{E}(t) = \exp\left(\frac{-k_3 t}{\varepsilon_2} + \frac{G_{Na}h_0}{F_h}\exp(\frac{-F_h t}{\varepsilon_1\varepsilon_2})\right) \times & \\ \quad \left[E_* \exp\left(\dfrac{k_3 t_{*1}}{\varepsilon_2} - \dfrac{G_{Na}h_0}{F_h}\exp(\dfrac{-F_h t_{*1}}{\varepsilon_1\varepsilon_2})\right) + E_{\mathrm{Na}}\, u(-k_3\varepsilon_1 + F_h, t)\right. & \\ \quad \dfrac{g_{22}\varepsilon_1}{G_{Na}h_0}\displaystyle\sum_{l=0}^{4}\binom{4}{l}(n_0-1)^l\, u(-k_3\varepsilon_1 + \varepsilon_1\varepsilon_2 l f_n, t) & \\ \quad \left. + \dfrac{k_3\varepsilon_1 E_3}{G_{Na}h_0}\, u(-k_3\varepsilon_1, t)\right], & t \in [t_{*1}, t_{*2}] \\ \overset{3}{E}(t) = (E_* - w(t_{*2}))\exp\left(\frac{k_2}{\varepsilon_2}(t - t_{*2})\right) + w(t), & t \in [t_{*2}, t_\dagger] \\ \overset{4}{E}(t) = (E_\dagger - m(t_\dagger))\exp\left(\frac{k_1}{\varepsilon_2}(t_\dagger - t)\right) + m(t), & t \in [t_\dagger, \infty) \end{cases} \tag{5.48c}$$

where

$$u(\varkappa, t) \equiv \frac{G_{Na}h_0}{F_h}\left(\frac{F_h}{G_{Na}h_0}\right)^{\frac{\varkappa}{F_h}}\left[\Gamma\left(\frac{\varkappa}{F_h}, \frac{G_{Na}h_0}{F_h}\exp\left(-\frac{F_h t}{\varepsilon_1\varepsilon_2}\right)\right) - \Gamma\left(\frac{\varkappa}{F_h}, \frac{G_{Na}h_0}{F_h}\exp\left(-\frac{F_h t_{*1}}{\varepsilon_1\varepsilon_2}\right)\right)\right],$$

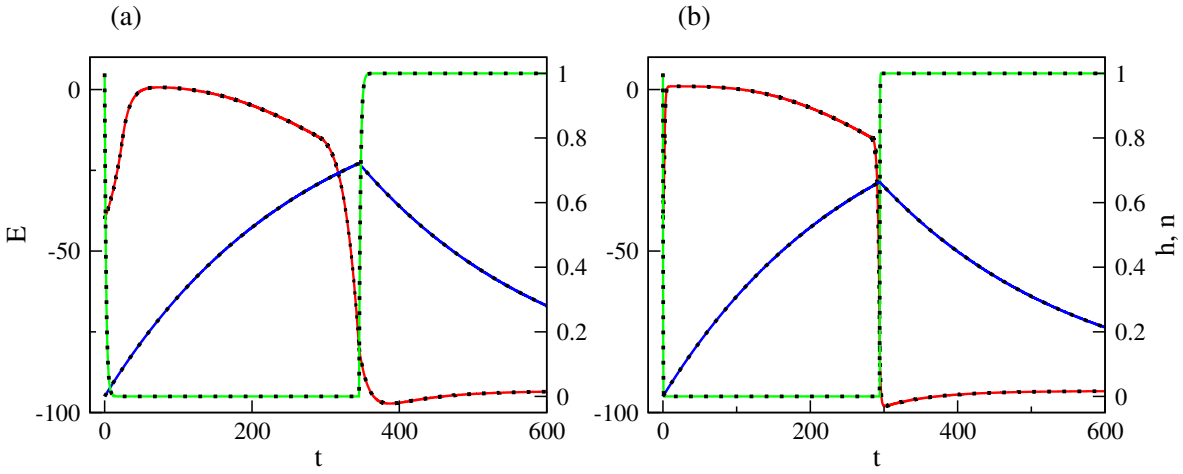

Figure 5.17: Exact solution of the full Caricature Noble model with voltage initial value considered in case 2. The numerical solution in comparison with the analytical solution of the full Caricature system (5.1). $E_0 = -30$, $h_0 = 1$ and $n_0 = 0$ for $t \in [0,600]$. In (a) $\varepsilon_1 = \varepsilon_2 = 1$ and in (b) $\varepsilon_1 = \varepsilon_2 = 0.1$.

$$w(t) \equiv E_2 + g_{22} \sum_{l=0}^{4} (n_0 - 1)^l \binom{4}{l} \frac{\exp(-l f_n t)}{-k_2 - l\varepsilon_2 f_n},$$

$$m(t) \equiv E_1 + \frac{g_{21}}{k_1 - 4\varepsilon_2 f_n r} \sum_{l=0}^{4} (n_0 - 1)^l \binom{4}{l} \exp\left((4 f_n r - l f_n) t_\dagger\right) \exp(-4 f_n r t),$$

and $\Gamma(a,x)$ is the upper incomplete gamma function, $\Gamma(a,x) \equiv \int_x^\infty z^{a-1} e^{-z} \mathrm{d}z$ for $\Re(a) > 0$ and $\Gamma(a+1,x) = a\Gamma(a,x) + x^a e^{-x}$ as defined in Abramowitz and Stegun (1965).

The exact analytical solution is plotted in Figure 5.17 where it is compared with the numerical solutions of the caricature model (5.1). Similar to the case 1 the parameters t_{*1}, t_{*2} and $t_\dagger$ can be found numerically as solutions of

$$\overset{1}{E}(t_{*1}) = \overset{2}{E}(t_{*1}) = E_*, \qquad \overset{2}{E}(t_{*2}) = \overset{3}{E}(t_{*2}) = E_*, \qquad \overset{3}{E}(t_\dagger) = \overset{4}{E}(t_\dagger) = E_\dagger. \tag{5.49}$$

For the standard values of parameters, $E_0 = -30$, $h_0 = 1$ and $n_0 = 0$ we obtain $t_{*1} \approx 24.5$ ms, $t_{*2} \approx 292.8$ ms and $t_\dagger \approx 345.24$ ms.

Solution of the periodic boundary value problem The periodic boundary conditions for this case are

$$E(0) = E_\dagger < E_0 < E_*, \quad h(0) = h(B), \quad n(0) = n(B), \tag{5.50}$$

Similar to the Case 1, the above boundary conditions (5.50) are imposed and the general solution is obtained as below

$$n(t) = \begin{cases} 1 - \mathrm{C}_4 \exp(-f_n t), & t \in [0, t_\dagger] \\ \big(1 - \mathrm{C}_4 \exp(-f_n t_\dagger)\big) \exp\big(f_n r (t_\dagger - t)\big), & t \in [t_\dagger, \infty) \end{cases} \tag{5.51a}$$

$$h(t) = \begin{cases} \mathrm{D}_4 \exp\big(-F_h t/(\varepsilon_1 \varepsilon_2)\big), & t \in [0, t_\dagger] \\ 1 - (\exp(F_h t_\dagger/(\varepsilon_1 \varepsilon_2)) - \mathrm{D}_4) \exp(-F_h t/(\varepsilon_1 \varepsilon_2)), & t \in [t_\dagger, \infty) \end{cases} \tag{5.51b}$$

$$E(t) = \begin{cases} \overset{1}{E}(t) = w(t) - (w(0) - E_0) \exp(\dfrac{k_2}{\varepsilon_2} t), & t \in [0, t_{*1}] \\ \overset{2}{E}(t) = \exp\left(\frac{-k_3 t}{\varepsilon_2} + \frac{G_{Na} \mathrm{D}_4}{F_h} \exp(\frac{-F_h t}{\varepsilon_1 \varepsilon_2}) \right) \times \\ \quad \left[E_* \exp\left(\dfrac{k_3 t_{*1}}{\varepsilon_2} - \dfrac{G_{Na} \mathrm{D}_4}{F_h} \exp(\dfrac{-F_h t_{*1}}{\varepsilon_1 \varepsilon_2}) \right) + E_{\mathrm{Na}}\, u(-k_3 \varepsilon_1 + F_h, t) \right. \\ \quad \frac{g_{22} \varepsilon_1}{G_{Na} \mathrm{D}_3} \sum_{l=0}^{4} \binom{4}{l} (-\mathrm{C}_3)^l \; u(-k_3 \varepsilon_1 + \varepsilon_1 \varepsilon_2 l f_n, t) \\ \quad \left. + \frac{k_3 \varepsilon_1 E_3}{G_{Na} \mathrm{D}_4}\, u(-k_3 \varepsilon_1, t) \right], & t \in [t_{*1}, t_{*2}] \\ \overset{3}{E}(t) = (E_* - w(t_{*2})) \exp\left(\frac{k_2}{\varepsilon_2} (t - t_{*2}) \right) + w(t), & t \in [t_* 2, t_\dagger] \\ \overset{4}{E}(t) = (E_\dagger - m(t_\dagger)) \exp\left(\frac{k_1}{\varepsilon_2} (t_\dagger - t) \right) + m(t), & t \in [t_\dagger, \infty) \end{cases} \tag{5.51c}$$

where

$$u(\varkappa, t) \equiv \frac{G_{Na} \mathrm{D}_3}{F_h} \left(\frac{F_h}{G_{Na} \mathrm{D}_3} \right)^{\frac{\varkappa}{F_h}} \left[\Gamma\left(\frac{\varkappa}{F_h}, \frac{G_{Na} \mathrm{D}_3}{F_h} \exp\left(-\frac{F_h t}{\varepsilon_1 \varepsilon_2} \right) \right) - \Gamma\left(\frac{\varkappa}{F_h}, \frac{G_{Na} \mathrm{D}_3}{F_h} \exp\left(-\frac{F_h t_{*1}}{\varepsilon_1 \varepsilon_2} \right) \right) \right],$$

$$w(t) \equiv E_2 + g_{22} \sum_{l=0}^{4} (-\mathrm{C}_3)^l \binom{4}{l} \frac{\exp(-l f_n t)}{-k_2 - l \varepsilon_2 f_n},$$

$$m(t) \equiv E_1 + \frac{g_{21}}{k_1 - 4 \varepsilon_2 f_n r} \sum_{l=0}^{4} (-\mathrm{C}_3)^l \binom{4}{l} \exp\big((4 f_n r - l f_n) t_\dagger\big) \exp(-4 f_n r t),$$

and $\Gamma(a,x)$ is the upper incomplete gamma function $\Gamma(a,x) \equiv \int_x^\infty z^{a-1} e^{-z} \mathrm{d}z$ for $\Re(a) > 0$ and $\Gamma(a+1,x) = a\Gamma(a,x) + x^a e^{-x}$ as defined in Abramowitz and Stegun (1965).

Constructing restitution curves

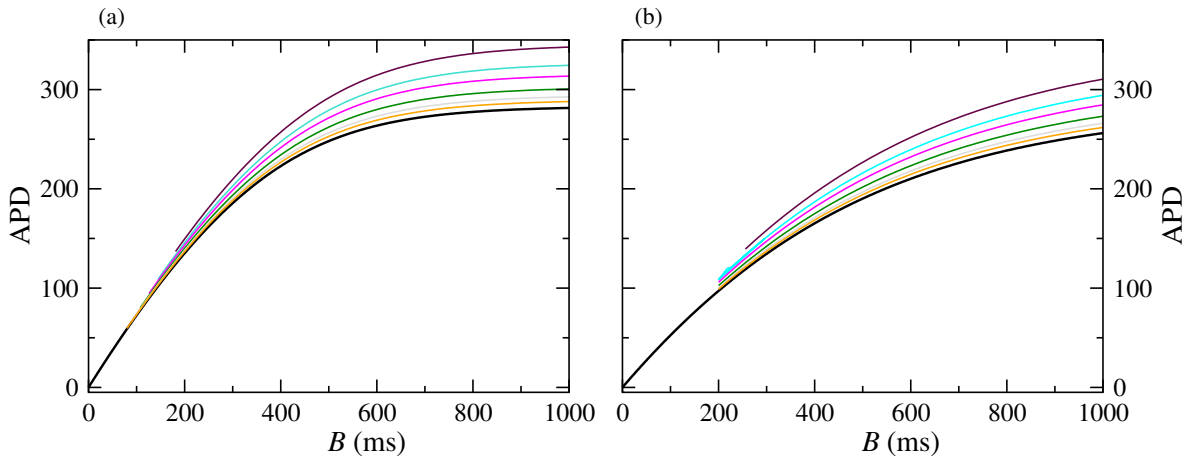

Figure 5.18: Action potential duration restitution curves exhibiting 1:1 response for the full system in case 2, in comparison with the asymptotic restitution curve (5.14). The value of ε_2 changes from 1 to 0 from top to bottom. In (a) $r = 1.8$ and in (b) $r = 0.8$.

1:1 restitution curves Imposing the conditions (5.45) on the exact solution of slow over-threshold response (5.51) and determine the coefficient functions C_4 and D_4 as below:

$$C_4 = \frac{1-\exp\left(f_n r(t_\dagger - B)\right)}{1-\exp\left((-f_n t_\dagger) - f_n r(B-t_\dagger)\right)}$$
$$D_4 = \frac{1-\exp\left(\frac{F_h(t_\dagger - B)}{\varepsilon_1\varepsilon_2}\right)}{\left(1-\exp\left(\frac{-F_h B}{\varepsilon_1\varepsilon_2}\right)\right)}$$

The 1:1 restitution curve for this case is illustrated in Figure 5.18 with curves denoted by diamond symbol. As can be seen in Figure 5.18 and 5.15, the curves for these two cases are identical. Since action potentials for both of these cases have similar duration. change in the value of ε_2 the action potential duration becomes shorter.

The 2:2 restitution curve Similar to the previous case, in order to construct the 2:2 restitution curve, the following conditions must be satisfied

$$\begin{cases} {}^{1}h_{\text{even}}(0) = {}^{2}h_{\text{odd}}(B), \\ {}^{2}h_{\text{even}}(B) = {}^{1}h_{\text{odd}}(0), \end{cases} \tag{5.52}$$

$$\begin{cases} {}^{1}n_{\text{even}}(0) = {}^{2}n_{\text{odd}}(B), \\ {}^{2}n_{\text{even}}(B) = {}^{1}n_{\text{odd}}(0), \end{cases} \tag{5.53}$$

The above equations are solved simultaneously using the solution of the initial value problem as an initial guess. Thus, similar to the previous part, we formulate the $E(t)$ solution as a function of B and $t_\dagger$. By decreasing the value of B and finding the $t_\dagger$ for each basic cycle length, the restitution curves for different ε_2 are constructed. For $r > 1$ the bifurcation is Supercritical and stable alternans occur. The restitution curves for this condition are illustrated in Figure 5.19(a) and when $r < 1$ the restitution curves demonstrate 1:1 response as can be seen in Figure 5.8(c). As $\varepsilon_2 \to 0$ the exact solution reaches the asymptotic solution (5.14).

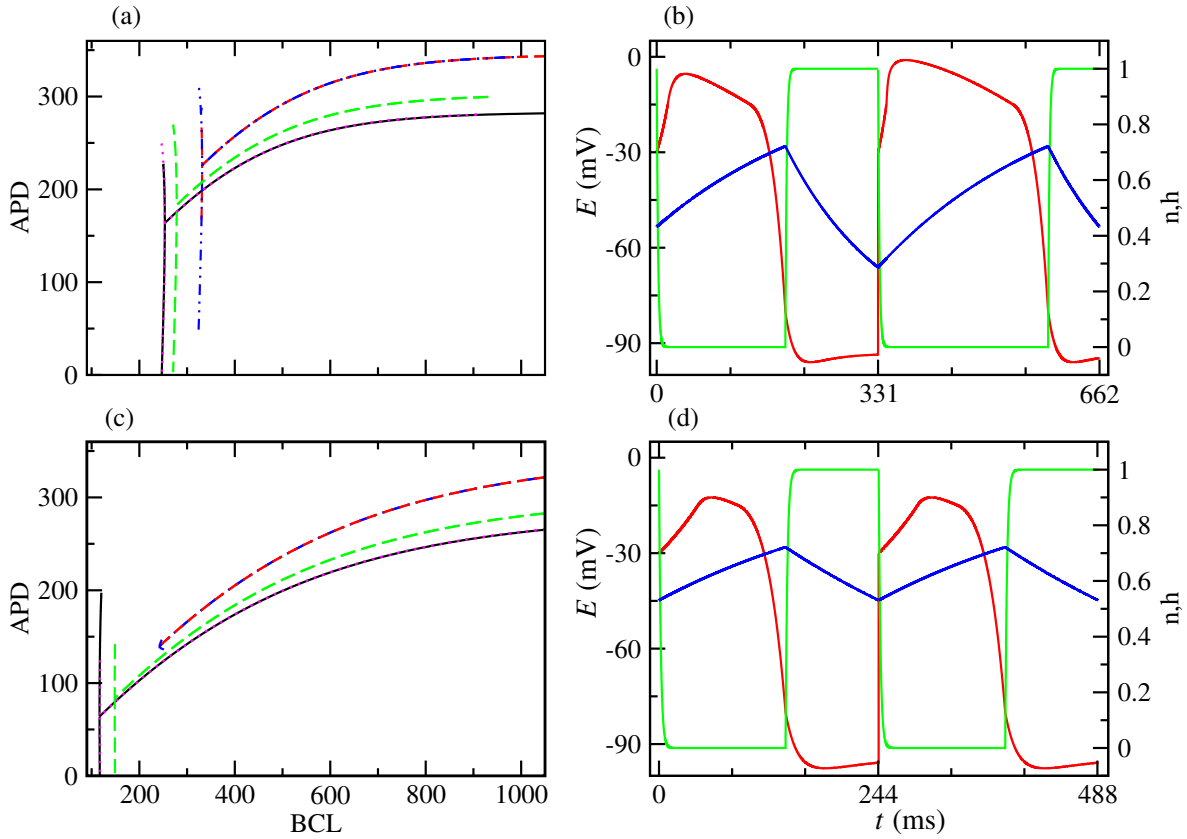

Figure 5.19: Action potential duration restitution curves from the exact analytical solution in comparison with asymptotic map. The red curve corresponds to the full model. The blue curve is for $\varepsilon_1 = 0$ and $\varepsilon_2 = 1$. The green curve corresponds to $\varepsilon_1 = 0$, $\varepsilon_2 = 0.2$, the magneta curve is for $\varepsilon_1 = 1$ and $\varepsilon_2 = 0.001$ and the black curve is for asymptotic map i.e.$\varepsilon_1 = \varepsilon_2 = 0$. In (a) $r = 1.8$ and in (b) stable alternans at $B = 331$ (ms) is shown. Plot (c) is for $r = 0.8$ and in (d) 1:1 response for $r = 0.8$ at $B = 244$ (ms).

5.6 Summary

In this chapter, a version of the classical model of Purkinje fibers (Noble, 1962) are studied. The Noble (1962) model was simplified by Biktashev et al. (2008) to a caricature model using asymptotic embedding approach. The caricature Noble model is simple enough to be solved analytically but at the same time it contains the essential time scales and parameters relevant to the physiology of the cardiac cell. Following the results described in the previous chapter and also the direction suggested by Mitchell and Schaeffer (2003), a dimensionless parameter r is introduced to the function of the slow gating variable n. We remark that Mitchell and Schaeffer (2003) described a procedure in the case of a simple model but in this chapter, we have applied the procedure to the Caricature Noble model which is a more relevant cardiac model.

Applying asymptotic reduction methods, the full Caricature Noble system (5.1) is reduced to two subsystems, the phase portrait of the system is studied and an explicit restitution map is derived from the model where the relevant parameters of the model are still present in the map. The stability of the map and bifurcations of equilibria of the map have been studied to determine the regions and the parameter space where normal response and alternans occur. We have found that the parameter r in the slow gating variable n, plays an important role in inducing instabilities including alternans. It has been presented that the map losses its stability at $r = 1$ and exhibits 2:2 response for $r > 1$. The results of the asymptotic action potential duration restitution curve is validated by comparing it with the full solutions of the system. The attention was focused not only on the role of the slow subsystem in inducing alternans but also on the role of the fast subsystem. We have found that the fast subsystem (5.4) determines the voltage stimulus, such that, since the n_{thr} is a function of E_{stim} according to (5.11), it can be large enough to prevent alternans in the full system.

Since the Caricature model (Biktashev et al., 2008) is a version of Noble (1962) model, its parameters and variables could have physiological meaning. Hence our results could be translated into Physiology. The variable n is activation gating variable for K^+ current. As stated previously, in more physiologically based models gating variables satisfy equations of the form

$$\frac{\mathrm{d}n}{\mathrm{d}t} = \frac{\overline{n}(E) - n(E)}{\tau_n(E)},$$

where $\overline{n}(E)$ and $\tau_n(E)$ are continuous function of voltage E. It follows from the equation (5.1c) that:

$$F_n(E) = \frac{1}{\tau_n(E)}.$$

Recall that n is activation gating variable, therefore, when $n = 1$ the channel is open and K^+ ions leave the cell causing the voltage to decrease. For $n = 0$, the channel closes and there is no I_K current. Parameter r is present in the $F_n(E)$ equation and in particular it appears at the diastolic phase of the model's action potential i.e. when $t > t_\dagger$ and $E < E_\dagger$. Thus, r determines the speed in which the n-gating variable decreases during the diastolic phase. When $r > 1$, $F_n(E)$ increases, consequently $\tau_n(E)$ reduces which means the time needed for activation of n-gating variable is small. As a result n-gating variable reaches its resting value quickly. Physiologically this means that the channel closes and the outward I_K current decreases. Thus alternans occurs.

When $r < 1$ the time scale at which the n gating variable evolves increases and the evolution of n gating variable slows down. Hence, n-gating variable closes slowly resulting in more K^+ ion leaving the cell and the membrane potential becoming more negative. As a result, increase in magnitude of the I_K suppresses alternans. Although literature supports the role of an increase in the I_K current in suppressing alternans (Fox et al., 2002), we wish to emphasise that there are other ionic mechanisms that play more important roles in inducing or suppression of alternans. For example Ca^{+2} as an important ion in excitation-contraction of cardiac cells believed to be responsible for inducing action potential duration alternans in cardiac cells. However, it is not included in the Noble (1962) model in the first place. Therefore, one interpretation of our finding in this chapter could be the fact that the slow gating variable responsible for inducing alternans in this model, is a combination of slow recovery variables of Ca^{+2} and K^+ channels.

Chapter 6

Restitution and alternans in the Courtemanche-Ramirez-Nattel model of a human atrial cell

6.1 Introduction

In this chapter the methods introduced and developed in the previous chapters are applied to a reduced version of the detailed Courtemanche et al. (1998) model of the human atrial cell action potential. The model of Courtemanche et al. (1998) is much more detailed than the models considered previously. Therefore, the results obtained from this model might be transferable to the physiology of the atrial cells. The model was reduced by Suckley (2004) where she used asymptotic methods and qualitative analysis to eliminate the variables of the system of Courtemanche et al. (1998) with 21 equations, called CRN-21, to a system with 3 equations (CRN-3).

A short summary of the reduction process of Suckley (2004) is given in the first section of this chapter where the steps are repeated to confirm that Suckleys reduction remains valid in the case of multiple periodic simulation not only for one single action potential. Then the system is further reduced to two equations, called CRN-2. The methodology presented in Chapter 3 is applied to the CRN-2 model and an asymptotic map describing the action potential duration as a function of the preceding diastolic interval for a fixed basic cycle length is derived. The stability of this map is studied and the region(s) of the model's parameters where instabilities occur are outlined. The CRN-2

is a simplified version of CRN-21, therefore the parameters and variables present in the CRN-2, are relevant to the physiology of the atrial cell. Moreover, the 2 equations in CRN-2 are expected to represent the membrane voltage and the slow inactivation gating variable for L-type Ca^{+2} current. Although the reduced version does not contain all the details present in the full Courtemanche model, since it is successful in inducing instability, we are therefore able to identify a factor responsible for alternans.

6.2 Courtemanche-Ramirez-Nattel model

The Courtemanche et al. (1998) is based on ionic current data obtained directly from human atrial cells. When human data were not available or were inadequate to describe an atrial ion current, they employed animal data. In particular they used the model of Luo and Rudy (1991) which is based on measurements of guinea pig ventricular cells. The Courtemanche et al. (1998) model action potential resembles action potentials recorded in human atrial samples. A schematic representation of the currents and subcellular compartments of a cardiac cell that is included in the Courtemanche et al. (1998) model is shown in Figure 6.1. As was explained in Section 2.2.1, in each heartbeat the Na^{+} channels are activated by a stimulus current, Na^{+} enters the cell and the cell membrane is depolarised. The voltage-dependent Ca^{+2} channels open due to the change in the membrane potential (Bers., 2002) and Ca^{+2} enters the cytoplasm. Ca^{+2} binds to ryanodine receptor (RyR) and activates them. Then the Ca^{+2} stored in the sarcoplasmic reticulum SR is released into the intracellular space. Courtemanche et al. (1998) used a similar approach to Luo and Rudy (1991) and represented the SR Ca^{+2} uptake and SR Ca^{+2} release as a two-compartment model. The intracellular Ca^{+2} is taken up into an SR uptake compartment called the network SR (NSR) and the SR Ca^{+2} release is released from a compartment called the junctional SR (JSR). The membrane potential for an equipotential cell is given by

$$\frac{\mathrm{d}E}{\mathrm{d}t} = -\frac{I_{\text{ion}}}{C_M}, \tag{6.1a}$$

where C_M is the membrane capacitance and I_{ion} is the total ionic current given by

$$I_{\text{ion}} = I_{\text{Na}} + I_{\text{K1}} + I_{\text{to}} + I_{\text{Kur}} + I_{\text{Kr}} + I_{\text{Ks}} + I_{\text{Ca,L}} + I_{\text{p,Ca}} + I_{\text{Na,K}} + I_{\text{b,Na}} + I_{\text{NaCa}} + I_{\text{b,Ca}}, \tag{6.1b}$$

where notations are presented below

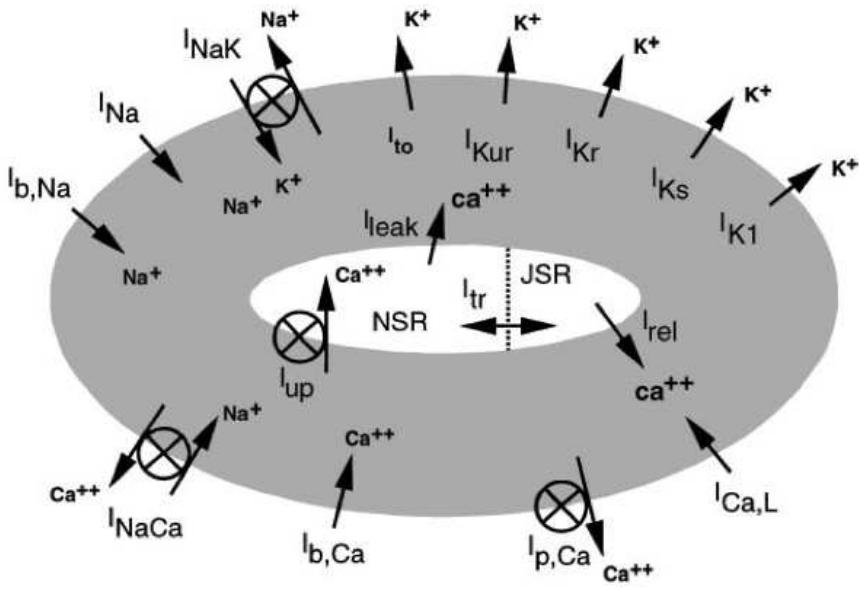

Figure 6.1: Diagram of intracellular compartments and ion fluxes included in the Courtemanche et al. (1998) model. The model considers the cell with 3 intracellular compartments: the myoplasm, the sarcoplasmic reticulum release compartment labeled JSR and the sarcoplasmic reticulum uptake compartment labeled NSR.

I_{Na}: fast inward Na^+ current,
I_{K1}: inward rectifier K^+ current,
I_{to}: transient outward K^+ current,
I_{Kur}: ultrarapid delayed rectifier K^+ current,
I_{Kr}: rapid delayed rectifier K^+ current,
I_{Ks}: slow delayed rectifier K^+ current,
$I_{\mathrm{Ca,L}}$: inward Ca^{+2} current,
$I_{\mathrm{p,Ca}}$: sarcoplasmic Ca^{+2} pump current,
$I_{\mathrm{Na,K}}$: $\mathrm{Na}^+ - \mathrm{K}^+$ pump current,
I_{NaCa}: $\mathrm{Na}^+ - \mathrm{Ca}^{+2}$ exchanger current,
$I_{\mathrm{b,Na}}$: background Na^+ current,
$I_{\mathrm{b,Ca}}$: Background Ca^{+2} current,
$I_{\mathrm{b,K}}$: Background K^+ current,
I_{rel}: Ca^{+2} release current from the JSR,
I_{up}: Ca^{+2} uptake current into the NSR,
I_{tr}: Ca^{+2} transfer current from NSR to JSR,
$I_{\mathrm{up,leak}}$: Ca^{+2} leak current from the NSR.

The model has 15 gating variables satisfying

$$\frac{\mathrm{d}y_{\mathrm{i}}}{\mathrm{d}t} = -\frac{\overline{y}_{\mathrm{i}} - y_{\mathrm{i}}}{\tau_{y_{\mathrm{i}}}}, \qquad \text{for i} = 1,..,15, \tag{6.1c}$$

$$y_{\mathrm{i}} \in [0,1].$$

For each gating variable y_i, $\overline{y}_\mathrm{i}$ is the steady state -activation and inactivation- relations for the gating variable y_i and τ_{y_i} is time. The gating variables included in this model are the following:

m: activation gating variable for I_Na,
h: fast inactivation gating variable for I_Na,
j: slow inactivation gating variable for I_Na,
o_a: activation gating variable for I_to,
o_i: inactivation gating variable for I_to,
u_a: activation gating variable for I_Kur,
u_i: inactivation gating variable for I_Kur,
x_r: activation gating variable for I_Kr,
x_s: activation gating variable for I_Ks,
d: activation gating variable for $I_\mathrm{Ca,L}$,
u: activation gating variable for I_rel,
v: Ca^{+2}-dependent inactivation gating variable for I_rel,
w: E-dependent inactivation gating variable for I_rel,
f: E-dependent inactivation gating variable for $I_\mathrm{Ca,L}$,
f_Ca: Ca^{+2}-dependent inactivation gating variable for $I_\mathrm{Ca,L}$.

In addition, the model keeps track of the intracellular concentrations of $[Na^+]_\mathrm{i}$, $[Ca^{+2}]_\mathrm{i}$ and $[K^+]_\mathrm{i}$ of Na^+, Ca^{+2} and K^+ while the extracellular ion concentrations are fixed. The evolution of these intracellular concentration are given by

$$\frac{\mathrm{d}[\mathrm{Na}^+]_\mathrm{i}}{\mathrm{d}t} = (FV_i)^{-1}\left(-3I_\mathrm{Na,K} + 3I_\mathrm{NaCa} + I_\mathrm{b,Na} + I_\mathrm{Na}\right), \tag{6.1d}$$

$$\frac{\mathrm{d}[\mathrm{K}^+]_\mathrm{i}}{\mathrm{d}t} = (FV_i)^{-1}\left(2I_\mathrm{Na,K} - I_\mathrm{K1} - I_\mathrm{to} - I_\mathrm{Kur} - I_\mathrm{Kr} - I_\mathrm{Ks} - I_\mathrm{b,K}\right),$$

$$\frac{\mathrm{d}[\mathrm{Ca}^{+2}]_\mathrm{i}}{\mathrm{d}t} = \frac{B_1}{B_2},$$

$$B_1 = (2FV_\mathrm{i})^{-1}\left(2I_\mathrm{NaCa} - I_\mathrm{p,Ca} - I_\mathrm{Ca,L} - I_\mathrm{b,Ca}\right) + (V_\mathrm{i})^{(-1)}\left(V_\mathrm{up}(I_\mathrm{up,leak} - I_\mathrm{up}) + I_\mathrm{rel}V_\mathrm{rel}\right),$$

$$B_2 = 1 + \frac{[\mathrm{Trpn}]_\mathrm{max}K_\mathrm{m,Trpn}}{([\mathrm{Ca}^{+2}]_\mathrm{i} + K_\mathrm{m,Trpn})^2} + \frac{[\mathrm{Cmdn}]_\mathrm{max}K_\mathrm{m,Cmdn}}{[\mathrm{Ca}^{+2}]_\mathrm{i} + K_\mathrm{m,Cmdn})^2}.$$

where F is the Faraday constant, V_i is the intracellular volume intracellular volume is the cytosolic volume, V_up is the SR uptake compartment volume, V_rel is the SR release compartment volume, $[\mathrm{Trpn}]_\mathrm{max}$ is the total troponin concentration in the myoplasm, $K_\mathrm{m,Trpn}$ is the Ca^{+2} half-saturation constant for troponin, $[\mathrm{Cmdn}]_\mathrm{max}$ is the total calmodulin concentration in the myoplasm and $K_\mathrm{m,Cmdn}$ is the Ca^{+2} half-saturation constant for calmodulin.

The change in the concentration of Ca^{+2} released from SR, denoted $[Ca^{+2}]_{rel}$, and the concentration of Ca^{+2} uptake to the SR, denoted $[Ca^{+2}]_{up}$, are also included in the Courtemanche et al. (1998) model with the following equations

$$\frac{d[Ca^{+2}]_{up}}{dt} = I_{up} - I_{up,leak} - I_{tr}\frac{V_{rel}}{V_{up}}, \tag{6.1e}$$
$$\frac{d[Ca^{+2}]_{rel}}{dt} = \frac{(I_{tr} - I_{rel})}{\left(1 + \frac{[Csqn]_{max}K_{m,Csqn}}{([Ca^{+2}]_{rel} + K_{m,Csqn})^2}\right)}.$$

Here $[Csqn]_{max}$ is total calsequestrin concentration in JSR and $K_{m,Csqn}$ is Ca^{+2} half-saturation constant for calsequestrin. The Courtemanche model is a sophisticated system of ordinary differential equations as can be seen from the system of equations (6.1). Hence a reduced version of this model with fewer variables would be an ideal tool to study and understand the role of physiological parameter. The reduced Courtemanche et al. (1998) model reproduces the four phases of the cardiac action potential, hence analysing its parameters provides insight into the initiation, plateau, decay, and recovery. With this motivation, we use a version of the Courtemanche et al. (1998) model which was reduced by Suckley (2004). We repeat the steps that she took to obtain the reduced system. The next section is a summary of the process we followed in order to reduce the system as Suckley did in her PhD thesis. We emphasise that in order to confirm that Suckleys reduction remains valid in the case of multiple periodic simulation not only for one single action potential, we repeated the process of reducing the model of Courtemanche et al. (1998).

6.3 Reduction of the CRN-21 model

The main idea of this reduction is to identify small and large terms and slow and fast time scales in the problem. Therefore, according to Definition (2.1) a set of small parameters can be introduced accordingly. This process was explained in Chapter 2. The first step in reducing the Courtemanche et al. (1998) model is to classify the dynamical variables according to their speed, using the following definition due to Biktashev and Suckley (2004); Suckley (2004).

Definition 6.1 *For a system of differential equations*

$$\frac{d\mathbf{y}}{dt} = \mathbf{f}(\mathbf{y}) \qquad \mathbf{y} = (y_1, y_2, ..., y_N),$$

the characteristic time-scale coefficients $\tau_{\mathbf{y}_i}$ *are*

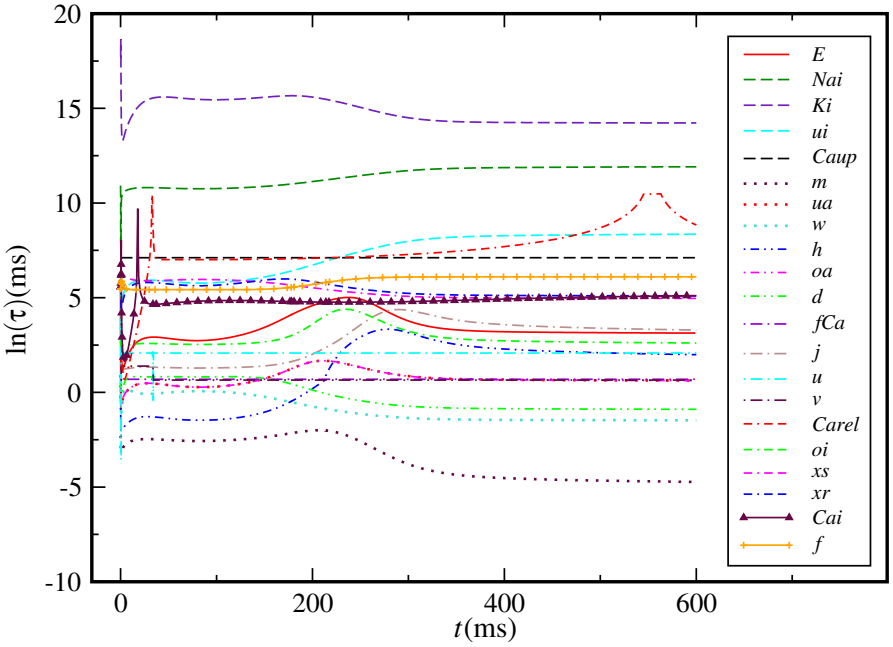

Figure 6.2: Graph of the $\ln(\tau)$'s for all the variables of the CRN-21 for $t \in [0, 600]$.

$$\tau_{y_i} \equiv \left| \left(\frac{\partial}{\partial y_i} \left(\frac{dy_i}{dt} \right) \right)^{-1} \right|.$$

The characteristic time-scale coefficients τ_{y_i} for all the dynamical variables of the Courtemanche et al. (1998) model is plotted in Figure 6.2. For gating variables $y_i = m$, h, j, o_a, o_i, u_a, u_i, x_r, x_s, d, f, f_{Ca}, u, v, w in the system (6.1), the time-scale coefficients τ_{y_i} corresponds to the τ_{y_i} already presented in the equations (6.1c). For the other variables in the system (6.1) such as E, $[Ca^{+2}]_i$, $[Na^{+}]_i$, $[K^{+}]_i$, $[Ca^{+2}]_{up}$ and $[Ca^{+2}]_{rel}$ the above definition is used. The variables with very small and very large time-scale coefficients are categorised into two groups of fast and slow variables, respectively. Having said that, some of the model's variables do not exactly fit into either of the two groups; during the time course of one action potential their speeds vary, behaving at times like fast variables and at other times like slow. This can be seen in Figure 6.2.

It is vital to remark that the focus of Suckley (2004) was on one particular solution rather than a series of solutions, whereas in this thesis each reduced system is solved many times to make sure that the reduced system is in agreement with the original system. The reason for doing this process is that, in order to study the restitution properties of the cardiac cells, the cell must be excited repeatedly. Hence, the system of equations must be solved for a series of solutions rather than one solution. As

can be seen in Figure 6.2 the largest time-scale coefficients are the super-slow variables $[Na^{+}]_i$, $[K^{+}]_i$, $[Ca^{+2}]_{up}$ and u_i. Variables with the smallest characteristic time-scales are the super-fast variables m, u_a and w. Super-fast variables are m, u_a and w. The green dashed dotted line that you mentioned in the correction list, corresponds to the variable d, it is considered fast variable but since at the beginning of the action potential, its time scale is very large, it is not considered as a super-fast variable. In Figure 6.3, the bottom part of the Figure 6.2 is zoomed in, to illustrate the time-scale coefficient for fast and super-fast variables.

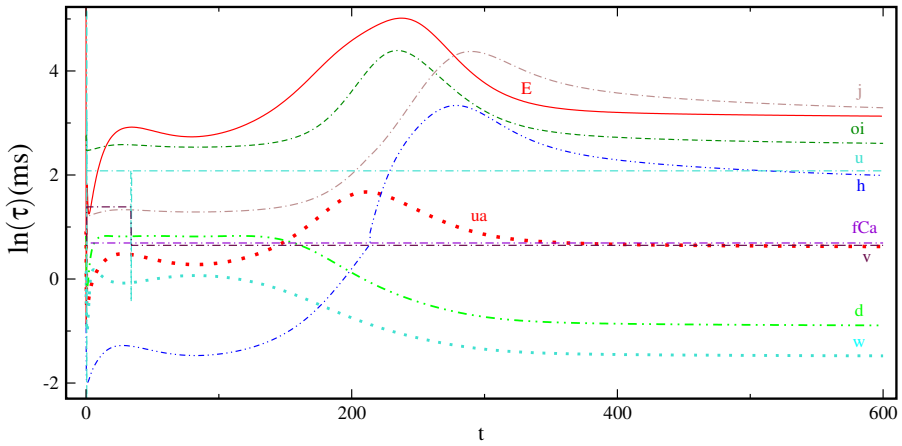

Figure 6.3: Graph of the $\ln(\tau)$'s for all the variables of the CRN-21 for $t \in [0, 600]$.

The super-slow variables don't differ significantly from their initial values, therefore they can be replaced with their initial conditions and the system of CRN-21 is reduced to CRN-17. The super-fast variables reach their quasi-stationary values $\overline{m}$, $\overline{u_a}$, $\overline{w}$, very quickly. Since the speed of these variables remains fast at all times during the action potential solution, Suckley (2004) introduced a small parameter $\varepsilon > 0$ to their equations as follows:

$$\varepsilon \frac{dy_i}{dt} = -\frac{\overline{y}_i - y_i}{\tau_{y_i}}, \quad \text{for} \quad y_i = m, u_a, w.$$

As ε tends to zero, $\overline{y}_i$ tends to y_i and the super-fast variables are replaced with their quasi-stationary functions. This allows the CRN-17 to be reduced to the new system of 14 variables (CRN-14). The solution of CRN-17 and CRN-14 are plotted in Figure 6.4 with red and blue curves, respectively and can be seen to agree closely with the CRN-21 solution.

It should be noted that the evolution of the super-fast variables m, u_a, w can be studied by re-scaling the independent time variable t to $T = t/\varepsilon$. When $\varepsilon \to 0$ all the other variables are parameters as

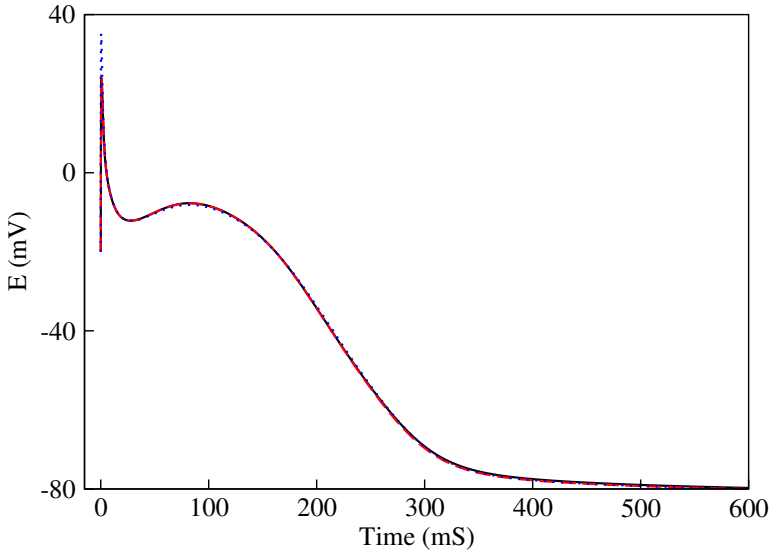

Figure 6.4: The human atrial action potential generated by the model of Courtemanche et al. (1998). A selected solution for the CRN-21, CRN-17 and CRN-14 is plotted in black, red and blue curves, respectively, when $t \in [0, 600]$

their change during the fast time-scale T is negligible. For further details see Biktasheva et al. (2006); Simitev and Biktashev (2006); Suckley (2004). Since the focus of this research is to study alternans in the repolarisation phase of an action potential, the fast subsystems are not studied here. After obtaining the reduced Courtemanche system with 14 variables (CRN-14), Suckley (2004) divided the action potential solution of this system into three time stages corresponding to different time-scales. The stages are explained briefly as follows and are also illustrated in Figure 6.5.

i. *The fast stage* $[t_0, t_1]$*:* This is the fastest stage of an action potential where I_{Na} enters the system and the variables h, o_{a} and d are fast as can be seen in Figure 6.5(a). The rest of the variables are slow and are taken as their initial value. So, a system of 4 equations for voltage E, gating variables h, o_{a} and d, describes this stage of an action potential.

ii. *Intermediate stage* $[t_1, t_2]$*:* During this stage I_{Na} is over and the fast gating variables h, o_{a} and d are replaced with their quasi-stationary values. This stage is described by the CRN-11 system, as can be seen in Figure 6.5(b). The gating variables f, x_{r} and x_{s} are slow during this stage, hence they are replaced with their initial values. The variables u and v are replaced with explicit functions of time. Therefore the CRN-6 system describes this stage of an action potential.

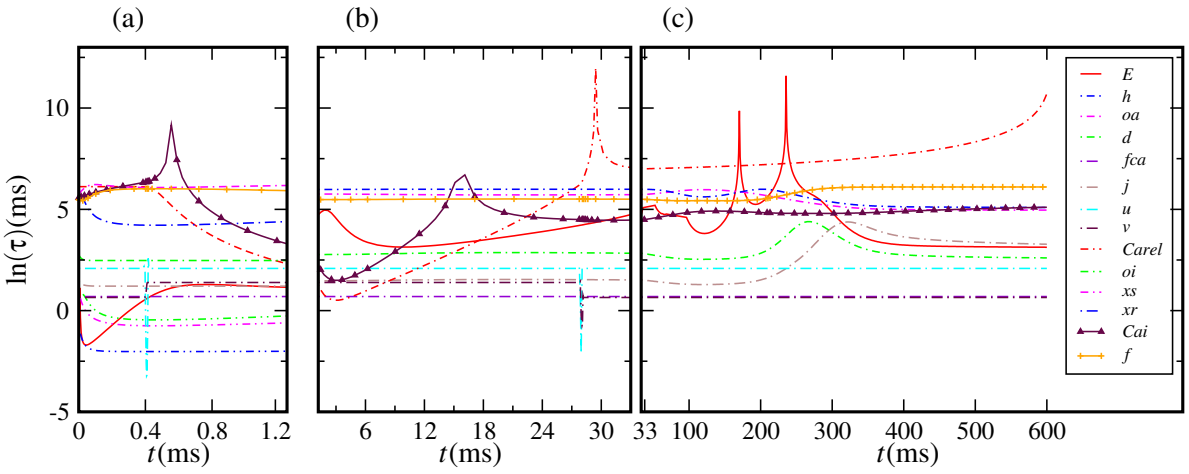

Figure 6.5: Graph of the $\ln(\tau)$ for various τ for the three stages of an action potential. Plots (a) is of CRN-14 for the fast stage $t \in [0, 1.2]$, plot (b) and (c) show CRN-11 during the intermediate stage $t \in [1.2, 33]$ and the slow stage $t \in [33, 600]$ of the action potential, respectively.

iii. *Slow stage* $[t_2, \infty)$*:* The system of CRN-11 is valid for this stage too (Figure 6.5(c)). The variables f_{Ca}, j, u and v are fast during this stage, so they can be replaced with their quasi-stationary values and the system of CRN-7 is obtained.

The asymptotic methods that Suckley (2004) applied to the CRN-21 system are summarised in the following system. She used small parameters ε_j for $j = 1, \ldots, 4$, to obtain the reduced systems for three stages of the action potential.

$$
\begin{aligned}
\frac{\mathrm{d}E}{\mathrm{d}t} &= -\frac{I_{\mathrm{ion}}}{C_M}, \\
I_{\mathrm{ion}} &= \frac{1}{\varepsilon_3} I_{\mathrm{Na}}(E, m, h, j) + I_{\mathrm{K1}}(E, [\mathrm{K}^+]_{\mathrm{i}}, \varepsilon_4) + I_{\mathrm{to}}(E, [\mathrm{K}^+]_{\mathrm{i}}, o_{\mathrm{a}}, o_{\mathrm{i}}) \\
&\quad + \; I_{\mathrm{Kur}}(E, [\mathrm{K}^+]_{\mathrm{i}}, u_{\mathrm{a}}, u_{\mathrm{i}}) + I_{\mathrm{Kr}}(E, [\mathrm{K}^+]_{\mathrm{i}}, x_{\mathrm{r}}, \varepsilon_4) + I_{\mathrm{Ks}}(E, [\mathrm{K}^+]_{\mathrm{i}}, x_{\mathrm{s}}, \varepsilon_4) \\
&\quad + \; I_{\mathrm{Ca,L}}(E, d, f, f_{\mathrm{Ca}}) + I_{\mathrm{p,Ca}}([\mathrm{Ca}^{+2}]_{\mathrm{i}}, \varepsilon_4) + I_{\mathrm{Na,K}}(E, [\mathrm{Na}^+]_{\mathrm{i}}, \varepsilon_4) \\
&\quad + \; I_{\mathrm{NaCa}}(E, [\mathrm{Na}^+]_{\mathrm{i}}, [\mathrm{Ca}^{+2}]_{\mathrm{i}}, \varepsilon_4) + I_{\mathrm{b,Na}}(E, [\mathrm{Na}^+]_{\mathrm{i}}, \varepsilon_4) + I_{\mathrm{b,Ca}}(E, [\mathrm{Ca}^{+2}]_{\mathrm{i}}, \varepsilon_4), \\
\frac{\mathrm{d}u_{\mathrm{i}}}{\mathrm{d}t} &= \varepsilon_1 \varepsilon_4 \frac{\overline{u_{\mathrm{i}}}(E) - u_{\mathrm{i}}}{\tau_{u_{\mathrm{i}}}(E)}, \\
\frac{\mathrm{d}[\mathrm{Na}^+]_{\mathrm{i}}}{\mathrm{d}t} &= \varepsilon_1 \varepsilon_4 (FV_i)^{(-1)} \left(-3I_{\mathrm{Na,K}} + 3I_{\mathrm{NaCa}} + I_{\mathrm{b,Na}} + I_{\mathrm{Na}}\right), \\
\frac{\mathrm{d}[\mathrm{K}^+]_{\mathrm{i}}}{\mathrm{d}t} &= \varepsilon_1 \varepsilon_4 \left((FV_i)^{(-1)} \left(2I_{\mathrm{Na,K}} - I_{\mathrm{K1}} - I_{\mathrm{to}} - I_{\mathrm{Kur}} - I_{\mathrm{Kr}} - I_{\mathrm{Ks}} - I_{\mathrm{b,K}}\right)\right),
\end{aligned}
$$

$$
\begin{aligned}
\frac{\mathrm{d}[\mathrm{Ca}^{+2}]_{\mathrm{up}}}{\mathrm{d}t} =& \varepsilon_1\varepsilon_4\left(I_{\mathrm{up}} - I_{\mathrm{up,leak}} - I_{\mathrm{tr}}\frac{V_{\mathrm{rel}}}{V_{\mathrm{up}}}\right),\\
\varepsilon_2\varepsilon_3\frac{\mathrm{d}m}{\mathrm{d}t} =& \frac{\overline{m}(E,\varepsilon_3) - m}{\tau_m(E)}, \qquad \overline{m}(E,0) = H(E - E_m),\\
\varepsilon_2\varepsilon_3\frac{\mathrm{d}u_{\mathrm{a}}}{\mathrm{d}t} =& \frac{\overline{u_{\mathrm{a}}}(E) - u_{\mathrm{a}}}{\tau_{u_{\mathrm{a}}}(E)},\\
\varepsilon_2\varepsilon_3\frac{\mathrm{d}w}{\mathrm{d}t} =& \frac{\overline{w}(E) - w}{\tau_w(E)},\\
\varepsilon_3\frac{\mathrm{d}h}{\mathrm{d}t} =& \frac{\overline{h}(E,\varepsilon_3) - h}{\tau_h(E)}, \qquad \overline{h}(E,0) = H(E_h - E),\\
\varepsilon_3\frac{\mathrm{d}o_{\mathrm{a}}}{\mathrm{d}t} =& \frac{\overline{o_{\mathrm{a}}}(E) - o_{\mathrm{a}}}{\tau_{o_{\mathrm{a}}}(E)},\\
\varepsilon_3\frac{\mathrm{d}d}{\mathrm{d}t} =& \frac{\overline{d}(E) - d}{\tau_d(E)},\\
\frac{\mathrm{d}u}{\mathrm{d}t} =& \frac{\overline{u}(F_n) - u}{\tau_u}, \qquad \overline{u}(F_n,0) = H(F_n - F_1),\\
\frac{\mathrm{d}v}{\mathrm{d}t} =& \frac{\overline{v}(F_n) - v}{\tau_v(F_n)}, \qquad \overline{v}(F_n,0) = H(F_n - F_2), \qquad \tau_v(F_n,0) = 2 + 2H(F_n - F_1),\\
\frac{\mathrm{d}x_{\mathrm{r}}}{\mathrm{d}t} =& \varepsilon_4\frac{\overline{x_{\mathrm{r}}}(E) - x_{\mathrm{r}}}{\tau_{x_{\mathrm{r}}}(E)},\\
\frac{\mathrm{d}x_{\mathrm{s}}}{\mathrm{d}t} =& \varepsilon_4\frac{\overline{x_{\mathrm{s}}}(E) - x_{\mathrm{s}}}{\tau_{x_{\mathrm{s}}}(E)},\\
\frac{\mathrm{d}f}{\mathrm{d}t} =& \varepsilon_4\frac{\overline{f}(E) - f}{\tau_f(E)},\\
\frac{\mathrm{d}j}{\mathrm{d}t} =& \frac{\overline{j}(E) - j}{\tau_j(E)},\\
\frac{\mathrm{d}f_{\mathrm{Ca}}}{\mathrm{d}t} =& \frac{\overline{f_{\mathrm{Ca}}}([\mathrm{Ca}^{+2}]_{\mathrm{i}}) - f_{\mathrm{Ca}}}{\tau_{f_{\mathrm{Ca}}}},\\
\frac{\mathrm{d}o_{\mathrm{i}}}{\mathrm{d}t} =& \frac{\overline{o_{\mathrm{i}}}(E) - o_{\mathrm{i}}}{\tau_{o_{\mathrm{i}}}(E)},\\
\frac{\mathrm{d}[\mathrm{Ca}^{+2}]_{\mathrm{i}}}{\mathrm{d}t} =& \frac{B_1}{B_2},\\
\frac{\mathrm{d}[\mathrm{Ca}^{+2}]_{\mathrm{rel}}}{\mathrm{d}t} =& \frac{(I_{\mathrm{tr}} - I_{\mathrm{rel}})}{\left(1 + \frac{[\mathrm{Csqn}]_{\max}K_{\mathrm{m,Csqn}}}{([\mathrm{Ca}^{+2}]_{\mathrm{rel}} + K_{\mathrm{m,Csqn}})^2}\right)},
\end{aligned}
$$

where

$$
\begin{aligned}
B_1 =& (2FV_{\mathrm{i}})^{(-1)}\left(2I_{\mathrm{NaCa}} - I_{\mathrm{p,Ca}} - I_{\mathrm{Ca,L}} - I_{\mathrm{b,Ca}}\right) + (V_{\mathrm{i}})^{(-1)}\left(V_{\mathrm{up}}(I_{\mathrm{up,leak}} - I_{\mathrm{up}}) + I_{\mathrm{rel}}V_{\mathrm{rel}}\right),\\
B_2 =& 1 + \frac{[\mathrm{Trpn}]_{\max}K_{\mathrm{m,Trpn}}}{([\mathrm{Ca}^{+2}]_{\mathrm{i}} + K_{\mathrm{m,Trpn}})^2} + \frac{[\mathrm{Cmdn}]_{\max}K_{\mathrm{m,Cmdn}}}{[\mathrm{Ca}^{+2}]_{\mathrm{i}} + K_{\mathrm{m,Cmdn}})^2}\\
F_n =& 10^{-12}V_{\mathrm{rel}}I_{\mathrm{rel}} - \frac{5\times 10^{-13}}{F}\left(\frac{1}{2}I_{\mathrm{Ca,L}} - \frac{1}{5}I_{\mathrm{NaCa}}\right),
\end{aligned}
$$

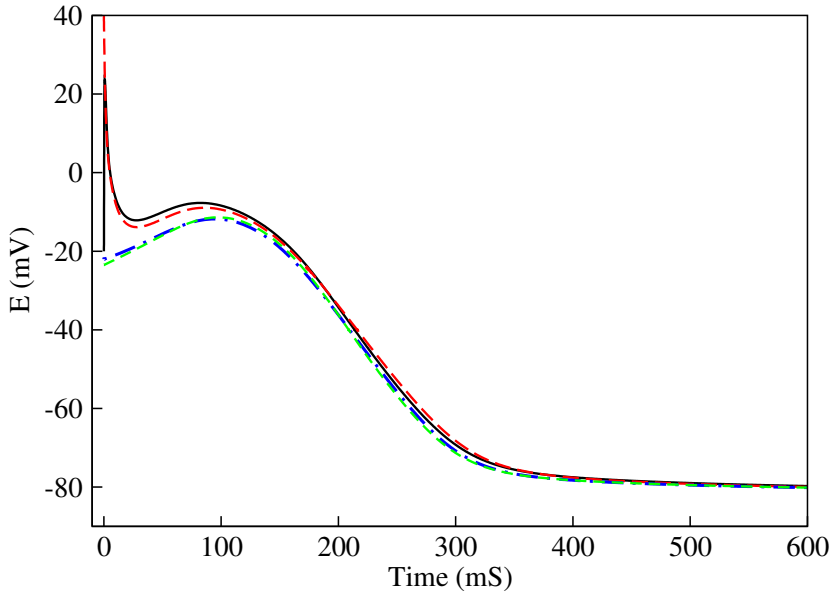

Figure 6.6: Solution of the full CRN-21 system denoted in black is compared with the reduced systems of CRN-11, CRN-7 and CRN-5 in red, blue and green respectively.

$$\overline{u} = (1 + H\exp(\frac{-F_n}{a}))^{-1}, \qquad \overline{v} = 1 - (1 + G\exp(\frac{-F_n}{a}))^{-1},$$
$$F_1 = a\ln G, \qquad F_2 = a\ln H.$$

A description of the ε_j for $j = 1,...,4$ is as follows.

ε_1 separates the super-slow variables from the slow variables, CRN-21 becomes CRN-17.

ε_2 distinguishes the super-fast variables from the fast variables, CRN-17 becomes CRN-14.

ε_3 classifies the fast variables from the intermediate variables, CRN-14 becomes CRN-11.

ε_4 separates the intermediate variables from the slow variables and CRN-14 gives CRN-6.

The reduced system CRN-7 obtained from the slow stage of an action potential is reduced further by Suckley (2004) where she proposed a series of less accurate reductions compared to the above reduction process. She showed that the $[Ca^{+2}]_{rel}$ equation in CRN-7 is decoupled and can be solved separately since it only contains $[Ca^{+2}]_{rel}$. This leads to the system CRN-6. Then speed analysis is applied as before and the remaining variables of the CRN-6 system are categorised into two groups of slow and fast variables. The variable o_i is identified as a fast variable that reaches its quasi-stationary value, relatively quick. Therefore, the variable is replaced with its quasi-stationary function and the system of CRN-5 is obtained. Figure 6.6 compares the solutions of the systems CRN-21, CRN-11, CRN-7 and CRN5 which are plotted with black, red, blue and green curves, respectively. From this

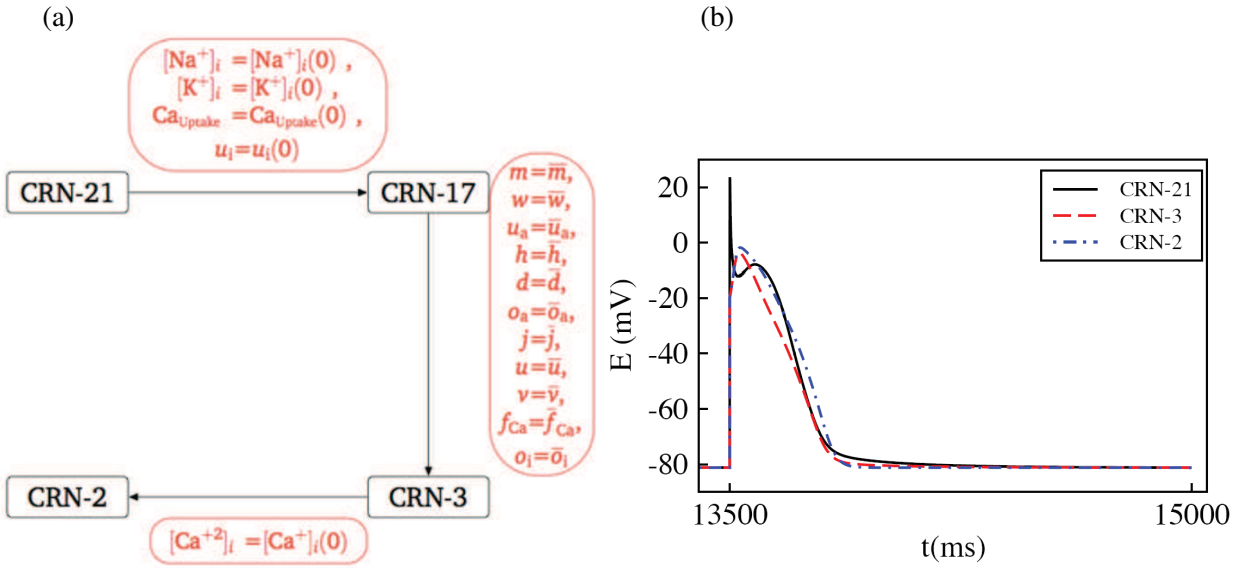

Figure 6.7: Plot (a) is a chart describing the reduction process of the CRN-21 model. Plot (b) shows the The solution of the full Courtemanche et al. (1998) model in comparison with CRN-3 and CRN-2, when $BCL = 1500$(ms).

figure it can be seen that during the repolarisation phase of the action potential, the solution of the reduced CRN-5 system is in agreement with the full CRN-21 model. The variables x_r and x_s are also identified as the fast variables of the system CRN-5 and are replaced with their quasi-stationary functions. Following this series of same accurate and same less accurate reductions, the system of CRN-3 involving only three variables E, f and $[Ca^{+2}]_i$ is obtained. Furthermore, we reduced the CRN-3 model one step further by replacing $[Ca^{+2}]_i$ with its initial value $[Ca^{+2}]_i(0)$ and the system of CRN-2 is obtained. A simple chart outlining the reduction process is plotted in Figure 6.7(a). The CRN-21, CRN-3 and CRN-2 systems are solved for series of solutions and their last solution is plotted in Figure 6.7(b). It can be seen that despite a difference between the shape of the action potential in these three systems, the solution of CRN-2 in the repolarisation phase agrees closely with the solution of the CRN-21 system. As a result, this system is studied and the role of its parameters in inducing repolarisation alternans are investigated.

6.4 The reduced Courtemanche system with two variables

The system of CRN-2 has two dynamical variables, the transmembrane voltage $E(t)$ and a gating variable $f(t)$. The voltage $E(t)$ is governed by

$$\frac{\mathrm{d}E}{\mathrm{d}t} = -\frac{I_1(E) + I_2(E,f)}{C_M}, \tag{6.3a}$$

where $I_1(E)$ is a combination of all the voltage dependent currents and $I_2(E,f)$ is a function of voltage E and variable f. The currents are given by

$$\begin{aligned} I_1(E) =& I_{\mathrm{K1}}\left(E,[\mathrm{K}^+]_{\mathrm{i}}(0)\right) + I_{\mathrm{to}}\left(E,\overline{o_{\mathrm{a}}},\overline{o_{\mathrm{i}}},[\mathrm{K}^+]_{\mathrm{i}}(0)\right) + I_{\mathrm{Kur}}\left(E,\overline{u_{\mathrm{a}}},\overline{u_{\mathrm{i}}},[\mathrm{K}^+]_{\mathrm{i}}(0)\right) \\ &+ I_{\mathrm{Kr}}\left(E,[\mathrm{K}^+]_{\mathrm{i}}(0),\overline{x_{\mathrm{r}}}\right) + I_{\mathrm{Ks}}\left(E,[\mathrm{K}^+]_{\mathrm{i}}(0),\overline{x_{\mathrm{s}}}\right) + I_{\mathrm{Na,K}}\left(E,[\mathrm{Na}^+]_{\mathrm{i}}(0)\right) \\ &+ I_{\mathrm{b,Na}}\left(E,[\mathrm{Na}^+]_{\mathrm{i}}(0)\right) + I_{\mathrm{NaCa}}\left(E,[\mathrm{Na}^+]_{\mathrm{i}}(0),[\mathrm{Ca}^{+2}]_{\mathrm{i}}(0)\right) + I_{\mathrm{b,Ca}}\left(E,[\mathrm{Ca}^{+2}]_{\mathrm{i}}(0)\right), \\ I_2(E,f) =& I_{\mathrm{Ca,L}}(E,f,\overline{d},\overline{f_{\mathrm{Ca}}}) = g_{\mathrm{Ca,L}}\overline{d}f\overline{f_{\mathrm{Ca}}}(E-65). \end{aligned} \tag{6.3b}$$

The current $I_2(E,f)$ is the inward Ca^{+2} current $I_{\mathrm{Ca,L}}$ and includes terms involving the maximum $I_{\mathrm{Ca,L}}$ conductance, denoted as $g_{\mathrm{Ca,L}}$, the voltage-dependent activation gate d, the voltage-dependent inactivation gate f and the Ca^{+2}-dependent inactivation gate f_{Ca}. As explained earlier, the gating variables d and f_{Ca} are replaced with their quasi-stationary functions and the only gating variable on which $I_{\mathrm{Ca,L}}$ depends is the voltage-dependent inactivation gating variable f which satisfies

$$\frac{\mathrm{d}f}{\mathrm{d}t} = \frac{\overline{f}(E) - f}{\tau_f(E)}, \tag{6.3c}$$

where

$$\begin{aligned} \overline{f}(E) &= \left(1 + \exp\left(\frac{E+28}{6.9}\right)\right)^{-1}, \\ \tau_f &= 9\left(0.0197\exp\left(-0.0337^2(E+10)^2\right) + 0.02\right)^{-1}. \end{aligned} \tag{6.3d}$$

The following initial conditions are imposed on the CRN-2 system (6.3)

$$E(0) = E_{\mathrm{stim}}, \quad f(0) = 1. \tag{6.3e}$$

The behaviour of the gating variable f affects the $I_{\mathrm{Ca,L}}$ and consequently the membrane potential. When f decreases, the inward $I_{\mathrm{Ca,L}}$ increases and the voltage rises. Hence an excursion occurs which happens during the depolarisation phase of an action potential. When f increases, the $I_{\mathrm{Ca,L}}$ decreases

and the voltage decays back towards its resting potential. This occurs during the repolarisation phase. The functions $\tau_f(E)$ and $\overline{f}(E)$ are continuous functions of voltage E. In order to understand their behaviour and their effect on the membrane potential, these functions and the voltage $E(t)$ are plotted as black curves in Figures 6.8(a), 6.8(b) and 6.8(c), respectively. As can be seen in Figure 6.8(a), the range of $\tau_f(E)$ is large, therefore the voltage-dependent inactivation of $I_{\mathrm{Ca,L}}$ is a slow process. According to Courtemanche et al. (1998) the $I_{\mathrm{Ca,L}}$ activates very quickly, due to its voltage-dependent activation d. Then it has rapid inactivation process mediated by Ca^{+2} and this is followed by a slow voltage-dependent inactivation process which occurs when voltage decays to its resting potential. From the Figure 6.8, it can be seen that the functions $\tau_f(E)$ and $\overline{f}(E)$ can be replaced by step func-

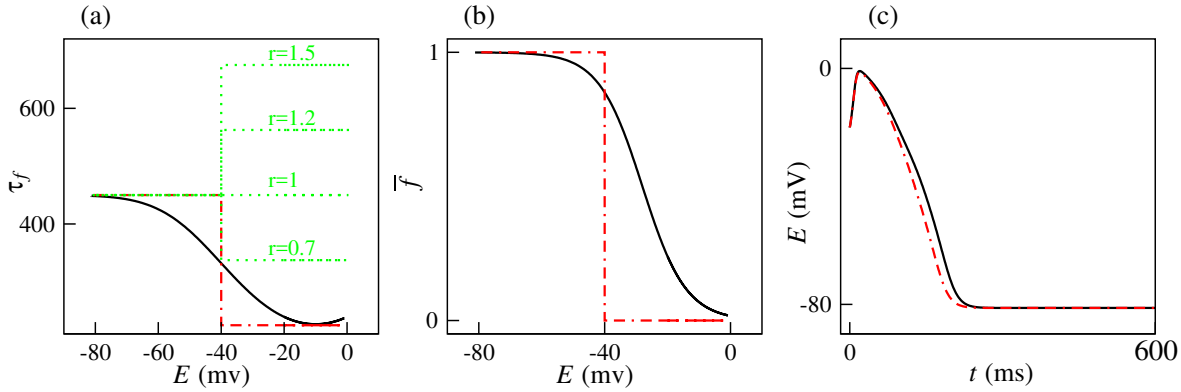

Figure 6.8: The original and modified functions for $\tau_f(E)$, $\overline{f}(E)$ and the membrane voltage E are plotted in (a), (b) and (c) respectively. The black curves correspond to the original functions and the red curves denote the modified functions where the model's constants are $E_f = -40$, $F_1 = 450$ and $r = \frac{1}{2}$. In plot (a) the green curves correspond to different values of the parameter r.

tions (6.3f) and (6.3g) as follow

$$\tau_f(E) = F_1\left(rH(E-E_f) + H(E_f-E)\right), \tag{6.3f}$$

$$\overline{f}(E) = H(E_f-E), \tag{6.3g}$$

where the values $E_f = -40$, $F_1 = 450$ and $r = \frac{1}{2}$ give the closest match to the original system. In Mitchell and Schaeffer (2003) it was determined that the voltage-dependent time function ($\tau(E)$ as a function of τ_{open} and τ_{close}) plays an important role in changing the behaviour of a system and inducing instabilities. Therefore in modifying the voltage-dependent inactivation time function $\tau_f(E)$ in CRN-2 system, a dimensionless parameter r is introduced into the function $\tau_f(E)$ and the role of r is studied. The parameter r determines the amplitude of the time function during the slow inactivation

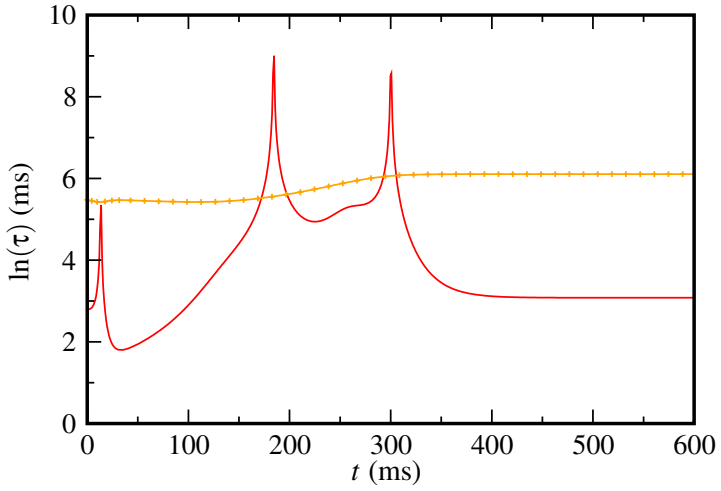

Figure 6.9: Graph of the timescale coefficient for CRN-2. The red curve is the time-scale coefficient function of voltage and the orange curve corresponds to f.

process of $I_{\mathrm{Ca,L}}$. When $r < 1$ the time required for the inactivation process to occur is small and consequently the gating variable f evolves quickly. For $r > 1$ the time required for the inactivation process is large. The dependence of $\tau_f(E)$ on the parameter r is illustrated in Figure 6.8(a). Now that the functions of CRN-2 have been modified using appropriate step functions and that the resulting membrane potential has been seen to agree closely with the original CRN-2 model, the system of CRN-2 is studied in more details. An explicit formula for its restitution curve is derived and the responses of the map are studied.

6.4.1 Asymptotic reduction

The CRN-2 system (6.3) is now considered in the domain $t \in [0,B]$ and when the boundary condition is $E(0) = E_{\mathrm{stim}}, f(0) = f(B)$. The speed of the voltage E and the gating variable f are compared. As described previously, the timescale coefficient can be plotted against time to analyse the speed of each variable during one solution. It can be seen in Figure 6.9 that the voltage E, despite having two peaks during the time course of one action potential, has a smaller timescale coefficient than the gating variable f. Therefore it is considered as the fast variable in the CRN-2 system. On the other hand the gating variable f has the larger timescale coefficient which indicates that f is the slow variable. As a result of the speed analysis, a small parameter $\varepsilon > 0$ can be introduced into the system (6.3) such that when $\varepsilon = 1$ the system CRN-2 (6.3) is recovered and in the limit $\varepsilon \to 0$ the variable E becomes much

faster then the gating variable f. Introducing ε, the system (6.3) becomes

$$\varepsilon\frac{\mathrm{d}E}{\mathrm{d}t} = -\frac{I_1(E)+I_2(E,f)}{C_M},$$
$$\frac{\mathrm{d}f}{\mathrm{d}t} = \frac{\overline{f}(E)-f}{\tau_f(E)}.$$

This indicates that the CRN-2 system can be analysed as fast and slow subsystems as follows.

The slow subsystem: When $\varepsilon \to 0$, the asymptotically reduced system becomes as follows

$$0 = I_1(E)+I_2(E,f), \tag{6.4a}$$
$$\frac{\mathrm{d}f}{\mathrm{d}t} = \frac{\overline{f}(E)-f}{\tau_f(E)}, \tag{6.4b}$$

where f is the only dynamical variable and (6.4b) describes its evolution along the slow branch (6.4a). As stated in previous chapters, the slow subsystem describes the plateau and the recovery stages of the action potential.

The fast subsystem: The fast transient of the system can be studied if the independent time variable is changed to $T = \frac{t}{\varepsilon}$. The fast subsystem is obtained as follows

$$\frac{\mathrm{d}E}{\mathrm{d}T} = -\frac{I_1(E)+I_2(E,f)}{C_M},$$
$$\frac{\mathrm{d}f}{\mathrm{d}T} = \varepsilon\frac{\overline{f}(E)-f}{\tau_f(E)}.$$

Taking the limit $\varepsilon \to 0$ the system (6.5) becomes:

$$\frac{\mathrm{d}E}{\mathrm{d}T} = -\frac{I_1(E)+I_2(E,f)}{C_M}, \tag{6.5a}$$
$$\frac{\mathrm{d}f}{\mathrm{d}T} = 0, \tag{6.5b}$$

where the evolution of f during the fast time scale is negligible since it is constant. The only dynamical variable in the fast time scale T is voltage E and its equation (6.5a) describes the upstroke and repolarisation stage of the action potential. In the next section, the phase portrait of the CRN-2 system (6.3) is studied.

6.4.2 Phase portrait

The phase portrait of the CRN-2 system (6.3) is shown in Figure 6.10 where the phase portrait for the original functions of CRN-2 (6.3d) and the modified functions (6.3f) and (6.3g) in Figures 6.10(a)

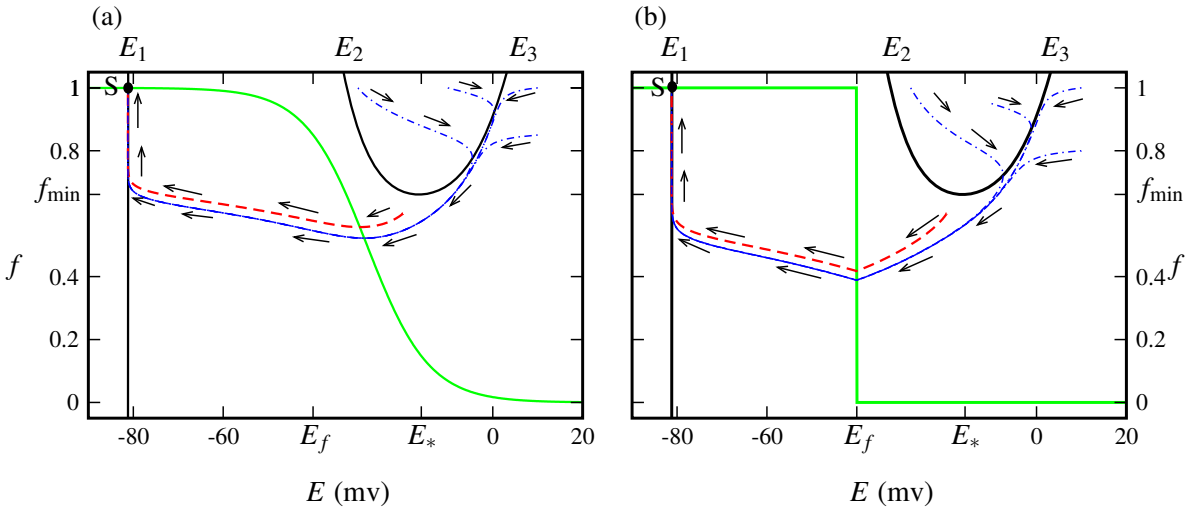

Figure 6.10: Phase portrait of CRN-2 system (6.3) with selected trajectories for different initial conditions (E_0, f_0). The black curve is the E-nullcline. The green f-nullcline is the original function (6.3d) in plot (a) and is the modified function (6.3g) in plot (b).in both (a) and (b) $\varepsilon = 1$, in (b) $r = 1$.

and 6.10(b), respectively are plotted. A few selected trajectories of the system (6.3) with original and modified functions are also shown in Figures 6.10(a) and 6.10(b) to outline the effects of the modification on the f-nullcline and the trajectories. Equation (6.4a) defines the slow manifold of the system which is plotted with a black solid curve in Figure 6.10 and is explicitly given by:

$$\mathcal{F}(E) = \frac{-I_1(E)}{g_{\text{Ca,L}}\,\overline{d}\,\overline{f_{\text{Ca}}}(E-65)}. \tag{6.6}$$

The f-nullcline $\dfrac{df}{dt} = 0$ is shown with green curves in plots (a) and (b) of Figure 6.10, and is defined by

$$f_{\text{Original}}(E) = \left(1 + \exp\left(\frac{E+28}{6.9}\right)\right)^{-1},$$

$$f_{\text{Modified}}(E) = \begin{cases} 1 & \text{if} \quad E < E_f \\ 0 & \text{if} \quad E > E_f. \end{cases}$$

The slow manifold is split into two parts with positive slope separated by a part with a negative slope. The positive slope branches, labelled E_1 and E_3, are stable and the negative slope branch E_2 is unstable. The stable and unstable branches are separated at the point $(E_*, f_{\min}) = (-15, 0.66)$ where E_* is the root of the equation $\mathcal{F}'(E_*) = 0$, where the slow gating variable f takes its minimum value at E_*.

$$\frac{df}{dE}(E_*) = 0 \tag{6.7}$$

$$f_{\min} = \frac{-I_1(E_*)}{g_{\mathrm{Ca,L}}\,\overline{d}\,\overline{f_{\mathrm{Ca}}}(E_* - 65)}.$$

The E_1 branch corresponds to the "diastolic" part $E \in (-\infty, E_f]$ and the E_3 branch is the "systolic" phase of an action potential when $E \in [E_f, +\infty]$. On the time scale $t \sim 1$ there is a slow movement along the slow manifold with its evolution described by (6.4b).

Consider the two nullclines intersect at the steady state $S = (E_{\mathrm{ss}}, f_{\mathrm{ss}})$. The point S is the equilibrium of the system (6.3) and as is shown in Figure 6.10, it is at the "diastolic" branch of the slow manifold. The direction of the trajectories are dependent on the signs of $\frac{\mathrm{d}E}{\mathrm{d}t}$ and $\frac{\mathrm{d}f}{\mathrm{d}t}$ as described in Chapter 2. If the equilibrium point is perturbed the resulting trajectory converges back to the steady state.

If the initial condition is chosen such that there is a sufficiently large perturbation from the steady state, then an action potential will be elicited. The initial condition for voltage must be large enough to pass the unstable middle branch E_2 of the E-nullcline. For a specific E_{stim} there is a threshold value for the gating variable f that is exactly the value of f on the E-nullcline when $E = E_{\mathrm{stim}}$. The equation that describes the threshold value of f, is as follows

$$f_{\mathrm{thr}} \equiv \frac{-I_1(E_{\mathrm{stim}})}{g_{\mathrm{Ca,L}}\,\overline{d}\,\overline{f_{\mathrm{Ca}}}(E_{\mathrm{stim}} - 65)}. \tag{6.8}$$

The k-th action potential will be formed if $f_k > f_{\mathrm{thr}}$. If this condition is not satisfied then the voltage decays back to its resting potential as it is illustrated in Figures 6.10 with red dashed curves. A trajectory starting from $E_{\mathrm{stim}} > E_2$ -satisfies the above condition- is repelled by E_2 and attracted by E_3 branch of the slow manifold. The trajectory then travels along the systolic branch of the slow manifold and at $(E_*, f_{\min})$ leaves the stable branch and jumps towards the diastolic branch. This is followed by another slow movement along the diastolic branch of E-nullcline approaching the global equilibrium, where the motion would eventually stops. As mentioned above, the entire cycle is repeated if the initial conditions are chosen in the excitable region of the phase portrait and the condition (6.8) is satisfied. The successful trajectories are shown in Figure 6.10 with blue curves. It is vital to note that f_{thr} is constrained to satisfy $f_{\mathrm{thr}} \in (f_{\min}, 1]$, since below the minimum value for f the solution is outside the excitable region. In the next section the action potential duration restitution map is derived from the modified CRN-2 system.

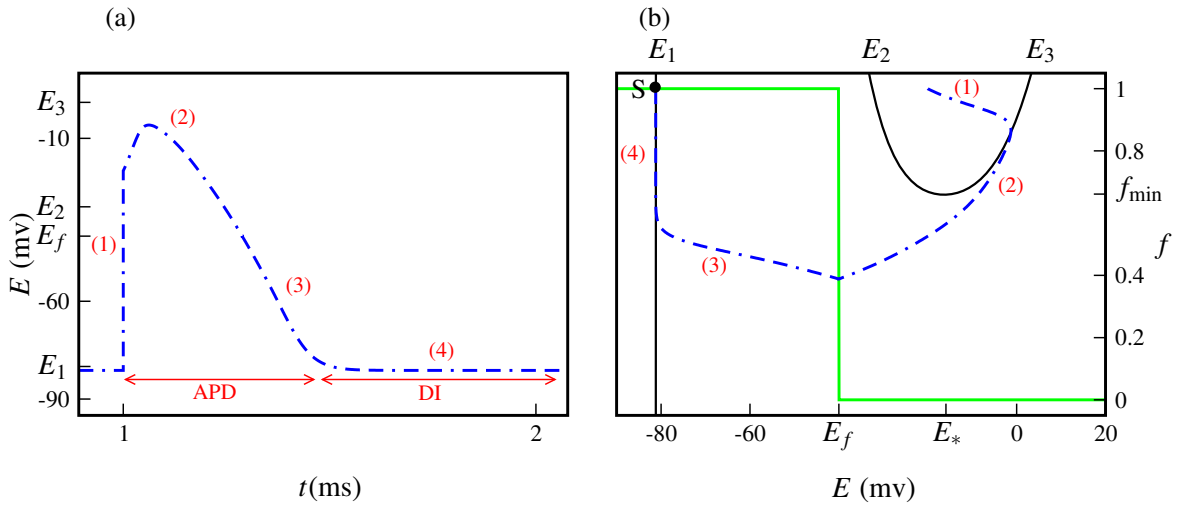

Figure 6.11: A typical action potential solution for CRN-2 system (6.3). Figure (a) illustrates the solution in (E,t) plane with action potential duration (APD) and diastolic interval (DI) shown as phases (2) and (4), respectively. In (b) the solution is shown in the (f,E) plane. The fast motion occurs at the phases (1) and (3), whereas the phases (2) and (4) are motion along the slow manifold.

6.5 Asymptotic action potential duration map

Figure 6.11 presents one selected trajectory corresponding to a typical action potential solution of the CRN-2 system (6.3) with modified functions (6.3f) and (6.3g) and initial conditions (6.3e). Four phases of the action potential are labelled 14 and are shown in the (t,E) plane and (E,f) plane. As mentioned earlier, the phase one of the action potential is a fast initial movement corresponding to the upstroke of the action potential. This phase is labelled as (1) in Figures 6.11(a) and 6.11(b). The movement of the trajectory along the systolic branch of the slow manifold (6.6) is labelled as phase (2) and corresponds to the plateau phase of the action potential. This phase occurs on a time scale of $\tau_f = rF_1$ and the inactivation gating variable f reaches its smallest value $\overline{f} = 0$. At the point $(E_*, f_{\min})$ the trajectory leaves the stable branch and jumps towards the diastolic branch which corresponds to the repolarisation phase of the action potential and it is shown as phase (3) of the action potential. Then at the phase (4) the trajectory travels slowly along the diastolic branch of the slow manifold (6.6) and stops at the steady state i.e. the action potential returns to its resting potential. This phase occurs on a time scale of $\tau_f = F_1$ in which the voltage-dependent inactivation gating variable f reaches its largest value, i.e. $\overline{f} = 1$. The action potential duration map of type (3.1) is now constructed in this section and the stability of the map is studied. Similar to the previous chapters, the approach in

obtaining the map is based on Mitchell and Schaeffer (2003).

Map The APD restitution map of the CRN-2 system (6.3) is obtained using the equation (6.4).

Lemma 6.1 *For an AP sequence generated in problem* (6.3)

$$\mathrm{A}_k = a(f_{k-1}), \qquad a(x) \equiv rF_1 \ln\left|\frac{x}{f_{\min}}\right|, \tag{6.9a}$$

$$\mathrm{D}_k = d(f_k), \qquad d(x) \equiv F_1 \ln\left|\frac{1-f_{\min}}{1-x}\right|, \tag{6.9b}$$

$$f_k \equiv f(kB), \quad k \in \mathbb{N}.$$

where $f_{k-1} = f((k-1)B)$ is the value of gating variable f at the beginning of the k-st AP and $k \in \mathbb{N}$.

Proof As can be seen in Figure 6.11 the time during which the voltage in greater than E_f is the action potential duration. The figure 6.11 is modified so that it can illustrate the APD. In general APD can be considered as the sum of phase 2 and some part of phase 3 of the action potential. But, here we considered phase 2 only. The value of the voltage also exceeds E_f during parts of the phase (3) but as stated previously, the motion away from the slow manifold is very fast and this phase like the phase (1) of the action potential is very brief. As a result, the time required for the f gating variable to travel from its preceding value to $f_{\min}$ is considered to be the duration of phase (2) and is obtained by integration of $\frac{\mathrm{d}f}{\mathrm{d}t}$ along the systolic branch $E \in [E_f, +\infty]$. The time required for the motion at the phase four of the action potential is diastolic interval D_k and is obtained by integration of (6.4b) along the diastolic branch of the slow manifold $E \in (-\infty, E_f]$. Thus the following equations are obtained:

$$\mathrm{A}_k = \int_{(k-1)B}^{(k-1)B+\mathrm{A}_k} \mathrm{d}t = \int_{f((k-1)B)}^{f_{\min}} (rF_1)\frac{\mathrm{d}f}{-f} = rF_1 \ln\left|\frac{f_{k-1}}{f_{\min}}\right|, \qquad E > E_f, \tag{6.10a}$$

$$\mathrm{D}_k = \int_{(k-1)B+\mathrm{A}_k}^{kB} \mathrm{d}t = \int_{f_{\min}}^{f(kB)} (F_1)\frac{\mathrm{d}f}{1-f} = F_1 \ln\left|\frac{1-f_{\min}}{1-f_k}\right|, \qquad E < E_f. \tag{6.10b}$$

Where $f_{k-1} = f((k-1)B)$ and $f_{\min}$ is the turning point for gating variable f, at which f is at its minimum value on the systolic branch of the slow manifold (6.6). Furthermore, $f_{\min}$ is the value in which the end of any plateau phase coincides with the beginning of the next recovery stage i.e.

$$f((k-1)B + \mathrm{A}_k) = f(kB + \mathrm{A}_{k+1}) = f_{\min} \quad \text{for any} \quad k \in \mathbb{N}$$

. ■

The propositions explained in this chapter are similar to those of previous chapters. However, since the equations are different, proofs are given for each proposition and the new terms are explained.

Proposition 6.1 *An action potential duration restitution map for the CRN-2 model is given by*

$$\begin{aligned} \mathrm{A}_{k+1} &= \Phi(\mathrm{A}_k), \\ \Phi(\mathrm{A}_k) = F(\tilde{\mathbf{a}}, B-\mathrm{A}_k) &= rF_1 \ln\left|\frac{1-(1-f_{\min})\exp\left(\frac{-(B-\mathrm{A}_k)}{F_1}\right)}{f_{\min}}\right|, \end{aligned} \tag{6.11}$$

where $\tilde{\mathbf{a}}$ *is a vector of CRN-2 parameters, i.e.* $\tilde{\mathbf{a}} = [r,\ B,\ E_{\text{stim}},\ f_{\text{thr}}]^T$.

Proof f_k is eliminated between expression (6.9a) written for A_{k+1} and expression (6.9b) written for $\mathrm{D}_k = B - \mathrm{A}_k$ and an action potential duration restitution map relating A_{k+1} to A_k is obtained. This Proposition gives an equivalent explicit representation of Lemma 6.1. ∎

Fixed points The fixed point of the maps Φ and Φ^2 correspond to the 1:1- and 2:2-responses as follows.

Proposition 6.2 *The equation* $\overline{\mathrm{A}} = \Phi(\overline{\mathrm{A}})$ *has a unique solution branch given in parametric form by*

$$\overline{\mathrm{A}} = a(\overline{f}), \qquad \overline{\mathrm{D}} = d(\overline{f}), \tag{6.12}$$

so that $a(\overline{f}) = B - d(\overline{f})$ *with a parameter* $\overline{f} \in [f_{\text{thr}}, 1]$.

Proof In order to solve $\overline{\mathrm{A}} = \Phi(\overline{\mathrm{A}})$, the parametric representation of Lemma 6.1 is used. Since in a 1:1 response

$$\mathrm{A}_k = \mathrm{A}_{k+1} \quad \text{and} \quad \mathrm{D}_k = \mathrm{D}_{k+1},$$

which is equivalent by (6.9) to

$$a(f_{k-1}) = a(f_k) \quad \text{and} \quad d(f_k) = d(f_{k+1}),$$

therefore, the solutions are $f_{k-1} = f_k \equiv \overline{f}$ and $f_k = f_{k+1} \equiv \overline{f}$, respectively. Hence all the action potentials start from identical values of the f gate, $\overline{f}$ in 1:1 response. The parameter $\overline{f}$ is a gating variable hence $\overline{f}$ must be in the range $[0,1]$. Furthermore, we stated in the equation (6.8) that no AP can be excited below f_{thr} so $\overline{f} \in [f_{\text{thr}}, 1]$. ∎

Proposition 6.3 *The equation* $\overline{\overline{\mathrm{A}}} = \Phi \circ \Phi(\overline{\overline{\mathrm{A}}})$ *has three solution branches: the first one is identical to* (6.12)*, and the other two are given in parametric form by*

$$\overline{\overline{\mathrm{A}}}_{\text{even}} = a(f_{\text{e}}) = a(\alpha f_{\text{o}}), \qquad \overline{\overline{\mathrm{D}}}_{\text{even}} = d(f_{\text{o}}), \tag{6.13a}$$

$$\overline{\overline{\mathrm{A}}}_{\mathrm{odd}} = a(f_{\mathrm{o}}), \qquad \overline{\overline{\mathrm{D}}}_{\mathrm{odd}} = d(f_{\mathrm{e}}) = d(\alpha f_{\mathrm{o}}), \tag{6.13b}$$

$$f_{\mathrm{o}} = \frac{1-\alpha^{r}}{1-\alpha^{r+1}}, \tag{6.13c}$$

with a parameter $\alpha \in (0,\infty)$.

Proof Similar to 5.3 rather than solving the equation $\overline{\overline{\mathrm{A}}} = \Phi \circ \Phi(\overline{\overline{\mathrm{A}}})$ directly, the equivalent parametric representation of Lemma 6.1 is used. In a 2:2 response

$$\mathrm{A}_{2k} = \mathrm{A}_{2k+2} \qquad \text{and} \qquad \mathrm{A}_{2k+1} = \mathrm{A}_{2k+3}, \qquad \forall k \in \mathbb{N}$$

as well as

$$\mathrm{D}_{2k} = \mathrm{D}_{2k+2} \qquad \text{and} \qquad \mathrm{D}_{2k+1} = \mathrm{D}_{2k+3}, \qquad \forall k \in \mathbb{N}.$$

Applying expressions (6.9), yields

$$f_{2k-1} = f_{2k+1} \equiv f_{\mathrm{e}} \qquad \text{and} \qquad f_{2k} = f_{2k+2} \equiv f_{\mathrm{o}}.$$

Since the basic cycle length is fixed, it is required that

$$B = \mathrm{A}_{2k} + \mathrm{D}_{2k} = \mathrm{A}_{2k+1} + \mathrm{D}_{2k+1} \iff a(f_{\mathrm{e}}) + d(f_{\mathrm{o}}) = a(f_{\mathrm{o}}) + d(f_{\mathrm{e}}). \tag{6.14}$$

Let f_{e} and f_{o} be rearranged as $f_{\mathrm{e}} = \alpha f_{\mathrm{o}}$, where $\alpha \in (0,\infty)$ then the results can be written as:

$$\overline{\overline{\mathrm{A}}}_{\mathrm{even}} = a(f_{\mathrm{e}}) = a(\alpha f_{\mathrm{o}}), \qquad \overline{\overline{\mathrm{D}}}_{\mathrm{even}} = d(f_{\mathrm{o}}),$$

$$\overline{\overline{\mathrm{A}}}_{\mathrm{odd}} = a(f_{\mathrm{o}}) \qquad \overline{\overline{\mathrm{D}}}_{\mathrm{odd}} = d(f_{\mathrm{e}}) = d(\alpha f_{\mathrm{o}}),$$

$$f_{\mathrm{o}} = \frac{1-\alpha^{r}}{1-\alpha^{r+1}}$$

It is now vital to establish the range of α. Clearly (6.13c) is invariant with respect to exchanging f_{e} and f_{o}, therefore without loss of generality the case $f_{\mathrm{e}} \geq f_{\mathrm{o}}$ is considered and since f_{e} and f_{o} are positive it follows that $f_{\mathrm{e}}/f_{\mathrm{o}} = \alpha \in (1,\infty)$. ∎

Stability and bifurcations of equilibria Again, similar to the previous chapters, in order to establish the stability properties of 1:1 and 2:2 responses, the condition (3.4b) and (3.5b) are imposed on (6.12) and (6.13), respectively.

Proposition 6.4 *The equilibrium* (4.16) *of the APD restitution map* (6.11) *loses stability in a flip (period-doubling) bifurcation at*

$$f_{\mathrm{bif}} = \frac{r}{1+r} \tag{6.15a}$$

or in terms of the BCL, alternatively at

$$B_{\text{bif}} = a(f_{\text{bif}}) + d(f_{\text{bif}}) = F_1 \ln \left| \frac{{f_{\text{bif}}}^r (1 - f_{\min})}{{f_{\min}}^r (1 - f_{\text{bif}})} \right|. \tag{6.15b}$$

B_{bif} *corresponds to the region where 2:2-response bifurcates from the 1:1-response and it is denoted as* S_1 *in Figure 6.12.*

Proof Substitution of (6.12) into (3.4b) and solve $\left|\partial_{\text{A}} F(\mathbf{a}, \text{A})\right|_{\overline{\text{A}}} = 1$, which is the border of stability, the following condition is obtained

$$\left| -\frac{r(1 - f_{\min}) \exp\left(\frac{-(B - \overline{\text{A}})}{F_1}\right)}{1 - (1 - f_{\min}) \exp\left(\frac{-(B - \overline{\text{A}})}{F_1}\right)} \right| = 1 \tag{6.16}$$

Clearly, at the end of the the k-st action potential, $f_k = 1 - (1 - f_{\min}) \exp\left(-\frac{\text{D}}{F_1}\right)$. It follows from $\text{D} = \text{D}_{\text{bif}}$ that $f_{\text{bif}} = 1 - (1 - f_{\min}) \exp\left(-\dfrac{(B_{\text{bif}} - \text{A}_{\text{bif}})}{F_1}\right)$. Thus by rewriting (6.16) in terms of f_{bif}, the following equation is obtained

$$\frac{r(1 - f_{\text{bif}})}{f_{\text{bif}}} = 1$$

which provides an expression for f_{bif} in terms of the models parameter r:

$$\overline{f} = f_{\text{bif}} = \frac{r}{(1 + r)}.$$

Evaluating (6.12) at f_{bif} yields:

$$\text{A}_{\text{bif}} = a(f_{\text{bif}}) = r F_1 \ln \left| \frac{f_{\text{bif}}}{f_{\min}} \right|, \tag{6.17a}$$

$$\text{D}_{\text{bif}} = d(f_{\text{bif}}) = F_1 \ln \left| \frac{1 - f_{\min}}{1 - f_{\text{bif}}} \right|, \tag{6.17b}$$

$$B_{\text{bif}} = a(f_{\text{bif}}) + d(f_{\text{bif}}) = F_1 \ln \left| \frac{{f_{\text{bif}}}^r (1 - f_{\min})}{{f_{\min}}^r (1 - f_{\text{bif}})} \right|. \tag{6.17c}$$

■

Proposition 6.5 *The equilibria* (6.13) *of the second-generation map* $\Phi \circ \Phi$ *bifurcate from the equilibrium* (6.12) *of the APD restitution map* (6.11) *at* (6.15a) *and lose their stability at* $r = 1$.

Proof It is evident that $f_{\text{o}} = f_{\text{e}}$ when $\alpha = 1$, therefore the intersection of (6.12) and (6.13) can be obtained if the expression (6.13c) is evaluated at $\alpha = 1$. Thus the following equation for the value where (6.13) first emerges, is obtained:

$$f_{\text{o}}(\alpha = 1) = \frac{r}{1 + r} = f_{\text{bif}},$$

In order to determine the stability of the equilibria, the methods explained in the previous chapters are employed. Thus, according to Strogatz (2001) a pitchfork bifurcation can be either supercritical if $[\partial_{\mathrm{A}}^3 \Phi \circ \Phi]_{\mathrm{A_{bif}}} < 0$ or subcritical if $[\partial_{\mathrm{A}}^3 \Phi \circ \Phi]_{\mathrm{A_{bif}}} > 0$. It is important to mention that a flip bifurcation for Φ is a pitchfork bifurcation for the second generation map $\Phi \circ \Phi$ as well. Substituting (6.17) into $[\partial_{\mathrm{A}}^3 \Phi \circ \Phi]_{\mathrm{A_{bif}}} = 0$ and solving this equation for r, the boundary between the subcritical and the supercritical cases is determined to be $r = 1$. As before, the subcritical case is characterised by one stable branch on one side and no stable branches on the other side of the bifurcation point. The supercritical case is characterised by one stable branch on one side and two stable and one unstable branches on the other side of the bifurcation point. ■

Thresholds The 1:1 responses are stable for $B > \overline{B}_{\mathrm{thr}}$ (condition (3.4c)), where $\overline{B}_{\mathrm{thr}}$ is the threshold value of BCL for excitation of a 1:1 response. Furthermore, the 2:2 responses are stable for $B > \overline{\overline{B}}_{\mathrm{thr}}$ (condition (3.5c)) such that $\overline{\overline{B}}_{\mathrm{thr}}$ is the threshold value for excitation of 2:2 response. These conditions are explained in propositions and respectively.

Proposition 6.6 *The threshold value of BCL for excitation of a 1:1 response is*

$$\overline{B}_{\mathrm{thr}} = \overline{\mathrm{A}}_{\mathrm{thr}} + \overline{\mathrm{D}}_{\mathrm{thr}} = rF_1 \ln \left| \frac{f_{\mathrm{thr}}}{f_{\mathrm{min}}} \right| + F_1 \ln \left| \frac{1 - f_{\mathrm{min}}}{1 - f_{\mathrm{thr}}} \right|. \tag{6.18}$$

The $\overline{B}_{\mathrm{thr}}$ given by the above equation, is a function of r and E_{stim} and is shown in Figure 6.12 as a blue surface denoted by S_2.

Proof Recall that E_{stim} is a value of the stimulus voltage which means the voltage must be large enough to generate the k-st action potential. Therefore E_{stim} must satisfy $E_{\mathrm{stim}} > E_2$ for which $f_{\mathrm{thr}} > f_{k-1}$ where f_{thr} is given by (6.8). The result then follows by evaluation of (6.12) at $\overline{f} = f_{\mathrm{thr}}$. ■

Proposition 6.7 *The threshold value of BCL for excitation of a 2:2 response is*

$$\overline{\overline{B}}_{\mathrm{thr}} = a\left(f_{\mathrm{thr}}\right) + d\left(\alpha\left(f_{\mathrm{thr}}\right) f_{\mathrm{thr}}\right) = a\left(\alpha(f_{\mathrm{thr}}) f_{\mathrm{thr}}\right) + d\left(f_{\mathrm{thr}}\right), \tag{6.19a}$$

where $\alpha(f_{\mathrm{thr}})$ is the solution of the below equation

$$f_{\mathrm{thr}} = \frac{1 - \alpha^r}{1 - \alpha^{r+1}}. \tag{6.19b}$$

$\overline{\overline{B}}_{\mathrm{thr}}$ *in* (6.19a) *is the threshold for existence of the 2:2 response and is a function of E_{stim} and r. The black surface denoted as S_3 in Figure 6.12, is the $\overline{\overline{B}}_{\mathrm{thr}}$.*

Proof As described in Section 6.4.2 in order to excite the k-th action potential E_{stim} must be greater than E_2 branch for which $f_{k-1} > f_{\text{thr}}$ where f_{thr} is given by (6.8). The result then follows by evaluation of (6.13) at $f_{\text{o}} = f_{\text{thr}}$. The equation (6.13c) is inverted and f_{thr} is used as a parameter. In order to obtain the exact solution of the equation (6.19b) for α, an approximation obtained by regular perturbations about $r = 1$ is represented below

Perturbation solution of equation (6.19b)*:* Equation (6.19b)for $r = 1$ has two roots $\alpha_1 = 1$ and $\alpha_2 = (1 - f_{\text{thr}})/f_{\text{thr}}$. When $\alpha_1 = \alpha_2$, $f_{\text{thr}} = 1/2 = 0.5$ which is below the f_{min} in CRN-2 model with the present parameters. Therefore, this solution is discarded as no action potential can be excited. The other solution α_2 corresponds to the threshold 2:2 response and it can be used as the basis of the perturbation expansion. The Taylor series expansion of the unknown α_2 -which is a function of r and f_{thr}- about $r = 1$ is as follows:

$$\alpha_2(r, f_{\text{thr}}) = \alpha_2(1, f_{\text{thr}}) + (1 - r)\frac{\partial \alpha_2(r, f_{\text{thr}})}{\partial r}\Big|_{r=1} + O\big((1 - r)^2\big).$$

Equation (6.19b) is rewritten as

$$f_{\text{thr}}\alpha_2\left(r, f_{\text{thr}}\right)^{r+1} - \alpha_2\left(r, f_{\text{thr}}\right)^{r} + 1 - f_{\text{thr}} = 0,$$

and $\dfrac{\partial \alpha_2(r, f_{\text{thr}})}{\partial r}$ which is the expansion coefficient, is obtained. Hence $\alpha_2(r, f_{\text{thr}})$ is described by the following equation

$$\alpha_2(f_{\text{thr}}) = \frac{1 - f_{\text{thr}}}{f_{\text{thr}}} - (1 - r)\frac{1 - f_{\text{thr}}}{1 - 2f_{\text{thr}}}\log\left(\frac{1 - f_{\text{thr}}}{f_{\text{thr}}}\right) + O\big((1 - r)^2\big). \tag{6.20}$$

As explained earlier, f_{thr} this a function of E_{stim}, therefore for each E_{stim} and each r, there is a unique $\alpha_2(f_{\text{thr}})$. By inserting α_2 into equation 6.3, the threshold value of basic cycle length for excitation of a 2:2 response is obtained. This finding is in contrast with Mitchell and Schaeffer (2003) approach where they claimed that 2:2 sequence exists until the threshold condition (6.18) for a 1:1 response is violated. ■

The four surfaces B_{bif}, $\overline{B}_{\text{thr}}$, $\overline{\overline{B}}_{\text{thr}}$ and $r = 1$ are plotted in Figure 6.12 as red, blue, black and green surfaces, respectively and the regions of parameters where the 1:1 and 2:2 responses occur, are illustrated. The figure is created by changing the dimensionless parameter r from 0 to 4 and E_{stim} from -30 mV to 0 mV. Note that the range of E_{stim} is chosen based on the phase portrait of the CRN-2 system (Figure 6.10). When $r < 1$ the responses of the CRN-2 system is stable 1:1 and this corresponds to the right side of the green surface ($r = 1$) in the Figure 6.12. As can be seen in this plot, the blue surface $\overline{B}_{\text{thr}}$ corresponding to the threshold of 1:1 response is well above the red surface

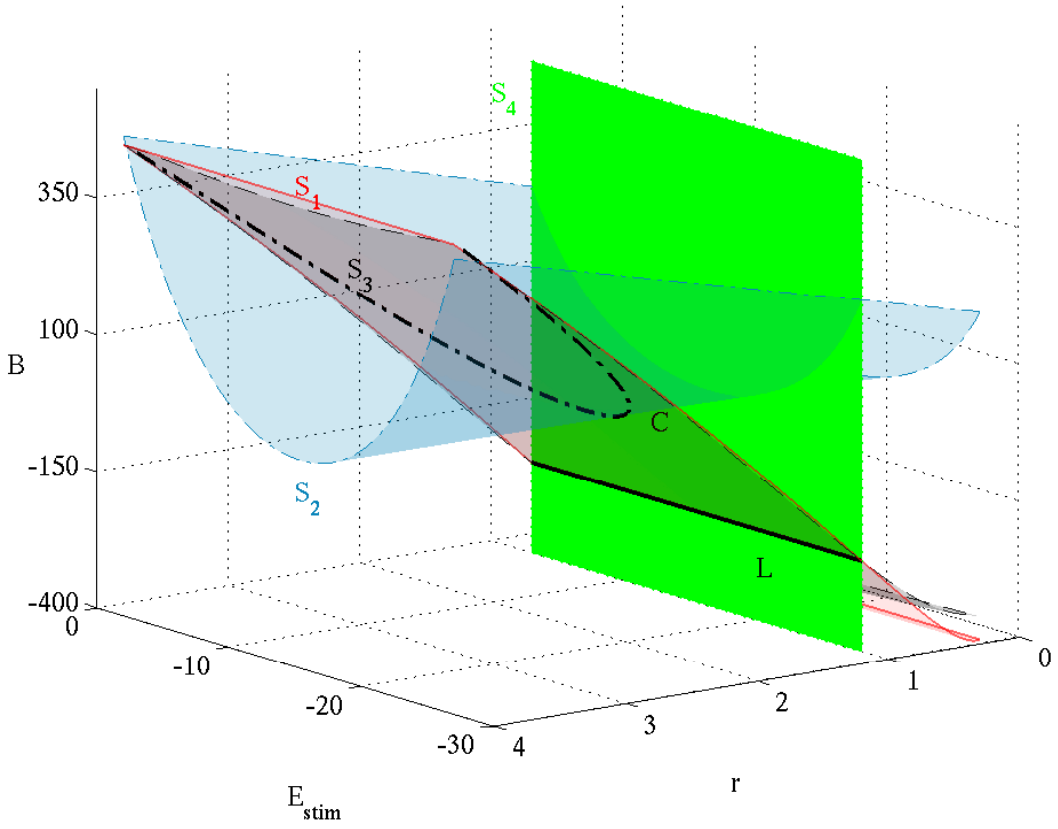

Figure 6.12: The bifurcation diagram of CRN-2 model in r-E_{stim}-B parameter space. The red surface S_1 is B_{bif} (6.15b). The blue surface S_2 is (6.18) and the black surface S_3 corresponds to (6.19a). The boundary between stable response and unstable response is denoted by a green surface S_4 which is $r = 1$.The intersection of three surfaces is shown in black lines.

B_{bif} as the basic cycle length decreases. This indicates that the if the parameters are chosen in this region, the system exhibits 1:1 response. Note that the bifurcation in fact occurs at a negative basic cycle length which does not even have a physiological meaning.

On the other hand when $r > 1$, depending on the range of E_{stim} the existence and the stability of 2:2 response changes. In order to gain better understanding of the bifurcation set in the E_{stim}-r-B parameter space, the restrictions to the hyperplanes $B =$ constant, $E_{\text{stim}} =$ constant and $r =$ constant are shown in Figure 6.13. The column (a) in Figure 6.13 illustrates a slice of the 3D Figure to the E_{stim}-r plane when B is fixed at $B = 127$ ms for the top figure and $B = 50$ ms for the bottom Figure. It can be seen that as r increases from 1 to 4, bifurcation occurs and the region of alternans is shown

as gray regions in Figure 6.13(a). When B decreases, alternans disappears. Another important point to remark is the the range of E_{stim} in which alternans occur which decreases by decreasing the basic cycle length and this is illustrated in Figure 6.13(a) bottom. Figures in column (b) are slices of 6.12 to the r-B plane. The top figure is a hyperplane $E_{\text{stim}} = -20$ mV and the gray area between B_{bif} and $\overline{B}_{\text{thr}}$ is the region of alternans. By increasing the value of E_{stim} this area disappears as it is illustrated in Figure 6.13(b) bottom for $E_{\text{stim}} = -5$ mV. In a large range of $r \in (0,3)$, alternans does not occur since the blue $\overline{B}_{\text{thr}}$ is above the B_{bif} and $\overline{\overline{B}}_{\text{thr}}$ and this simply means first bifurcation occur and then it reaches the threshold value for 1:1 solution and this is not correct. Therefore, the region at which instability arises is when r is chosen much bigger than three.

Furthermore, Figures in column (c) of 6.13 show hyperplanes $r = 2.5$ and $r = 0.8$ for the top and the bottom figure, respectively. When $r = 2.5$ 2:2 response occurs and this is shown as gray area, whereas at $r = 0.8$ there is no alternans as it was explained above. It is important to mention that the $\overline{B}_{\text{thr}}$ depends on E_{stim} which indeed indicates the strength of the stimulus current. Hence by increasing the stimulus strength and consequently increasing the E_{stim}, the range of 1:1 response can be extended. This also indicates the importance of the fast system which is responsible for the E_{stim} in the full system.

6.6 Numerical solution of the restitution boundary value problem

In this section the BVP formulation (3.8) and (3.10) are imposed on the full CRN-2 system for 1:1 and 2:2 responses, respectively, in order to verify the validity of the asymptotic results. The 1:1 and 2:2 restitution curves are constructed by imposing the boundary conditions (3.8) and (3.10) on the gating variable f, respectively. These conditions are not applied on the voltage equation since as stated in the previous chapters, at the beginning of each action potential, the voltage is prescribed at (or greater than) the threshold value of excitation E_{stim} (6.3e). Furthermore, no action potential is formed if this condition is not satisfied.

In deriving the map (6.11), the voltage at which f gating variable changes its behaviour and separates the systole part from the diastole part i.e. $E_f = -40$ mV, is used as a measure to construct the restitution curves as can be seen in the proof of the Lemma (6.1). Hence, in constructing the restitution curves t_f is plotted against B, such that

$$E(t_f) = E_f.$$

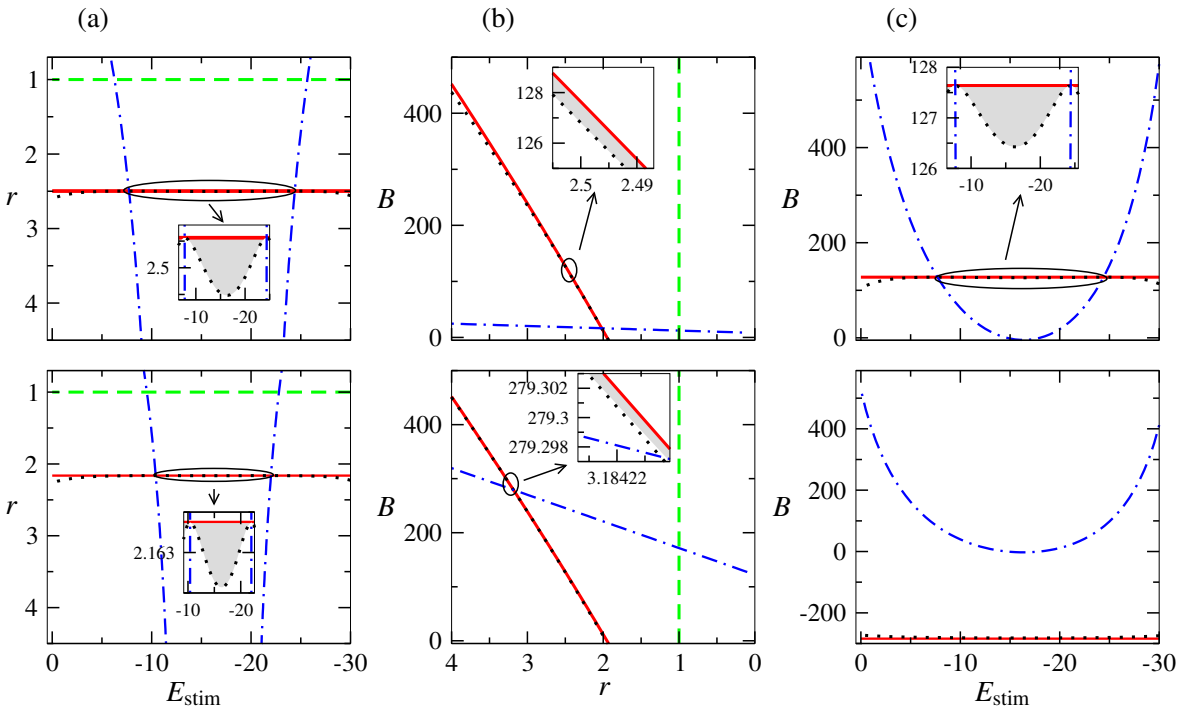

Figure 6.13: Restriction of the 3D figure to various hyperplanes. The colour coding is the same as in Figure 6.12. Figures in each column (a), (b) and (c), correspond to a projection of the figure in E_{stim}-r plane, r-B plane and E_{stim}-B plane, respectively. Top (a) $B = 127$ ms, bottom (a) $B = 50$ ms, top (b) $E_{\text{stim}} = -20$ mV, bottom (b) $E_{\text{stim}} = -5$ mV, top (c) $r = 2.5$ and bottom (c) $r = 0.8$. The region of alternans is denoted by gray surfaces in each plot.

Constructing 1:1 solution In order to produce the 1:1-response restitution curve, the condition (3.8) must be satisfied:

$$\begin{cases} E(kB,\ r,\ \varepsilon) = E((k+1)B,\ r,\ \varepsilon) = E_{\text{stim}}, \\ f(kB,\ r,\ \varepsilon) = f((k+1)B,\ r,\ \varepsilon), \end{cases} \tag{6.21}$$

The restitution curves for $r = 0.5$ and $r = 1.5$ are plotted in Figure 6.14, where t_f is plotted against the basic cycle length. The black solid curve is the asymptotic action potential duration map (6.11) which corresponds to $\varepsilon = 0$ and the thick red curves illustrate the restitution curve for the full CRN-2 model which corresponds to $\varepsilon = 1$. The coloured curves describe the restitution curves for different values of ε from 1 to 0 and it can be seen that as ε decreases, the exact analytical solution approaches the asymptotic map (6.11). The difference between the value of t_f in Figures 6.14(a) and 6.14(b), is understandable from the formula (6.9). As r increases, the action potential duration also increases.

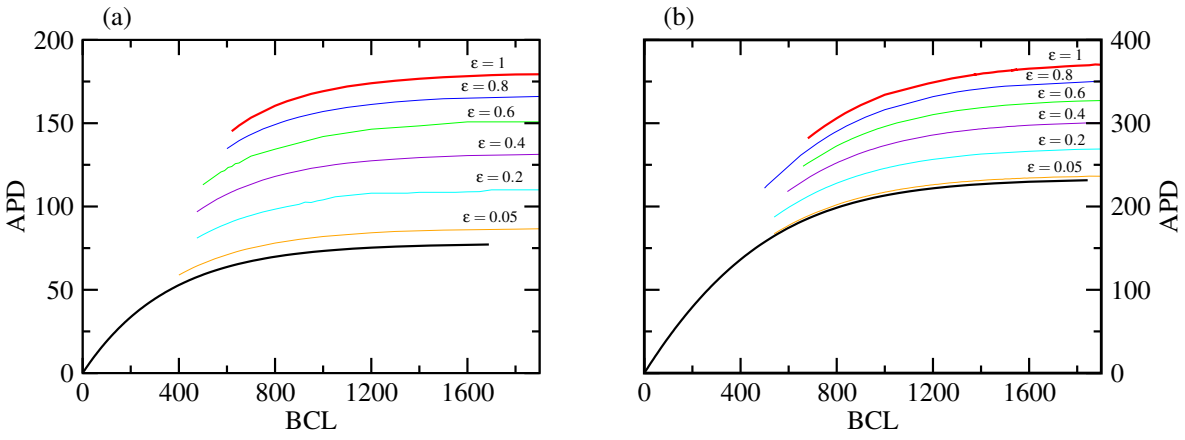

Figure 6.14: The 1:1 restitution curves for the CRN-2 system of equations (6.3) as $\varepsilon \to 0$. The parameters of the model are $E_{\text{stim}} = -20$ mv, $E_f = -40$ mv and $F_1 = 350$. The black solid curve is the solution of the asymptotic map (6.11) (i.e. $\varepsilon = 0$) and the solid red curve corresponds to $\varepsilon = 1$. The coloured curves denote different values of ε. As $\varepsilon \to 0$ the numerical solutions formulated as boundary value problem, approach the asymptotic map. In plot (a) $r = 0.5$ and in (b) $r = 1.5$.

Although the 1:1 restitution curve is constructed for all the values of B, this solution loses its stability at some basic cycle length $B = \overline{B}_{\text{thr}}$. The occurrence of the "unstable" solution is explained as below.

Constructing 2:2 solution As demonstrated in Chapter 3, in order to construct the 2:2 restitution curve, the condition (3.10) must be satisfied. (1) denotes the first action potential (2) indicates the second action potential.

$$E_1(0,\ r,\ \varepsilon) = E_{\text{stim}}, \tag{6.22}$$

$$E_2(0,\ r,\ \varepsilon) = E_{\text{stim}}, \tag{6.23}$$

$$f_1(0,\ r,\ \varepsilon) = f_2(B,\ r,\ \varepsilon), \tag{6.24}$$

$$f_2(0,\ r,\ \varepsilon) = f_1(B,\ r,\ \varepsilon). \tag{6.25}$$

The boundary value formulated restitution curves for $r = 0.8$ and $r = 2.5$ are illustrated in plots (a) and (b) in Figure 6.15. The red solid curve corresponds to the restitution curve for the full CRN-2 system ($\varepsilon = 1$) with the imposed above boundary conditions. The black solid curve shows the stable solutions of the map $\overline{\mathrm{A}} = \Phi(\overline{\mathrm{A}})$ and the stable solutions of the second generation map $\overline{\overline{\mathrm{A}}} = \Phi \circ \Phi(\overline{\overline{\mathrm{A}}})$. These solutions in the parametric form are explained in (6.12) and (6.13), respectively. It can be seen

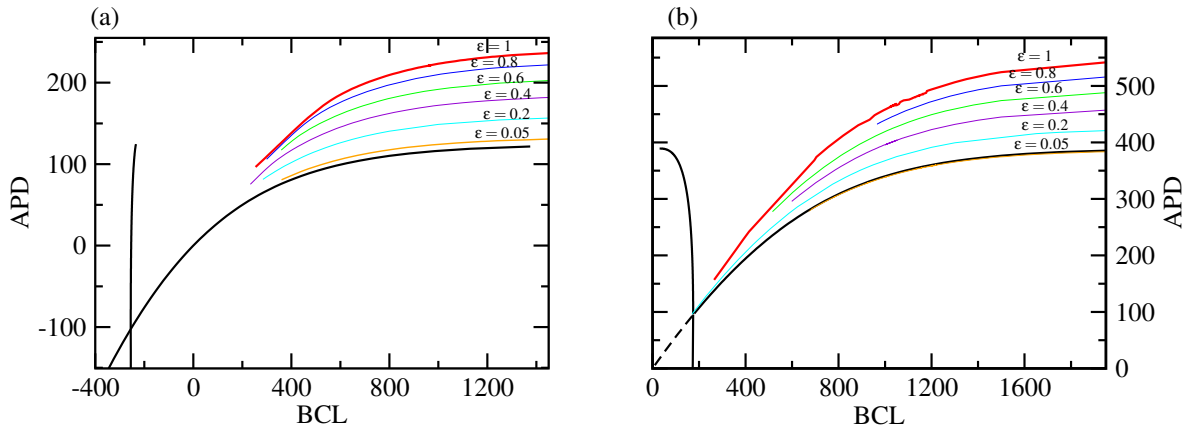

Figure 6.15: The 2:2 restitution curves for the CRN-2 system (6.3) when $\varepsilon \to 0$. The parameters of the model are $E_{\text{stim}} = -20$ mv, $E_f = -40$ mv and $F_1 = 350$. The thick black curve is the solution of the asymptotic map $\varepsilon = 0$ and the thick red curve corresponds to the solution of the full CRN-2 system $\varepsilon = 1$. Plot (a) illustrates the curves for $r = 0.8$ and (b) shows the restitution curves for $r = 2.5$.

from the plots (a) and (b) in Figure 6.15 that as $\varepsilon \to 0$, the numerical solution approaches the asymptotic solutions. Another key point to mention here is the occurrence of supercritical bifurcation and subcritical bifurcation for $r > 1$ and $r < 1$, respectively. For $r = 2.5$ the 2:2 solution has a supercritical bifurcation which corresponds to a persistent alternans. The solution of the CRN-2 system (6.3) when alternation of action potential occurs is shown in Figure 6.16. When $r = 0.8$, the bifurcation is subcritical which indicates a transient alternans. However, as it can be seen in Figure 6.15(a), the transient alternans appear on the negative basic cycle length which does not make sense. Hence the action potential solutions plotted in 6.16 show a normal and healthy response when $r < 1$.

6.6.1 Preliminary results of CRN-21

Now that the system of CRN-2 produces alternans, the simplified functions for $\tau_f(E)$ and $\overline{f}(E)$ are fitted to the full model and for different values for r, the system of CRN-21 is solved numerically. When $r > 1$, the modified full model produces alternans. Figure 6.17 illustrates the last 1200 (ms) of the solutions after 300 pacing times, for two different basic cycle lengths. As can be seen from Figure 6.17(a), the original system of CRN-21 at $B = 400$ (ms) does not produce alternans whereas the modified version of the full system with $r > 1$, has shown action potential duration alternans. Figure 6.17(b) illustrates the solutions for $B = 600$ (ms), where the change in r does not affect the behaviour of the system at this basic cycle length. Figure 6.17 demonstrates the correspondent $I_{\text{Ca,L}}$

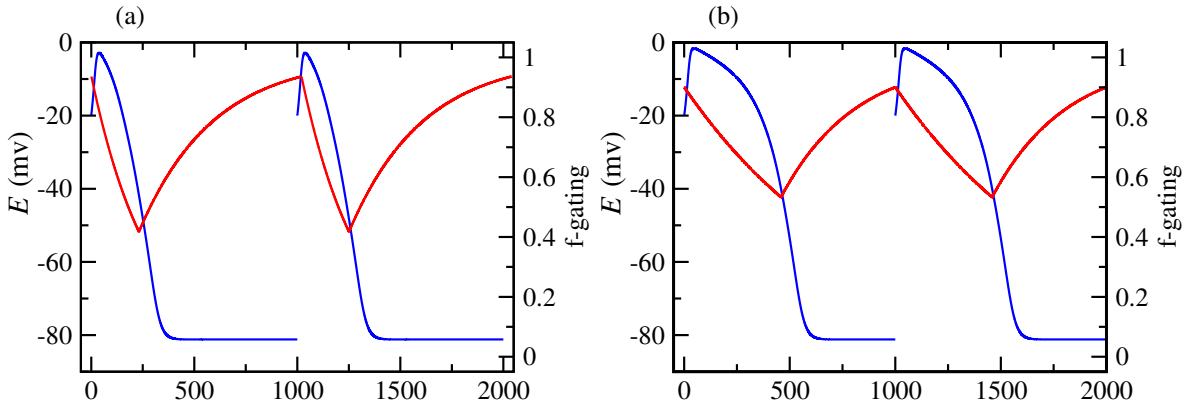

Figure 6.16: The action potential and f-gating variable for the CRN-2 system (6.3). The solid blue curve is the membrane potential E and the red curve illustrates the evolution of the f-gating variable. The parameters are $E_{\text{stim}} = -20$ (mv), $E_f = -40$ (mv), $F_1 = 350$, $\varepsilon = 1$ and $B = 1000$ (ms). In Figure (a) $r = 0.8$ and in Figure (b) $r = 2.5$ and alternans occur.

for these basic cycle length. From this figure it can be seen that for $B = 400$ (ms) there is alternation in the L-type Ca current. Based upon the preliminary results from the full physiological model, we found alternans as predicted by the analysis of the simplified models. This acts as a validation of our analysis. The identified mechanism is increasing r and subsequently increasing τ_f as the inactivation time for f-gating variable is slow. The slow inactivation of the f-gating variable leads to an increase in Ca^{+2} that enters the cell via L-type Ca^{+2} channel. Therefore, $[Ca^{+2}]_i$ will rise and this leads to alternans in the system (Fox et al., 2002; Weiss et al., 2006)

6.7 Summary

In this chapter, after reducing a detailed physiology-based model to a simplified system following the steps done by Suckley (2004), the role of the remaining variables was studied. The reduced CRN-2 system was modified such that a dimensionless parameter r was introduced to the time function of the gating variable $f(t)$. The parameter r determines the amplitude of the time required for the inactivation of the Ca^{+2} channel. The sequence of action potential duration was determined by iteration of the map $A_{k+1} = \Phi(A_k)$ and the stability of the map was studied. It was clearly shown that the map loses its stability at $r = 1$ and exhibits 2:2 response for $r > 1$. Furthermore, a parameter space specifying different regions corresponding to different responses, was presented.

The voltage-dependent time function is thought to play an important role in inducing instabilities

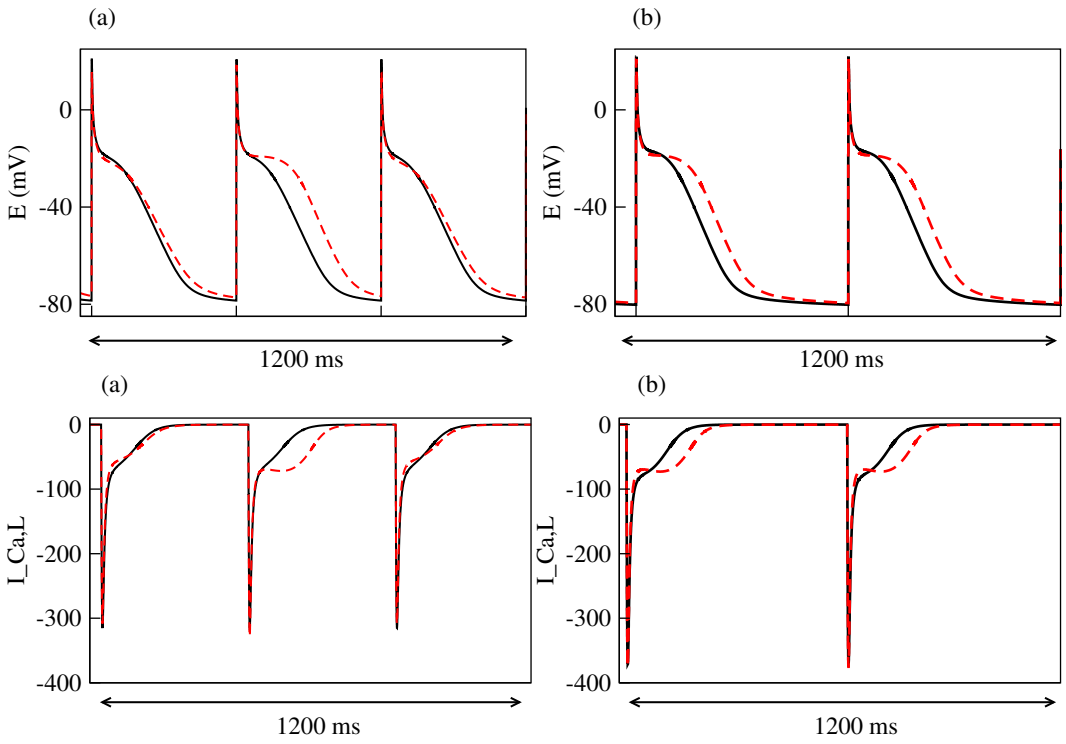

Figure 6.17: The last 1200 ms of the solutions, after 300 times pacing. The solid black curve is the solution for the original system and the dashed red curve indicates the solutions for the modified CRN-21 system when $r = 4$. (a) Action potential duration alternans when $B = 400$ (ms), (b) $B = 600$ (ms).

in the CRN-2 model. Therefore an increase in r and subsequently in τ_f implies that the voltage-dependent inactivation process of $I_{\mathrm{Ca,L}}$ becomes slower. The slow inactivation of the f-gating variable leads to an increase in Ca^{+2} which enters the cell via L-type Ca^{+2} channel, since total calcium influx during each action potential depends on the area under the $I_{\mathrm{Ca,L}}$ curve. Therefore, $[Ca^{+2}]_{\mathrm{i}}$ may rise and this could lead to action potential duration alternans.

On the other hand, as r decreases and τ_f decreases, the voltage-dependent inactivation gating variable $f(t)$ evolves faster. This indicates fast inactivation and less activation which leads to less inward $I_{\mathrm{Ca,L}}$. Furthermore, the equation that describes the evolution of the gating variable $f(t)$ is as follows:

$$f(t) = \exp(-t/rF_1).$$

When $r > 1$, the gating variable $f(t)$ stops before reaching its resting value which results in a short

diastolic interval. Therefore, the next action potential starts while the gating variable $f(t)$ has not recovered fully. Thus, for the next action potential the variable $f(t)$ starts at the point it was stopped before, rather than its resting value. Consequently it reaches its minimum value very quickly and it results in a short action potential duration. This is followed by a longer diastolic interval and consequently a longer action potential duration and so on so forth. When r increases the gating variable $f(t)$ decreases, consequently inactivation in $I_{\mathrm{Ca,L}}$ decreases. Thus, there is more activation which means more $I_{\mathrm{Ca,L}}$. For $r < 1$ the gating variable $f(t)$ decreases, the inactivation decreases and activation increases. Therefore, the inward current increases which leads to having a positive membrane voltage. When $f(t)$ increases, the inactivation becomes large, there is less inward current and the membrane goes toward negative potentials.

For long diastolic intervals, the inactivation recovers to its maximum value and long $I_{\mathrm{Ca,L}}$ during the next action potential causes Long action potential duration. This leads to a short diastolic interval, hence inactivation gate does not recover fully by the time the next action potential is generated. Therefore $I_{\mathrm{Ca,L}}$ was smaller and APD shorter. To conclude it should be mentioned that an increase in $I_{\mathrm{Ca,L}}$, increases alternans and the before the reduction in $I_{\mathrm{Ca,L}}$ may decrease the alternans magnitude. These results establish an ionic basis for action potential alternans which could help the development of pharmacological approaches to eliminate alternans.

Chapter 7

Conclusion and future work

In this thesis, we have studied the characteristics and potentials underlying mechanisms of action potential duration alternans in several mathematical models of action potentials. The models that are studied in this research are the McKean (1970) model which is a simplified version of the classical FitzHugh (1961) model in Chapter 4, the Caricature version of the Noble (1962) model derived by Biktashev et al. (2008) in Chapter 5 and an asymptotically reduced version of the Courtemanche et al. (1998) model of the atrial cell, reduced by Suckley (2004) in Chapter 6.
We have applied asymptotic reduction methods to reduce theses systems and to derive an explicit formula for action potential duration as a function of preceding diastolic interval. We have studied the stability of the map and have investigated the existence of bifurcations of equilibria. For each of the above mentioned models, the parameter regions where normal response and alternans occur, are presented.

In addition, we have developed a general framework formulated in terms of a boundary value problem and we have classified different responses of general excitable systems. We have applied the methods to the full excitable systems mentioned above, to derive analytically or compute numerically different branches of the action potential duration restitution curve. Finally we have presented that the asymptotic action potential duration restitution map and the boundary value problem formulated restitution curve for each model, are in close agreement. This indicate that the technique we have developed here, are applicable to general excitable systems.

The summary of the results is presented in the next section, followed by the last section as open questions and future directions.

7.1 Summary of results

While each of the models studied in this research provide a better understanding of the variables and parameters of excitable systems in inducing instabilities, the results obtained from all the of models has an important factor in common. All the models have demonstrated that the time scaling function in the voltage dependent slow gating variable is responsible for inducing alternans. In other words, the time that atrial cells need to relax, determines the time required for the next excitation.

In Chapter 4, a plausible explanation for the occurrence of alternans on a simplified model of spiking neurons is provided. Although the McKean model is simple and consists of two functions, we have been able to produce alternans by altering the time scale of the slow recovery gating variable. We have shown that the slow recovery dynamic suppresses electrical instabilities. In addition, the gating variable in the McKean model is analogous to the slow gating variables responsible for the repolarisation of the action potential in detailed cardiac models. Hence, in Chapters 5 and 6, we have assessed this finding by applying our methodology to two mathematical models of Cardiac action potentials.

The Caricature Noble model with three variables, has been studied in Chapter 5. The additional variable in Caricature Noble model is a superfast variable, thus, the whole action potential with the fast upstroke phase is presented. Biktashev et al. (2008) indicate that the asymptotic properties of the super fast variable in Caricature Noble model, is similar to Na^+ current in modern detailed models. Therefore, in order to investigate the role of the superfast system in inducing alternans, the Caricature Noble model with and without the super fast variable has been studied. We have found that the super fast variables -its existence is dependent on ε_1 in the Caricature Noble model- affects the region of alternans. Although we have shown that the role of ε_1 is mostly on the fast depolarisation and fast repolarisation of the action potential i.e.the front and back of the action potential, these two phases also contribute to the duration of an action potential (Mitchell and Schaeffer, 2003; Tolkacheva et al., 2002). In deriving the asymptotic maps, the role of these phases were neglected, but the bifurcation diagram of the full model in Chapter 5, well illustrated that the bifurcation point of the basic cycle length is displaced when the superfast variable is included in the system. Moreover, the superfast variable can shift the region of alternans by affecting the E_{stim} such that in the system without superfast variable, the E_{stim} of the system equals to the E_{stim} of the slow system. In contrast, for the full model (with superfast, fast and slow variables), the E_{stim} of the slow system is the value that superfast variable imposed on the system which in the case of the Caricature Noble model this is E_{Na}. This finding

suggests that the region of E_{stim} is affected by the super fast system and this system can suppress or promote instabilities which are produced by the slow system.

Furthermore, we have taken into account that the Caricature Noble model is based on the first mathematical model of cardiac action potentials and its parameters have physiological meaning. Hence, we have shown that the variable responsible for inducing instabilities in cardiac action potential, is the slow activation of outward I_{K} current. We have found that decreasing the K^+ current via shortening the recovery of the slow activation gating variable in Caricature Noble model, promotes alternans. Furthermore, by increasing the recovery time of the activation gating variable, it evolves slowly, therefore, the outward K^+ current increases and consequently suppresses alternans. This finding is in agreement with experimental results that suggest the variation of K^+ currents do not promote alternans but increasing this current can suppress alternans (Fox et al., 2002; Merchant and Armoundas, 2012).

In Chapter 6 we have assessed our methodology on a reduced version of the detailed human atrial action potential (Courtemanche et al., 1998). Hence, our results provide concurrence to the real physiology of the cardiac cell and we expect the existence of these responses to be directly observable experimentally.

We have found that the slow inactivation time in L-type $I_{\text{Ca,L}}$ current, has a crucial role in promoting and suppressing action potential alternans. Although the literature suggests that Ca^{+2}-mediated process may play a more important role than the voltage-dependent mechanism in inactivating Ca^{+2} channels, the role of voltage-dependent inactivation mechanism is not negligible (Sun et al., 1997). We have demonstrated that the time course of the voltage dependent inactivation of $I_{\text{Ca,L}}$ is identified as a pro-alternans factor based on studying a restitution map. Furthermore, we have shown that our reduced version of the Courtemanche et al. (1998) model with only one gating variable -the voltage-dependent inactivation variable for $I_{\text{Ca,L}}$- is capable of producing alternans.

At the cellular level, the relationship between membrane voltage and Ca^{+2} dynamics is complex. Membrane voltage and calcium dynamics are bidirectionally coupled and it is not clear whether alternation in ionic currents and membrane voltage leads to alternation in intracellular Ca^{+2} concentration, or alternation of intracellular Ca^{+2} concentration causes alternation of membrane voltage (Merchant and Armoundas, 2012; Valdivia, 2015; Weiss et al., 2006). According to Weiss et al. (2006) alternation in ionic currents and membrane voltage leads to alternation in intracellular Ca^{+2} concentration. Fox et al. (2002); Merchant and Armoundas (2012) also stated that alternation of sarcolemmal Ca^{+2} and

K^+ currents due to change in action potentials morphology have an affect on alternation in $[Ca^{+2}]_i$ cycling.

The role of alternation in $[Ca^{+2}]_i$ in producing voltage alternans is considered as a stronger rationale and one of the mechanisms inducing $[Ca^{+2}]_i$ alternans considered as variations of $[Ca^{+2}]_i$ influx into the cytoplasm. Consequently, alternation of intracellular Ca^{+2} concentration causes alternation of membrane voltage Merchant and Armoundas (2012); Valdivia (2015); Weiss et al. (2006). Our finding is in agreement with this mechanism as we have shown that the slow inactivation of the f-gating variable leads to an increase in Ca^{+2} which enters the cell via L-type Ca^{+2} channel. Therefore $[Ca^{+2}]_i$ will rise and this leads to alternans in the system. Moreover, alternans of $I_{Ca,L}$ due to change in voltage-dependent inactivation properties of $I_{Ca,L}$, can show how voltage-alternans and $[Ca^{+2}]_i$-alternans are interconnected.

Although literature suggests that Ca^{+2}-mediated process may play a more important role than the voltage-dependent mechanism in inactivating Ca^{+2} channels, the role of voltage-dependent inactivation mechanism is not negligible (Sun et al., 1997). In fact, an increase in $I_{\mathrm{Ca,L}}$, increases alternans and therefore reduction in $I_{\mathrm{Ca,L}}$ may decreases the alternans magnitude. These results establish an ionic basis for action potential alternans which could help the development of pharmacological approaches to eliminate alternans.

We conclude that the slow gating variables play important role in determining the slope of the action potential duration restitution curve. In other words, the time scale at which the slow gating variable evolves has a direct effect on the duration of the action potential and consequently on the occurrence of alternans. This finding is in agreement with the research done by Mitchell and Schaeffer (2003). However, we derive action potential duration restitution maps from the models that have physiological meaning. The novel contribution to the knowledge of this study is formulating methods that enable us to relate the cellular properties of cardiac cells in detailed cardiac models. Consequently we are able to predict the onset of alternans by controlling the amplitude of two important currents during the repolarisation phase of the action potential; the slow activation of the I_{K} or the L-type calcium current slow phase of inactivation or combination of both. This result is also in agreement with Fox et al. (2002); Merchant and Armoundas (2012). Our overall results establish an ionic basis for action potential alternans which could help the development of pharmacological approaches to eliminate alternans.

7.2 Open questions and future direction

The proposed method presented in this research, is applicable to any detailed cardiac model. The findings suggest that this approach could also be useful for studying other instabilities and irregular cardiac rhythms for prevention, control and suppression of abnormal rhythms. For example Ca^{+2} alternans or spatially extended alternans.

Another important direction is to investigate the role of the fast subsystem in promoting or suppressing alternans in more detailed model. For instance including the fast subsystem to the reduced Courtemanche et al. (1998) model would certainly extend our knowledge of the whole system of the cardiac cell.

It would be interesting to investigate coupling between voltage and the Ca^{+2} subsystem, in different reduced versions of the Courtemanche et al. (1998) model. Deriving asymptotic action potential duration restitution maps similar to Schaeffer et al. (2007) and Tolkacheva et al. (2006) and constructing restitution curves based on the formulation proposed in Chapter 3, would be the first step.

Bibliography

M. Abramowitz and I. A. Stegun, editors. *Handbook of mathematical functions: with formulas, graphs, and mathematical tables*. Dover, New York, 1965.

B. Alberts, D. Bray, J. Lewis, M. Raff, K. Roberts, and J. D. Watson. *Molecular biology of the cell*. Garland Publishing, 1994.

R. R. Aliev and A. V. Panfilov. A simple two-variable model of cardiac excitation. *Chaos, Solutions and Fractals*, 7:293–301, 1996.

G. W. Beeler and H Reuter. Reconstruction of the action potential of ventricular myocardial fibres. *JPL*, 268:177–210, 1977.

Donald M. Bers. Cardiac excitation-contraction coupling. *Nature*, 415:198–205, 2002.

V. N. Biktashev and R. Suckley. Non-Tikhonov asymptotic properties of cardiac excitability. *Phys. Rev. Lett.*, 93(16):168103, 2004.

V. N. Biktashev, R. Suckley, Y. E. Elkin, and R. D. Simitev. Asymptotic analysis and analytical solutions of a model of cardiac excitation. *Bulletin of Mathematical Biology*, 70:517–554, 2008.

I. V. Biktasheva, R. D. Simitev, R. Suckley, and V. N. Biktashev. Asymptotic properties of mathematical models of excitability. *Philosophical Transactions of the Royal Society of London A: Mathematical, Physical and Engineering Sciences*, 364(1842):1283–1298, 2006. doi: 10.1098/rsta.2006.1770.

J. W. Cain, E. G. Tolkacheva, D. G. Schaeffer, and D. J. Gauthier. Rate-dependent propagation of cardiac action potentials in a one-dimensional fibre. *The American Physical Society*, 2004.

E. M. Cherry, F. H. Fenton, and R. F. Gilmour. Mechanisms of ventricular arrhythmias: a dynamical systems-based perspective. *Am. J. Phys.*, 302(12):H2451–H2463, 2012.

D. R. Chialvo, D. C. Michaels, and J. Jalife. Supernormal excitability as a mechanism of chaotic dynamics of activation in cardiac Purkinje fibers. *CR*, 66:525–545, 1990.

P. Comtois and S. Nattel. Atrial repolarization alternans as a path to atrial fibrillation. *Journal Of Cardiovascular Electrophysiology*, 23:1013–1015, 2012.

M. Courtemanche, R. J. Ramirez, and S. Nattel. Ionic mechanisms underlying human atrial action potential properties: insights from a mathematical model. *Am. J. Physiol.*, 275:H301–H321, 1998.

B. Echebarria and A. Karma. Spatiotemporal control of cardiac alternans. *Chaos*, 12:923–930, 2002. doi: 10.1063/1.1501544.

V. Elharrar and B. Surawicz. Cycle length effect on restitution of action potential duration in dog cardiac fibers. *Am JPhysiol*, 244:H782–H792, 1983.

G. B. Ermentrout and D. H. Terman. *Mathematical foundations of neuroscience*. Interdisciplinary applied mathematics. Springer, New York, Dordrecht, Heidelberg, 2010. ISBN 978-0-387-87707-5. URL `http://opac.inria.fr/record=b1130863`.

S. J. Evans, O. Hotomaroglu, J. Geetha, K. Gittelson, J. Nilson, A. Garfinkel, H. M. Hastings, and F. H. Fenton. Alternans and the onset of ventricular fibrillation. *The American Physical Society*, 62:4043–4048, 2000.

F. Fenton and A. Karma. Vortex dynamics in three-dimensional continuous myocardium with fiber rotation: Filament instability and fibrillation. *Chaos*, 8:20–47, 1998.

R. FitzHugh. Impulses and physiological states in theoretical models of nerve membrane. *Biophysical Journal*, 1:445–456, 1961.

J.J. Fox, J.L McHARG, and R.F. GILMOUR. Ionic mechanism of electrical alternans. *Am J Physiol Heart Circ Physiol*, 282:H516–H530, 2002.

M. R. Franz, S. M. Jamal, and S. M. Narayan. The role of action potential alternans in the initiation of atrial fibrillation in humans: a review and future direction. *European society of cardiology*, 14: v58–v64, 2012. doi: 10.1093/europace/eus273.

R. F. Gilmour and N. F. Otani. Memory models for the electrical properties of local cardiac systems. *Journal of Theor Biol*, 187:409–436, 1997.

R. F. Gilmour, J. J. Fox, and E. Bodenschatz. Period doubling instability and memory in cardiac tissue. *Phys Rev E*, 89:138101–138104, 2002.

E. Grandi, F. S. Pasqualini, and D. M. Bers. A novel computational model of the human ventricular action potential and ca transient. *J Mol Cell Cardiol*, 48:112–121, 2010.

E. Grandi, S. V. Pandit, N. Voigt, A. J. Workman, D. Dobrev, J. Jalife, and D. M. Bers. Human atrial action potential and ca2+ model: Sinus rhythm and chronic atrial fibrillation. *Circulation research.*, 109:1055–1066, 2011.

M. R. Guevara, G. Ward, A. Shrier, and L. Glass. Electrical alternans and period-doubling bifurcations. *Computers in Cardiology*, 562:167–170, 1984.

R. M. Gulrajani. Computer simulation of action potential duration changes in cardiac tissue. *IEEE Comp Cardiol.*, 244:629–632, 1987.

G. M. Hall, S. Bahar, and D. J. Gauthier. Prevalence of rate-dependent behaviours in cardiac muscle. *PRL*, 82:2995–2998, 1999.

A. L. Hodgkin and A. F. Huxley. A quantitative description of membrane current and its application to conduction and excitation in nerve. *J. Physiol. Lond.*, 117:500–544, 1952.

S. S. Kalb, H. M. Dobrovolny, E. G. Tolkacheva, S. F. Idriss, W. Krassowska, and D.J. Gauthier. The restitution portrait: A new method for investigating rate-dependent restitution. *Cardiovascular Electrophysiol*, 15:698–709, 2004.

S. S. Kalb, E. G. Tolkacheva, D. G. Schaeffer, D.J. Gauthier, and W. Krassowska. Restitution in mapping models with an arbitrary amount of memory. *American Institute of Physics*, 15:023701–1–023701–11, 2005. doi: 1054-1500/2005/15(2)/023701/11.

A. Karma. Electrical alternans and spiral wave breakup in cardiac tissue. *Chaos*, 4:461–472, 1994.

J. Keener and J. Sneyd. *Mathematical Physiology*, volume 1. 2nd edition, 2008.

J. P. Keener and J. Sneyd. *Mathematical physiology. I. , Cellular physiology*. Interdisciplinary applied mathematics. Springer, New York, London, 1998.

D.P. Leong, J.W. Eikelboom, J.S. Healey, and S.J. Connolly. Atrial fibrillation is associated with increased mortality: causation or association? *European Heart Journal*, 34:1027–1030, 2013. doi: 10.1093/eurheartj/eht044.

D. Li, S. Fareh, T. K. Leung, and S. Nattel. Promotion of atrial fibrillation by heart failure in dogs. *Circulation*, 100(1):87–95, 1999. ISSN 0009-7322. doi: 10.1161/01.CIR.100.1.87. URL `http://circ.ahajournals.org/content/100/1/87`.

C. H. Luo and A. Rudy. A model of the ventricular cardiac action potential. *Circ Res*, 68:1501–1526, 1991.

H. P. McKean. Nagumo's equation. *Advances in Mathematics*, 4:209–223, 1970.

F. M. Merchant and A. A. Armoundas. Role of substrate and triggers in the genesis of cardiac alternans, from the myocyte to the whole heart: implications for therapy. *Circulation*, 125:539–549, 2012.

D. C. Michaels, J. Jalife, A. Vinet, and D. R. Chialvo. Nonlinear dynamics of rate- dependent activation in models of single cardiac cells. *Circulation Research*, 67:1510–1524, 1990.

C. Mitchell and D.G. Schaeffer. A two-current model for the dynamics of cardiac membrane. *BMB*, 65(3):767–793, 2003.

J. Nagumo, S. Arimoto, and S. Yoshizawa. An active pulse transmission line simulating nerve axon. *Proc. IRE*, 50:2061–2070, 1962.

S. Nattel. New ideas about atrial fibrillation 50 years on. *Nature*, 415:219–226, 2002. doi: 10.1038/415219a.

D. Noble. A modification of the Hodgkin-Huxley equations applicable to purkinje fibre action and pace-maker potentials. *J. Physiol.*, 160:317–352, 1962.

D. Noble, A. Garny, and P. J. Noble. How the hodgkin-huxley equations inspired the cardiac physiome project. *J Physiol*, 590.11:2613–2628, 2012.

J. B. Nolasco and R. W. Dahlen. A graphic method for the study of alternation in cardiac action potentials. *J. Appl. Physiol.*, 25:191–196, 1968.

A. Nygren, C. Fiset, L. Firek, J. W. Clark, D. S. Lindblad, R. B. Clark, and W. R. Giles. Mathematical model of an adult human atrial cell: the role of k^+ currents in repolarization. *Circ Res*, 82:63–81, 1998.

Z. Qu, J. N. Weiss, and A. Garfinkel. Cardiac electrical restitution properties and stability of reentrant spiral waves: a simulation study. *Am. J. Physiol.*, 276:H269–H283, 1999.

M. A. Richards, J. D. Clarke, P. Saravanan, N. Voigt, D. Dobrev, D. A. Eisner, and A. W. Trafford. Transverse tubules are a common feature in large mammalian atrial myocytes including human. *Am J Physiol Heart Circ Physiol*, 301:H1996–H2005, 2011.

D. G. Schaeffer, J. W. Cain, D. J. Gauthier, S. S. Kalb, R. A. Oliver, E. G. Tolkacheva, W. Ying, and W. Krassowska. An ionically based mapping model with memory for cardiac restitution. *Bulletin of Mathematical Biology*, 69:459–482, 2007.

D.G. Shaeffer, W. Ying, and X. Zhao. Asymptotic approximation of an ionic model for cardiac restitution. *Nonlinear Dyn*, 51:189–198, 2008. doi: 10.1007/s11071-007-9202-9.

R. D. Simitev and V. N. Biktashev. Conditions for propagation and block of excitation in an asympthotic model of atrial tissue. *Biophysical Journal*, 90:2258–2269, 2006.

R. D. Simitev and V.N. Biktashev. Asymptotics of conduction velocity restitution in model of electrical excitation in the hearts. *Springer*, 73:72–115, 2011.

SH Strogatz. Nonlinear dynamics and chaos: With applications to physics, biology, chemistry and engineering, 2001.

R. Suckley. *The Asymptotic Structure Of Excitable Systems Of Equations*. PhD thesis, Department of Mathematical Sciences, University of Liverpool, Liverpool L69 7ZL, UK., 2004.

Hui Sun, Normand Leblanc, and Stanley Nattel. Mechanisms of inactivation of l-type calcium channels in human atria1 myocytes. *Am. J. Physiol.*, 272:H1625–H1635, 1997.

A. N. Tikhonov. Systems of differential equations, containing small parameters at the derivatives. *Mat. Sbornik*, 31(3):575–586, 1952.

E. G. Tolkacheva, D. G. Schaeffer, D. J. Gauthier, and C. C. Mitchell. Analysis of the fenton karma model through an approximation by a one-dimensional map. *American Institute of Physics*, 12, 2002. doi: 10.1063/1.1515170.

E. G. Tolkacheva, D. G. Schaeffer, D. J. Gauthier, and W. Krassowska. Condition for alternans and stability of the 1:1 response pattern in a "memory" model of paced cardiac dynamics. *Physical Review*, 67:031904–1– 031904–10, 2003.

E. G. Tolkacheva, J. M. B. Anumonwo, and J. Jalife. Action potential duration restitution portraits of mammalian ventricular myocytes: Role of calcium current. *Biophysical Journal.*, 91:2735–2745, 2006.

M. A. Tsadok, C. A. Jackevicius, E. Rahme, K. H. Humphries, H. Behlouli, and L. Pilote. Sex differences in stroke risk among older patients with recently diagnosed atrial fibrillation. *JAMA*, 307(18):1952–1958, 2012. doi: 10.1001/jama.2012.3490.

H.H. Valdivia. Mechanisms of cardiac alternans in atrial cells. intracellular ca2+ disturbances lead the way. *Circ Res*, 116:778–780, 2015. doi: 10.1161/CIRCRESAHA.115.305923.

R. Visweswaran, S. D. McIntire, K. Ramkrishnan, X. Zhao, and E. G. Tolkacheva. Spatiotemporal evolution and prediction of [Ca2+]i and APD alternans in isolated rabbit hearts. *JCE*, 24(11): 1287–1295, 2013.

J. E. P. Waktare. Atrial fibrillation. *Circulation*, 106:14–16, 2002. doi: 10.1161/01.CIR.0000022730.66617.D9.

M. L. Walker and D. S. Rosenbaum. Repolarization alternans: implications for the mechanism and prevention of sudden cardiac death. *Cardiovascular Research.*, 57:599–614, 2003. doi: 10.1016/S0008-6363(02)00737-X.

J. N. Weiss, A. Karma, Y. Shiferaw, P. S. Chen, A. Garfinkel, and Z. Qu. From pulsus to pulseless: the saga of cardiac alternans. *Circ Res*, 98:1244–1253, 2006.

R.L. Winslow, J. Rice, S. Jafri, E. Marban, and B. ORourke. Mechanisms of altered excitation-contraction coupling in canine tachycardia-induced heart failure, ii: model studies. *Circ Res*, 84: 571586, 1999.

A. J. Workman, K. A. Kane, and A. C. Rankin. Cellular bases for human atrial fibrillation. *Heart Rhythm*, 5:S1–S6, 2008. doi: 10.1016/j.hrthm.2008.01.016.